Nucleon imaging at the femtoscale via elastic electron-nucleon scattering

Andrew Puckett
University of Connecticut

Colloquium at UTK

March 11, 2019

Acknowledgements

- Support from US DOE, Office of Science, Office of Nuclear Physics, Award ID DE-SC0014230 (Early Career research program)
- SBS and Hall A Collaborations
- Additional support from Jefferson Lab and University of Connecticut

Historical/pedagogical digression—Rutherford scattering and the discovery of the nucleus

OR: Imaging the microscopic structure of a target using "high-energy" scattering

Discovery of the Nucleus—Rutherford Scattering

By scattering α particles from a radioactive source from a thin gold foil, Rutherford, Geiger and Marsden demonstrated the existence of the atomic nucleus and put upper limits on its size.
[Simulation]

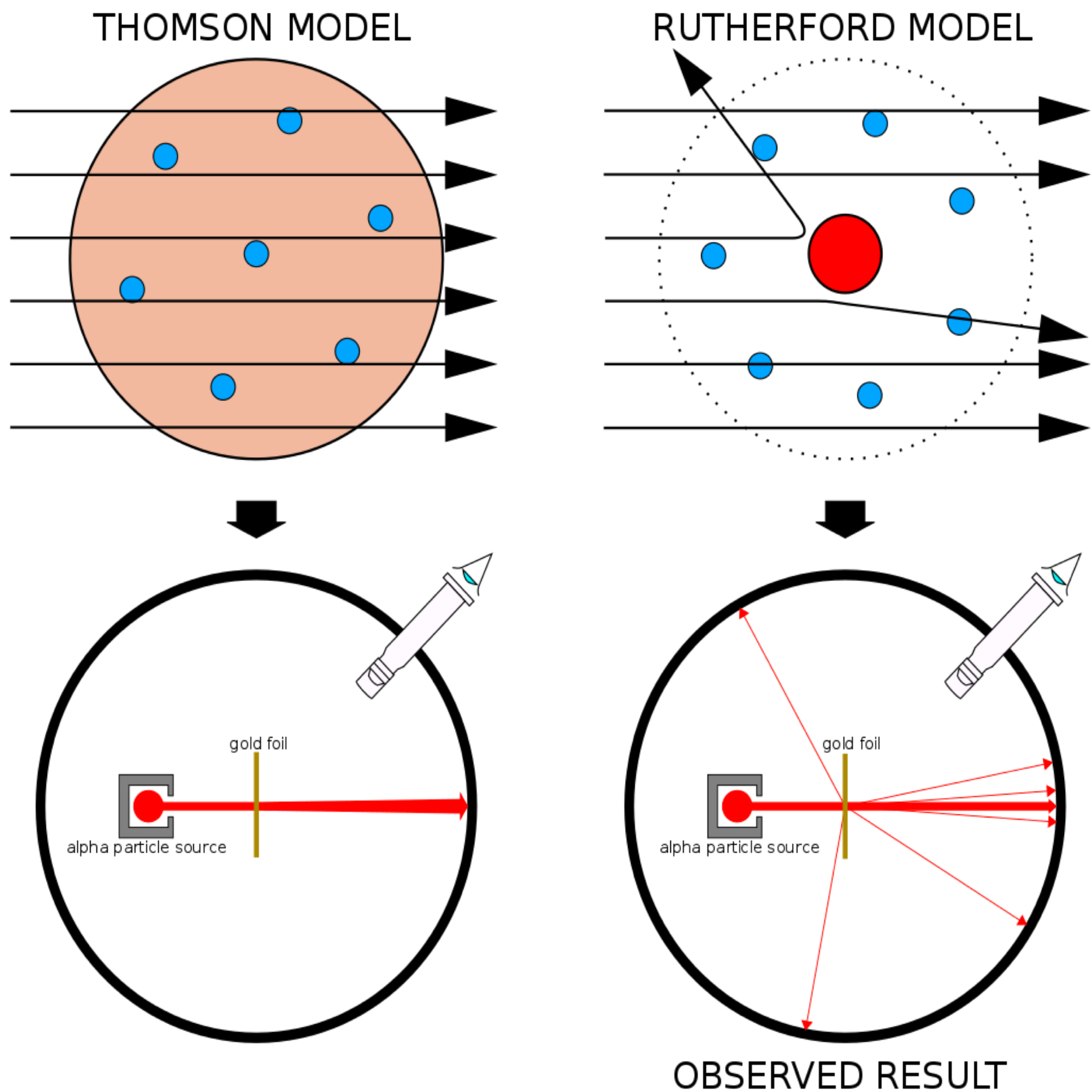

Classical Analysis of Rutherford Scattering

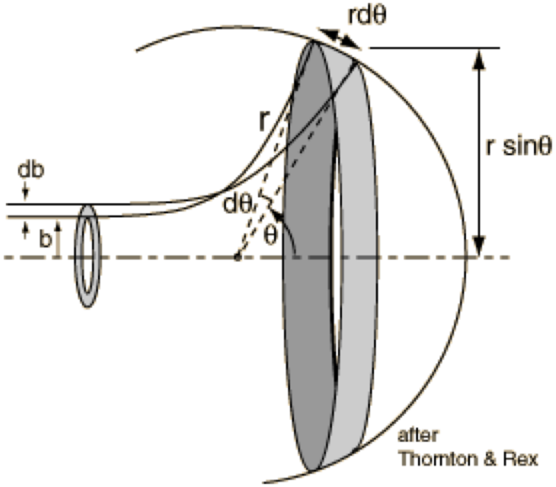

Figure credit: http://hyperphysics.phy-astr.gsu.edu/hbase/Nuclear/ruthcross.html

$$\alpha_{em} \equiv \frac{e^2}{4\pi\epsilon_0 \hbar c} \approx \frac{1}{137.036}$$

Assumptions:

- The incident α particle ($Z_\alpha = +2$) scatters from a *stationary, point-like* gold nucleus ($Z_{Au} = +79$).
- The interaction is repulsive and pure Coulomb: $U = \frac{Z_\alpha Z_{Au} e^2}{4\pi\epsilon_0 r}$
- Angular momentum conservation for a central force confines the motion to a plane
- The equation of the orbit $u(\theta) = \frac{1}{r(\theta)}$ is the solution to the *Binet* equation: $\frac{d^2u}{d\theta^2} + u = -\frac{Z_\alpha Z_{Au} e^2}{8\pi\epsilon_0 E b^2}$, where E is the α particle kinetic energy and b is the impact parameter.
- The impact parameter and scattering angle are related by:
  - $b = \frac{Z_\alpha Z_{Au} e^2}{8\pi\epsilon_0 E} \cot\frac{\theta}{2} = \frac{Z_\alpha Z_{Au} \alpha_{em} \hbar c}{2E} \cot\frac{\theta}{2}$
- Closest-approach distance and scattering angle are related by:
  - $r_{min} = \frac{Z_\alpha Z_{Au} e^2}{8\pi\epsilon_0 E}\left(1 + \csc\frac{\theta}{2}\right) = \frac{Z_\alpha Z_{Au} \alpha_{em} \hbar c}{2E}\left(1 + \csc\frac{\theta}{2}\right)$

- Rutherford differential cross section formula:

$$\frac{d\sigma}{d\Omega} = \left|\frac{b\,db}{\sin\theta\, d\theta}\right| = \frac{(\alpha_{em}\hbar c)^2 Z_\alpha^2 Z_{Au}^2}{16E^2 \sin^4\frac{\theta}{2}}$$

Example trajectories in α-gold Coulomb scattering @4.8 MeV

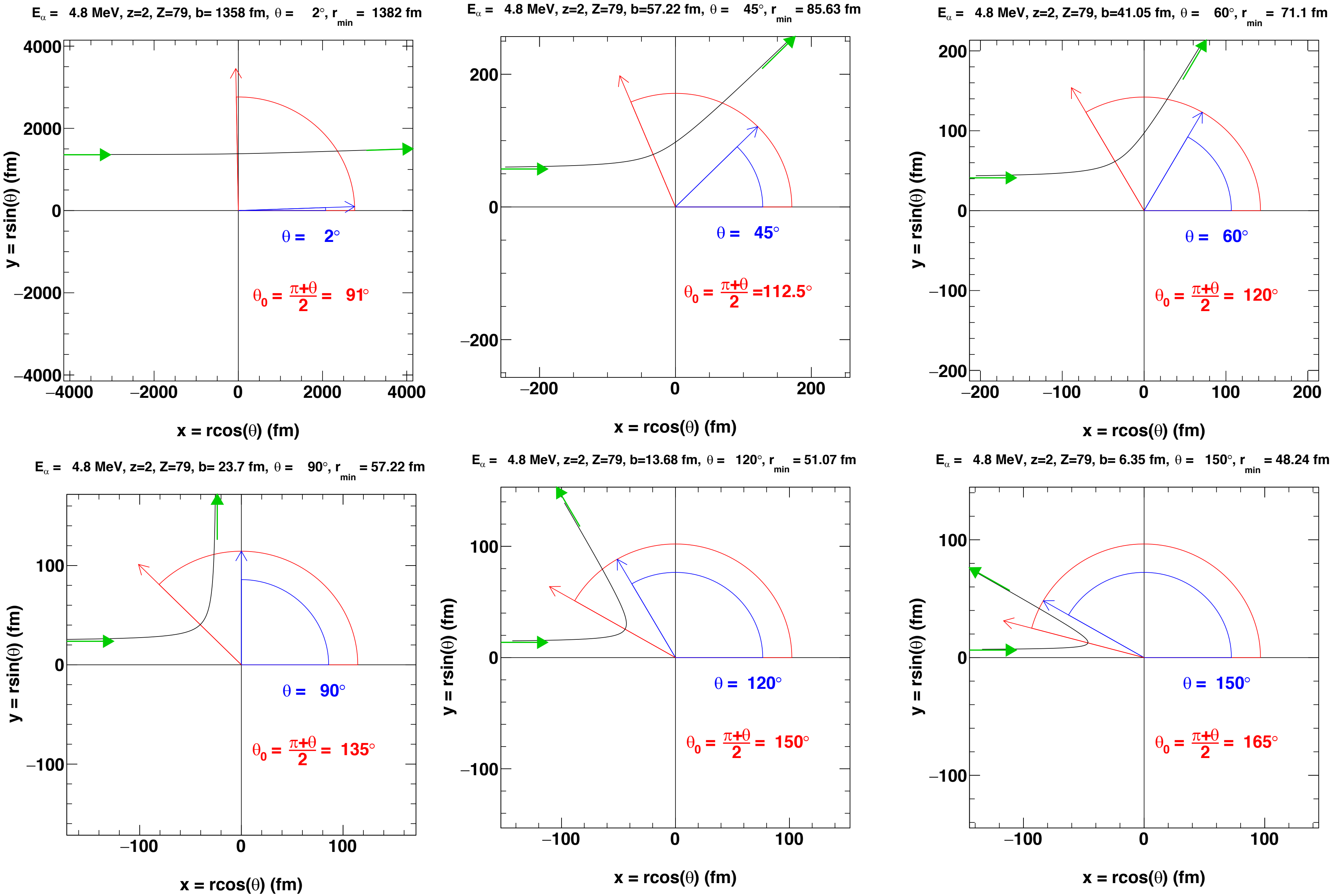

$$\text{Gauss' Law: } \mathbf{E} = \left\{ \begin{array}{c} \frac{Ze}{4\pi\epsilon_0 r^2}\hat{r}, r > R \\ \frac{Zer}{4\pi\epsilon_0 R^3}\hat{r}, r < R \end{array} \right\}$$

$$\text{Coulomb Force: } \mathbf{F} = \left\{ \begin{array}{c} \frac{zZe^2}{4\pi\epsilon_0 r^2}\hat{r}, r > R \\ \frac{zZe^2 r}{4\pi\epsilon_0 R^3}\hat{r}, r < R \end{array} \right\}$$

$$\text{Potential energy } U = \left\{ \begin{array}{c} \frac{zZe^2}{4\pi\epsilon_0 r}, r > R \\ \frac{zZe^2}{4\pi\epsilon_0 R}\left[\frac{3}{2} - \frac{r^2}{2R^2}\right], r < R \end{array} \right\}$$

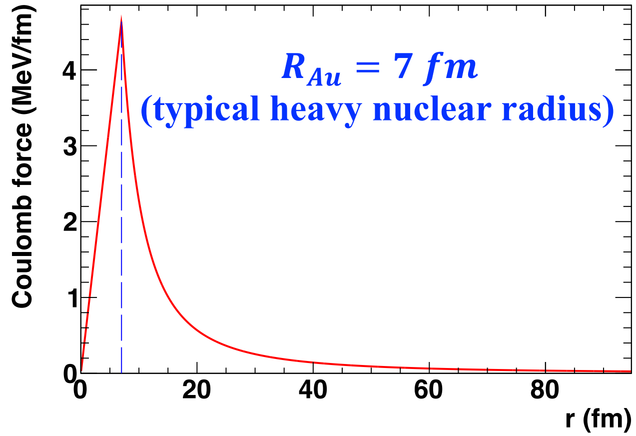

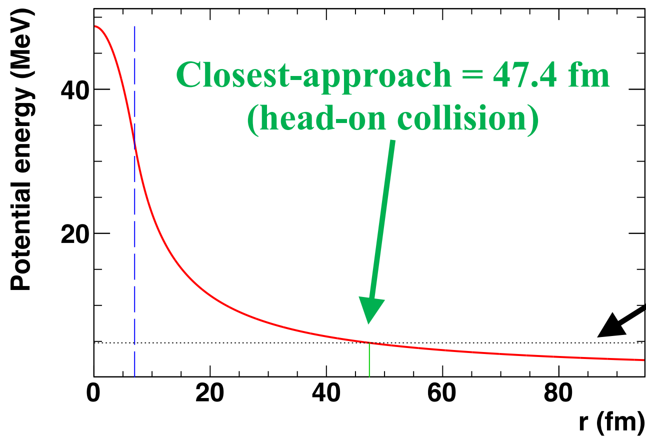

$E_\alpha = 4.8\ MeV$

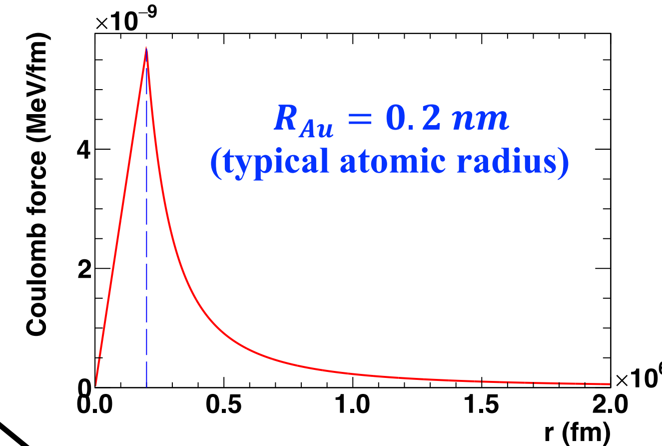

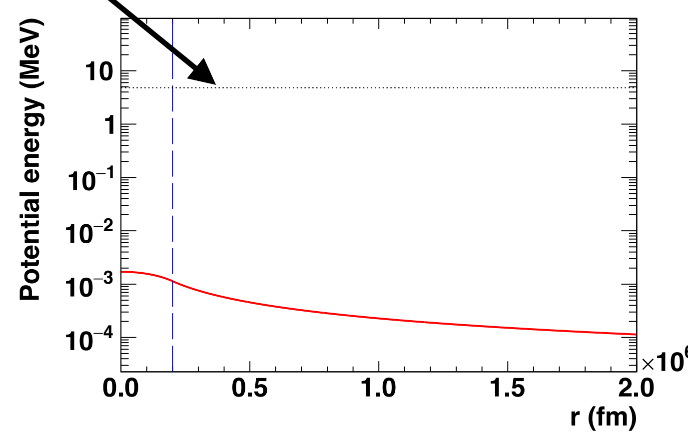

- Imagine the nucleus as a sphere of positive charge with uniform density throughout its volume (this approximation is not actually that far off)
- Even ignoring the atomic electrons, a Thomson-model nuclear charge density cannot produce large-angle deflections for MeV-scale kinetic energies

Deviations from the Rutherford formula and Nuclear size

Plots from: Eisberg and Porter, [Rev. Mod. Phys, 33, 190 (1961)]()

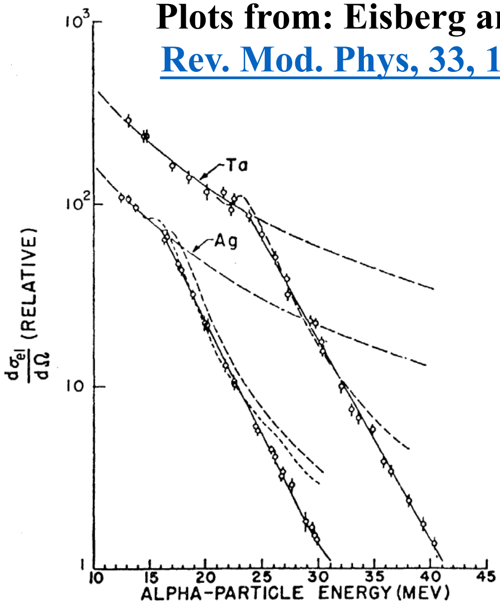

FIG. 14. Comparison of the differential cross section calculated from the APB model and experimental data for Ag and Ta. Experimental points were obtained from measurements at 60°. The broad dashed curve gives the Coulomb cross section and solid curves represent the experimental data of Farwell and Wegner. For Ag, two theoretical curves are shown; for the finer, $R=9.67\times10^{-13}$ cm; and for the coarser, $R=8.84\times10^{-13}$ cm. For Ta, the finer dashed curve gives the theoretical cross section for $R=10.54\times10^{-13}$ cm.

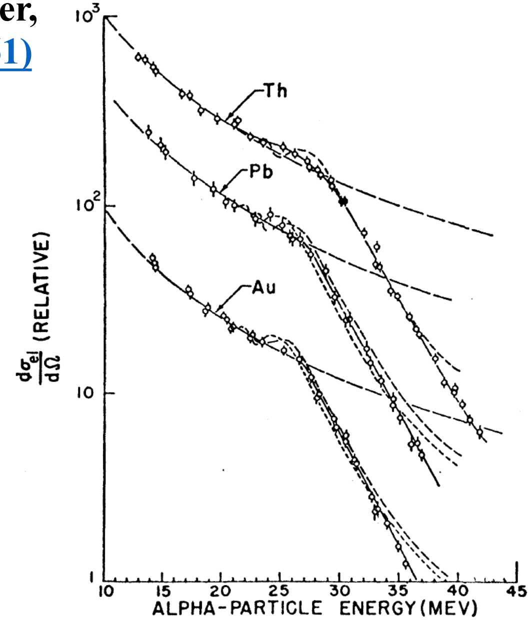

FIG. 15. Similar graphs for Au, Pb, and Th. For Au, the finer theoretical curve corresponds to $R=10.58\times10^{-13}$ cm and the coarser to $R=10.3\times10^{-13}$ cm. For Pb, the finer curve corresponds to $R=10.87\times10^{-13}$ cm and the coarser to $R=10.42\times10^{-13}$ cm. For Th, the dashed curve corresponds to $R=11.01\times10^{-13}$ cm.

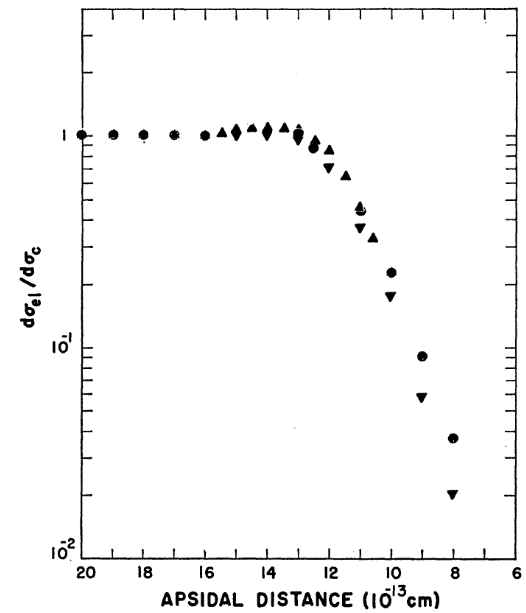

FIG. 19. Wegner plot of the experimental ratio of the differential cross section to the Coulomb cross section for the scattering of alpha particles by Au as a function of apsidal distance. Both angular data at fixed energy and energy data at fixed angle are shown. These data coincide for at least $(d\sigma_{el}/d\sigma_c)\geqslant0.1$ suggesting that the major variation of the ratio for heavy nuclei enters primarily through the apsidal distance. ▲, α's on Au, 22 Mev, 20°–60°; ●, α's on Au, 13–44 Mev, 60°; ▼, α's on Au, 13–44 Mev, 95°.

- Recall: closest approach distance ("apsidal distance") in Coulomb scattering is given by:

$$r_{min}=\frac{Z_\alpha Z_{Au}e^2}{8\pi\epsilon_0 E}\left(1+\csc\frac{\theta}{2}\right)=\frac{Z_\alpha Z_{Au}\alpha_{em}\hbar c}{2E}\left(1+\csc\frac{\theta}{2}\right)$$

- With the advent of high-energy accelerators, the α's could be accelerated to sufficiently high energies to penetrate the charge distribution of the nucleus, leading to deviations from Rutherford's formula
- The distance of closest approach at which the drop-off occurs provides a measure of the size of the nuclear charge distribution.
- The energy/angle dependence of the deviation from point-like behavior is sensitive to the details of nuclear structure and the alpha-nucleus interaction

Electron scattering for Nucleon/Nuclear Structure

Motivation: protons and neutrons are not elementary

$$\mu_{Dirac} = \frac{q\hbar}{2M}$$

$$\mu_{proton} \approx 2.793 \times \frac{e\hbar}{2M_p}$$

$$\mu_{neutron} \approx -1.913 \times \frac{e\hbar}{2M_p}$$

$$M_p = 938.272 \text{ MeV/c} \approx M_n = 939.565 \text{ MeV/c}$$

- Proton magnetic moment, first measured by Otto Stern in 1933, is nearly three times the value predicted by the Dirac equation for a spin-1/2 particle of charge e, mass M
- Approximate equality of proton and neutron masses suggests they are different quantum states of the same entity (the nucleon)
- Modern understanding: Quark model explains observed spectrum of baryons (mesons) as three-quark (quark-antiquark) bound states falling into flavor SU(N) multiplets for N quark flavors
- Nucleon is made of light quarks (uud/ddu). SM quarks have $M_u \sim M_d \sim$ 2-5 MeV, but $M_N \sim$ 1 GeV—where does nucleon mass come from?

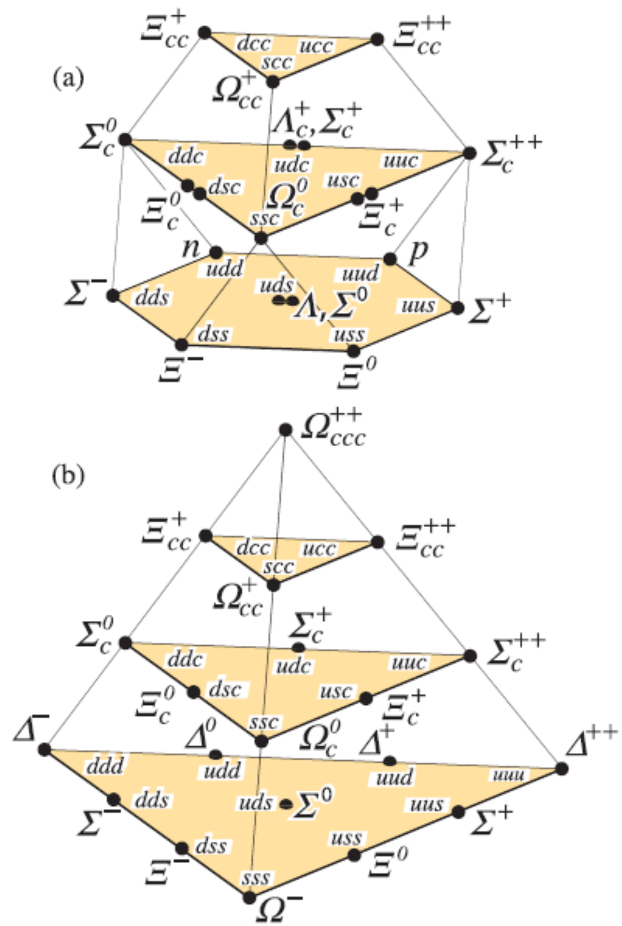

The modern baryon spectrum, PDG 2012: J. Beringer et al. (Particle Data Group), Phys. Rev. D86, 010001 (2012)

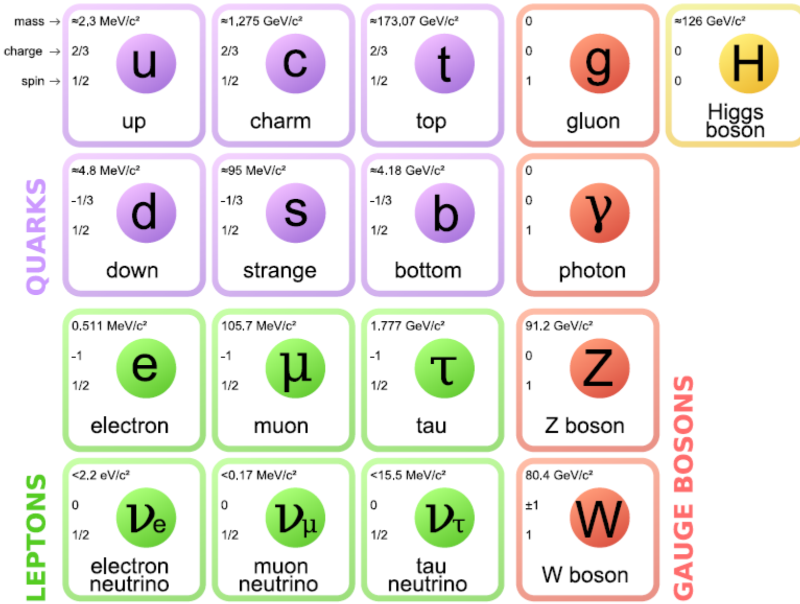

The Standard Model of Elementary Particles and Interactions

- Three families of elementary fermions: quarks & leptons
- Quarks → strong, EM and weak interactions
- Charged leptons → EM and weak
- Neutrinos → weak only
- **In this talk, we will focus on the strong interaction sector of the SM, described by Quantum Chromodynamics (QCD)**

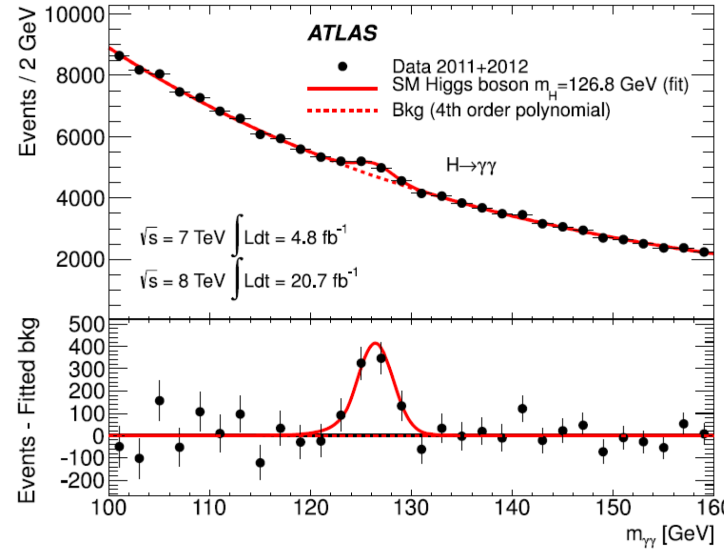

ATLAS Collaboration: Phys. Lett. B, 726, 88 (2013)

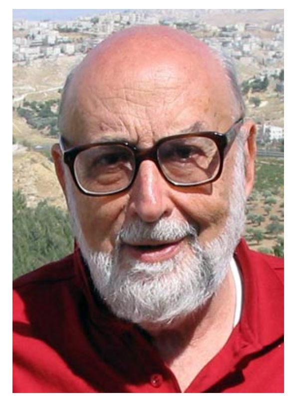

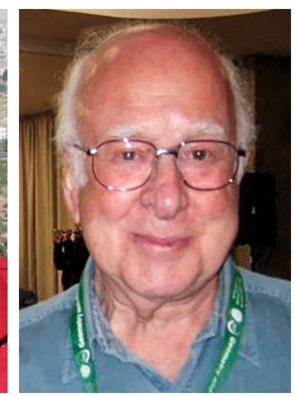

The Nobel Prize in Physics 2013: F. Englert and P. Higgs

Nucleon structure—conceptual aspects

- Elementary quarks of QCD are almost massless on the scale of the nucleon mass:
  - $m_u \sim m_d \sim$2-3 MeV
  - $M_p \sim M_n \sim$940 MeV
- The "binding energy" of quarks is of order $M_N/3$; Ratio of binding energy/constituent mass is ~100 → Quarks in the nucleon are highly relativistic!
  - In nuclei: Binding energy ~few MeV, constituent mass ~ 1 GeV → $\frac{E_B}{M_N} \sim \frac{1}{100}$
  - In atoms: Binding energy ~eV-keV, electron mass ~0.5 MeV, nuclear mass ~1-200 GeV → $\frac{E_B}{M_{atom}} \ll 1$
- $E = mc^2$ → quark-antiquark creation/annihilation is involved, occurs with regularity! "Bare" quarks are "dressed" by gluons/quark-antiquark pairs, complicated structure of QCD vacuum
- QCD is a non-Abelian gauge theory—as a consequence, the force carriers (gluons) also have self-interactions.
- QCD is confining—force increases as two quarks are pulled apart—no direct observation of quarks in the lab.
- QCD is strongly coupled at low energies—theoretical description of hadron formation/binding is inherently non-perturbative—prediction of hadron properties from first principles very difficult
- QCD is "asymptotically free"—force is weak at high energies/short distance scales—perturbation theory applicable
- Precise measurement and empirical understanding of nucleon structure is unavoidable if we hope to understand the physical world. Roughly 99% of the mass of visible matter in the universe is dynamically generated by strong interactions!

Electron-Nucleon Scattering in QED

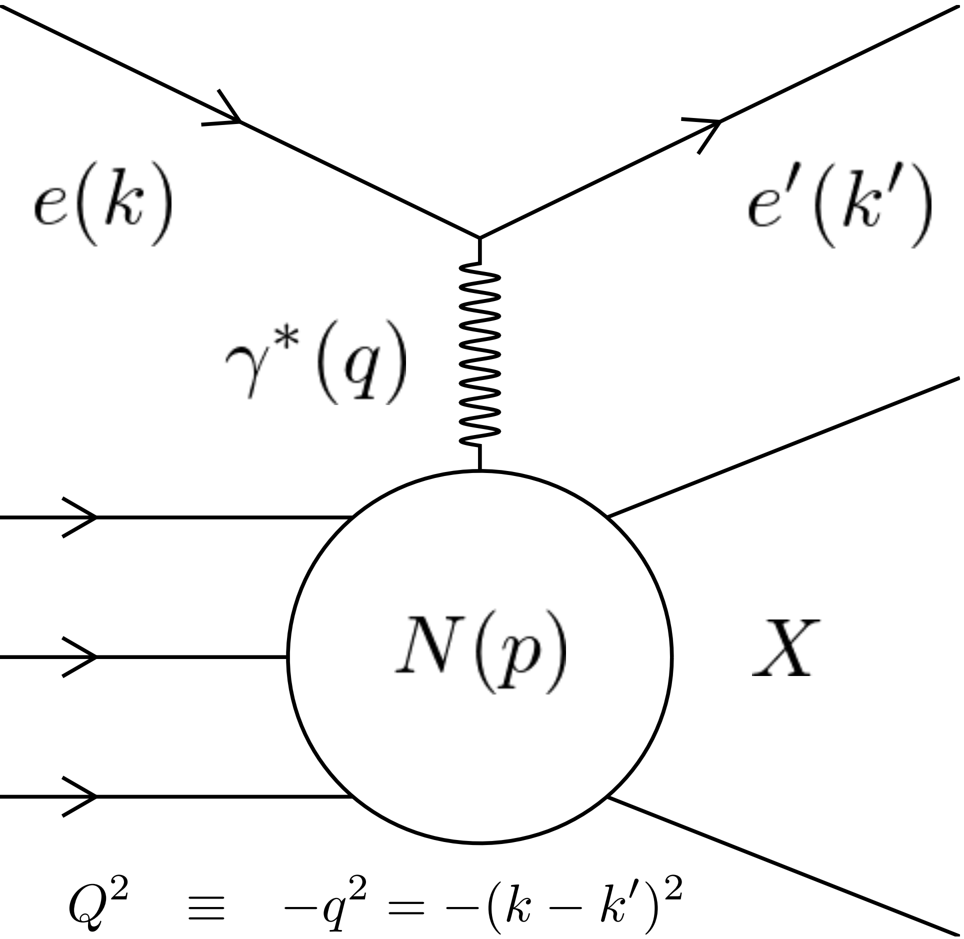

$$Q^2 \equiv -q^2 = -(k-k')^2$$

Feynman diagram for electron-nucleon scattering in the one-photon-exchange (Born) approximation

$$\alpha_{em} \equiv \frac{e^2}{4\pi\varepsilon_0\hbar c} = 1/137.035999074(44) \text{ (PDG 2012)}$$

- Charged leptons (e.g., electrons) interact with the charged constituents of nuclei predominantly via electromagnetic (EM) interaction (but also weak interaction).
- Electrons are point-like
- EM interaction is "weak"→low-order QED perturbation theory works well→"clean" theoretical interpretation
- EM interaction is well-described by the exchange of a single virtual photon of four-momentum q.
- Analogous to impulse approximation in classical mechanics
- Availability of high-quality electron beams w/ well-defined properties (energy, intensity, polarization, etc.) makes electron scattering a precision probe of nuclear structure

Scattering of ultrarelativistic electrons from a stationary charge distribution

$$\frac{d\sigma}{d\Omega} = \left(\frac{d\sigma}{d\Omega}\right)_{Mott} |F(\mathbf{q})|^2$$

$$\left(\frac{d\sigma}{d\Omega}\right)_{Mott} \equiv \frac{\alpha^2(\hbar c)^2}{4E_e^2 \sin^4\frac{\theta}{2}} \frac{E_e'}{E_e} \cos^2\frac{\theta}{2}$$

$$F(\mathbf{q}) = \int \rho(\mathbf{x}) e^{i\mathbf{q}\cdot\mathbf{x}} d^3x$$

- In the one-photon-exchange approximation in QED (equivalent to the first Born approximation in nonrelativistic quantum scattering theory), the cross section factorizes as the product of the "Mott" cross section, and the square of the *form factor* $F(\boldsymbol{q})$, equal to the Fourier transform of the charge density with respect to the three-momentum transfer $\boldsymbol{q} = \boldsymbol{k} - \boldsymbol{k}'$
- The Mott cross section represents the theoretical cross section for scattering of ultrarelativistic, spin-1/2 electrons from a point-like, spin-less target of charge *e*.
- Compared to the Rutherford cross section, the Mott cross section is modified by:
  - Relativistic kinematics of the electron (Rutherford formula is non-relativistic)
  - The "target recoil" factor $\frac{E_e'}{E_e}$ (which equals 1 for a static charge density)
  - The $\cos^2\frac{\theta}{2}$ suppression of large-angle scattering, which is a consequence of helicity conservation (a static charge density cannot flip the electron spin)

Elastic *eN* scattering and form factors: formalism

$$\mathcal{M} = \frac{4\pi\alpha}{q^2}\bar{u}(k')\gamma^\mu u(k) g_{\mu\nu}\bar{u}(p')\left[F_1(q^2)\gamma^\nu + F_2(q^2)\frac{i\sigma^{\nu\alpha}q_\alpha}{2M}\right]u(p)$$

Invariant amplitude for elastic eN scattering in the one-photon-exchange approximation

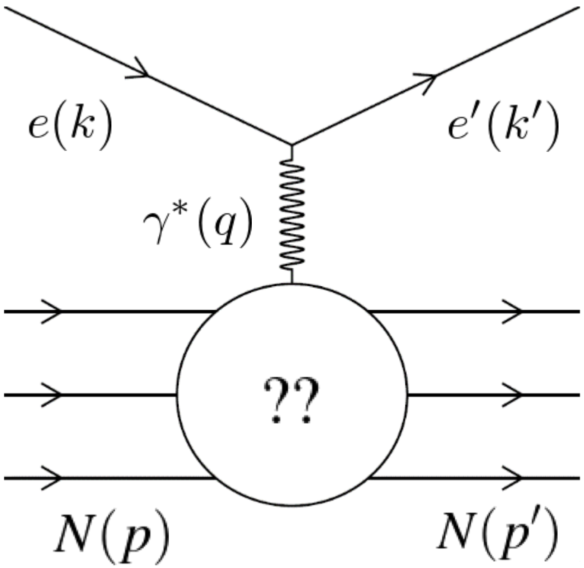

- The most general possible form of the virtual photon-nucleon vertex consistent with Lorentz invariance, parity conservation and gauge invariance is described by two form factors F_1 (Dirac) and F_2 (Pauli):
  - F_1 describes the helicity-conserving amplitude (charge and Dirac magnetic moment)
  - F_2 describes the helicity-flip amplitude (anomalous magnetic moment contribution)

$$G_E \equiv F_1 - \tau F_2$$
$$G_M \equiv F_1 + F_2$$
$$\tau \equiv \frac{Q^2}{4M^2}$$

Sachs Form Factors G_E (electric) and G_M (magnetic), are experimentally convenient linearly independent combinations of F_1, F_2

$$\frac{d\sigma}{d\Omega_e} = \frac{\alpha^2(\hbar c)^2\cos^2\frac{\theta_e}{2}}{4E_e^2\sin^4\frac{\theta_e}{2}}\frac{E_e'}{E_e}\left[\frac{\epsilon G_E^2 + \tau G_M^2}{\epsilon(1+\tau)}\right]$$
$$\frac{1}{\epsilon} \equiv 1 + 2(1+\tau)\tan^2\frac{\theta_e}{2}$$

Differential cross section in the nucleon rest frame:
Rosenbluth formula

$$\sigma_R \equiv \frac{\epsilon(1+\tau)\left(\frac{d\sigma}{d\Omega_e}\right)}{\left(\frac{d\sigma}{d\Omega_e}\right)_{Mott}} = \epsilon G_E^2 + \tau G_M^2$$

Rosenbluth Separation Method: Measure cross section at fixed Q^2 as a function of ε to obtain G_E^2 (slope) and G_M^2 (intercept).

Form Factors for a point nucleon

$$\begin{aligned}
G_E^p(Q^2=0) &= 1 \\
G_M^p(Q^2=0) &= \mu_p = +2.793 \\
G_E^n(Q^2=0) &= 0 \\
G_M^n(Q^2=0) &= \mu_n = -1.913 \\
F_1^p(0) &= 1 \\
F_2^p(0) &= \kappa_p = \mu_p - 1 = +1.793 \\
F_1^n(0) &= 0 \\
F_2^n(0) &= \kappa_n = -1.913
\end{aligned}$$

- In the low-Q^2 (long-wavelength) limit, the electric and magnetic form factors reduce to the proton and neutron charges and magnetic moments.
- If the nucleon was pointlike, the form factors would have these constant values at any Q^2

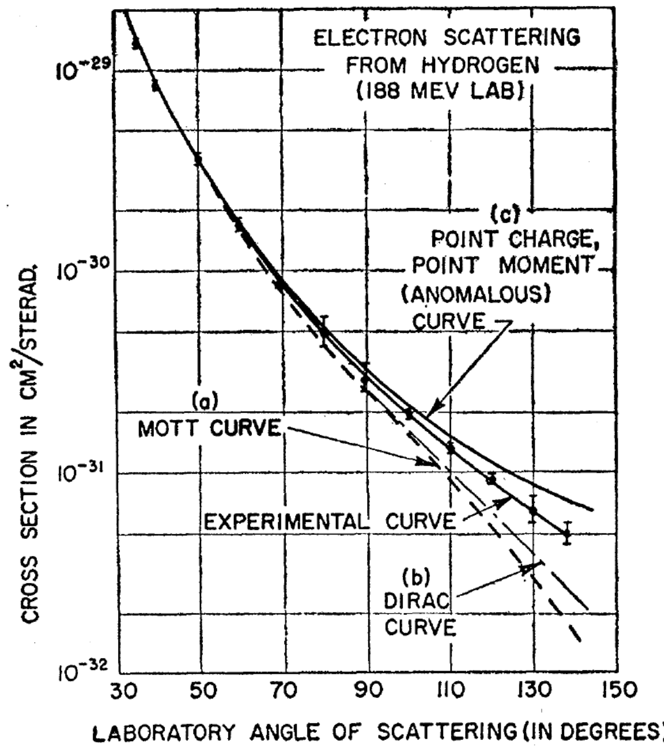

FIG. 24. Electron scattering from the proton at an incident energy of 188 Mev. The experimental points lie below the point-charge point-moment curve of Rosenbluth, indicating finite size effects.

R. Hofstadter, Rev. Mod. Phys., 28, 214 (1956)

R. Hofstadter
Nobel Prize 1961

"for his pioneering studies of electron scattering in atomic nuclei and for his thereby achieved discoveries concerning the structure of the nucleons"

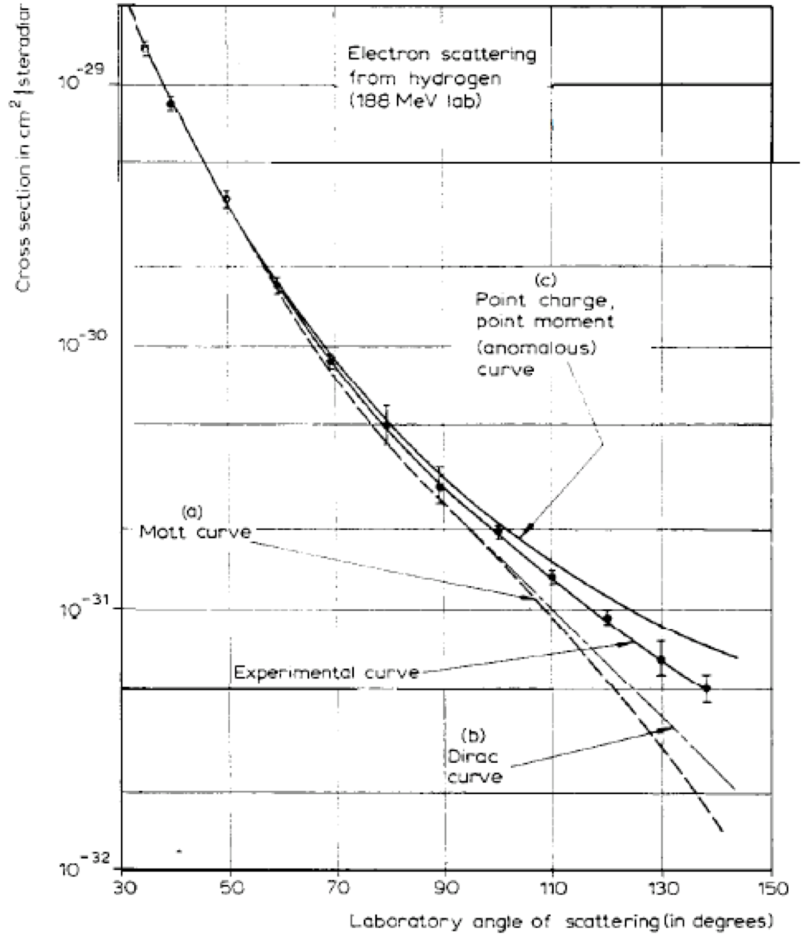

Fig. 9. Electron scattering from the proton at an incident energy of 188 MeV. *Curve (a)* shows the theoretical Mott curve for a spinless point proton. *Curve (b)* shows the theoretical curve for a point proton with a Dirac magnetic moment alone. *Curve (c)* shows the theoretical behavior of a point proton having the anomalous Pauli contribution in addition to the Dirac value of the magnetic moment. The deviation of the experimental curve from the Curve (*c*) represents the effect of form factors for the proton and indicates structure within the proton. The best fit in this figure indicates an rms radius close to $0.7 \cdot 10^{-13}$ cm.

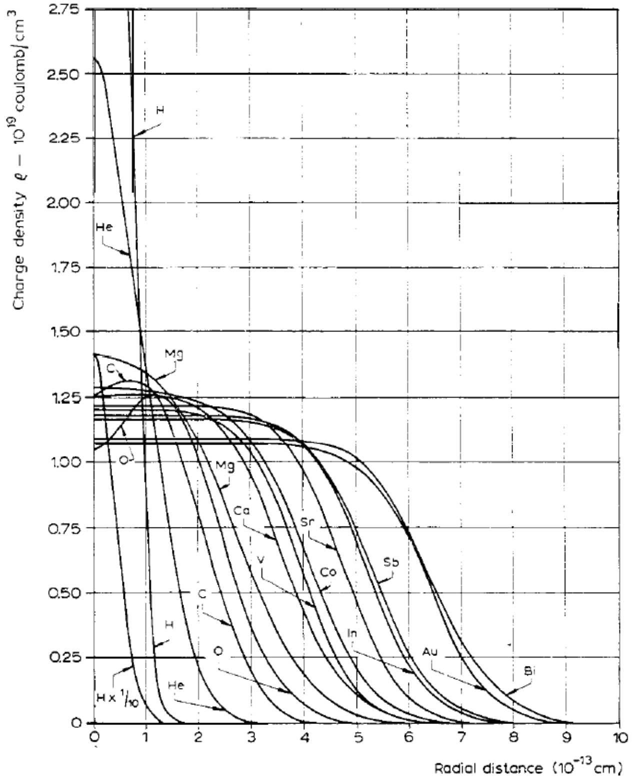

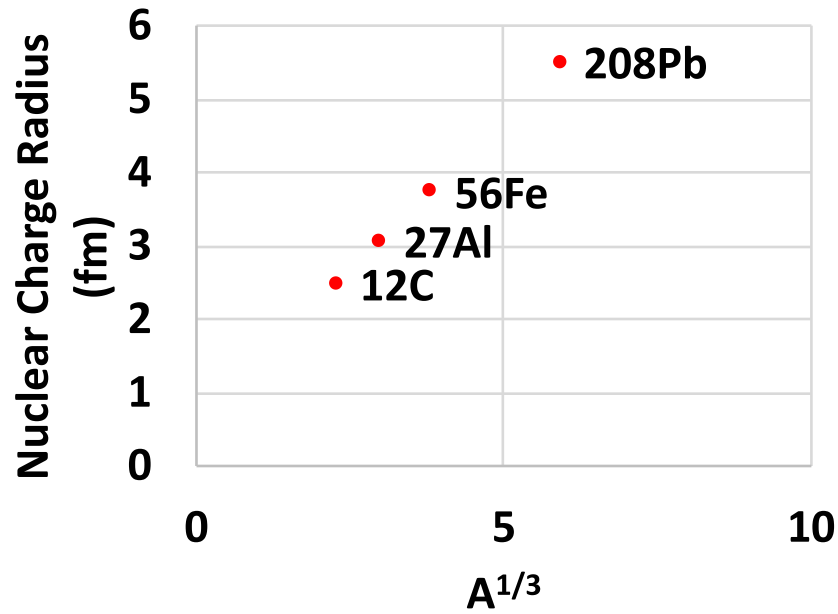

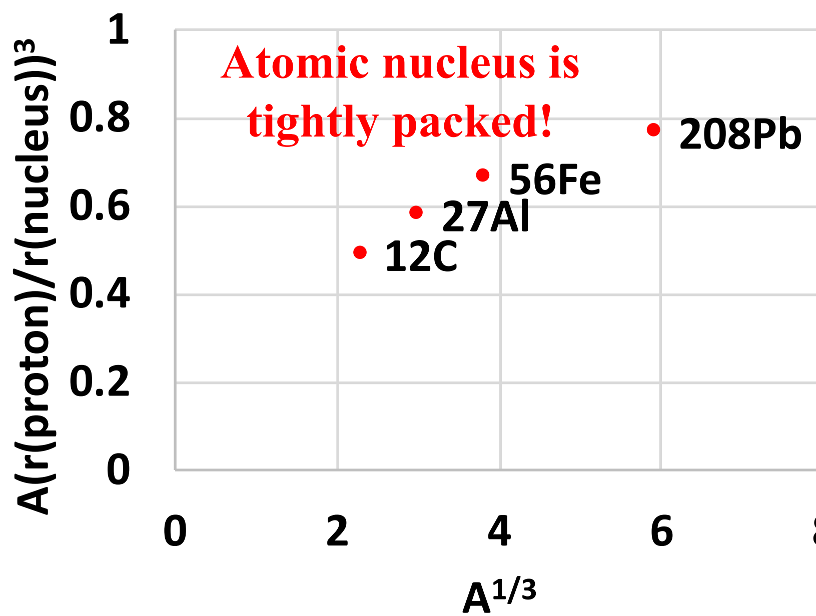

- Above: (R. Hofstadter Nobel lecture): Nuclear charge densities as measured in electron scattering, within Fermi model of the shape
- Top right: example nuclei, $r \sim A^{1/3}$ (volume proportional to number of nucleons)
- Bottom right: “Packing fraction” = ratio of volume of A nucleons to nuclear volume

*In*elastic electron-nucleon scattering and "scaling"

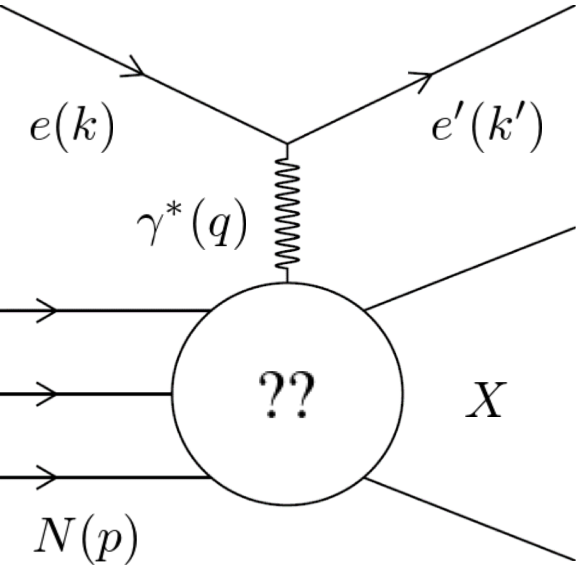

$$\frac{d^2\sigma}{dx\,dQ^2} = \frac{4\pi\alpha^2}{xQ^4}\left[\left(1-y-\frac{M^2x^2y^2}{Q^2}\right)F_2(x,Q^2)+xy^2F_1(x,Q^2)\right]$$

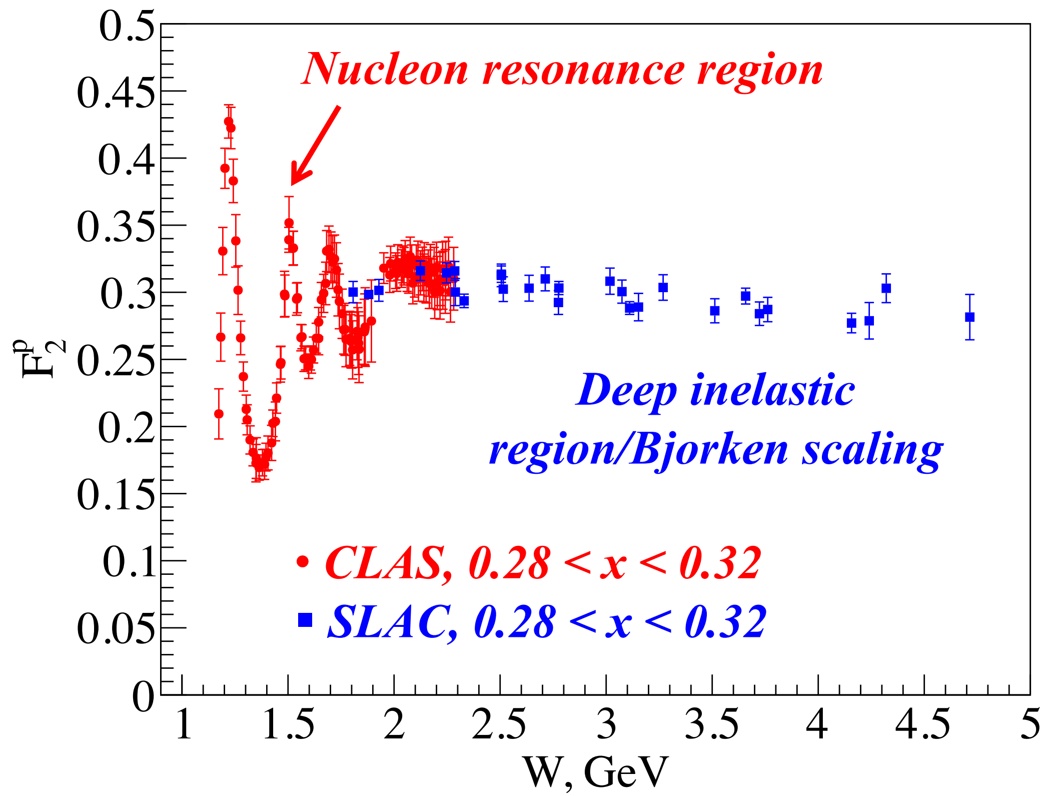

$$x = \frac{Q^2}{2p\cdot q}$$

$$W^2 = (p+q)^2 = M^2 + 2p\cdot q - Q^2 = M^2 + Q^2\frac{1-x}{x}$$

As Q^2/W^2 becomes "large" at fixed x, the proton structure functions exhibit the phenomenon of "scaling"—becoming independent of Q^2 for fixed "x"—this is called the ***"deep inelastic"*** regime

Friedman, Kendall, Taylor, Nobel Prize 1990

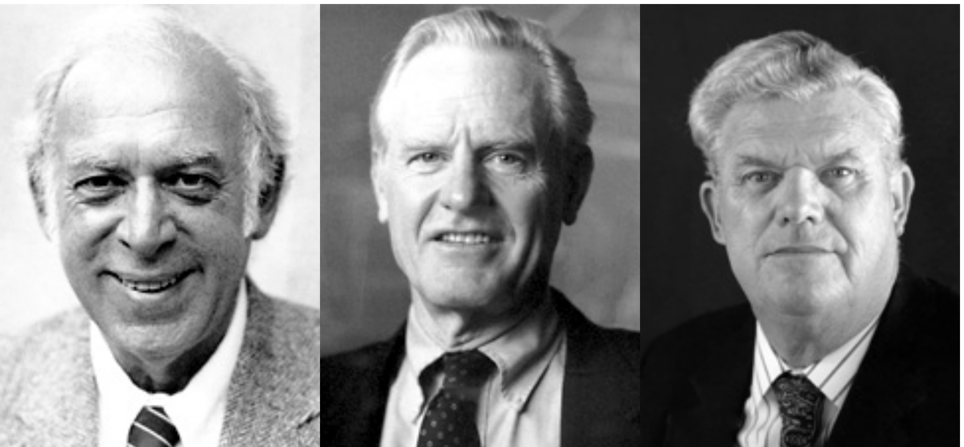

"for their pioneering investigations concerning deep inelastic scattering of electrons on protons and bound neutrons, which have been of essential importance for the development of the quark model in particle physics"

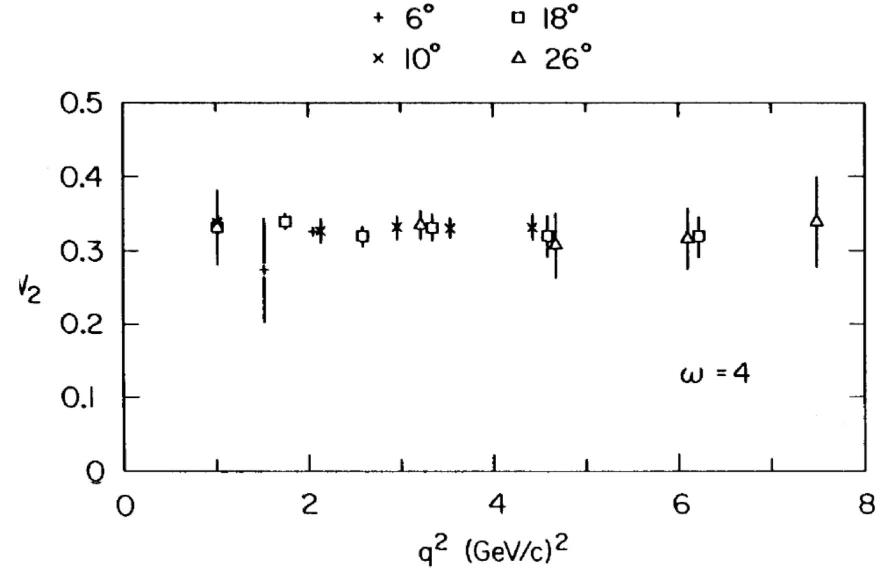

Fig. 13. An early observation of scaling: νW_2 for the proton as a function of q^2 for W > 2 GeV, at ω = 4.

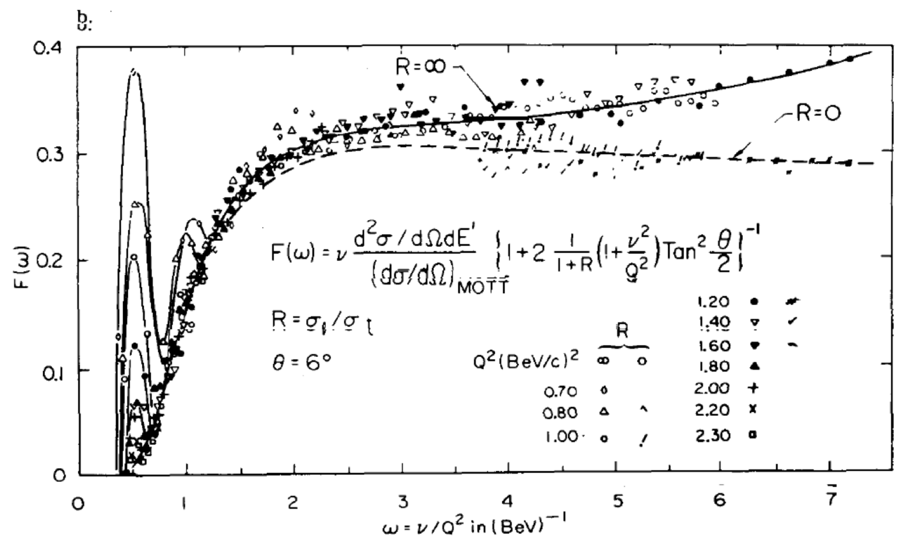

Fig. 12. **(a) The inelastic structure function $W_2(\nu,q^2)$ plotted against the electron energy loss ν.** (b) The quantity $F_1 = \nu W_2(\omega)$. The "nesting" of the data observed here was the first evidence of scaling. The figure is discussed further in the text.

Parton Distribution Functions

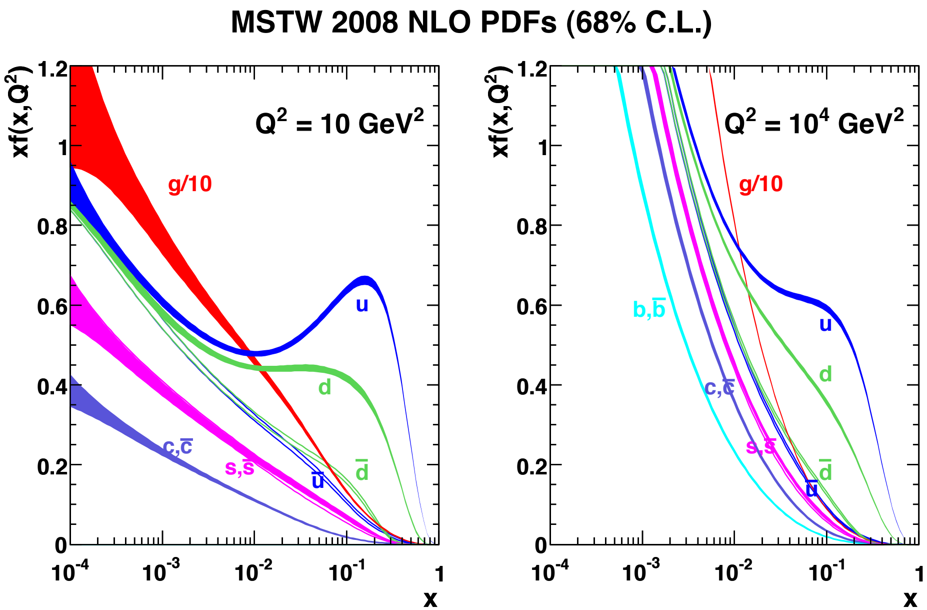

MSTW2008 NLO PDFs:
arXiv:0901.0002v3

- DIS structure functions mapped 5 orders of magnitude in x, Q^2
- Triumph of pQCD—description of scaling violations (Q^2 evolution)

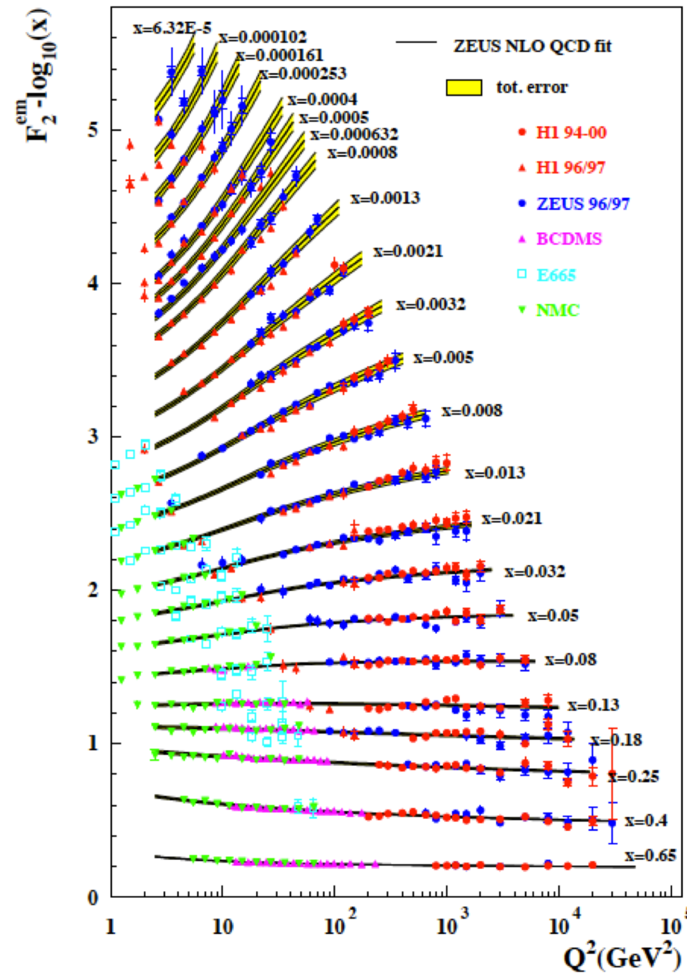

HERA F_2^p
arXiv:hep-ex/0211051v1

Gross, Politzer and Wilczek: Nobel Prize 2004

"for the discovery of asymptotic freedom in the theory of the strong interaction".

$$\beta(g) = -\frac{g^3}{16\pi^2}\left(\frac{11}{3}N_C - \frac{4}{3}\frac{N_F}{2}\right)$$

$$\beta < 0 \quad \Rightarrow \quad \alpha(\mu) \xrightarrow[\mu\to\infty]{} 0$$

Slides from D. Gross Nobel Lecture

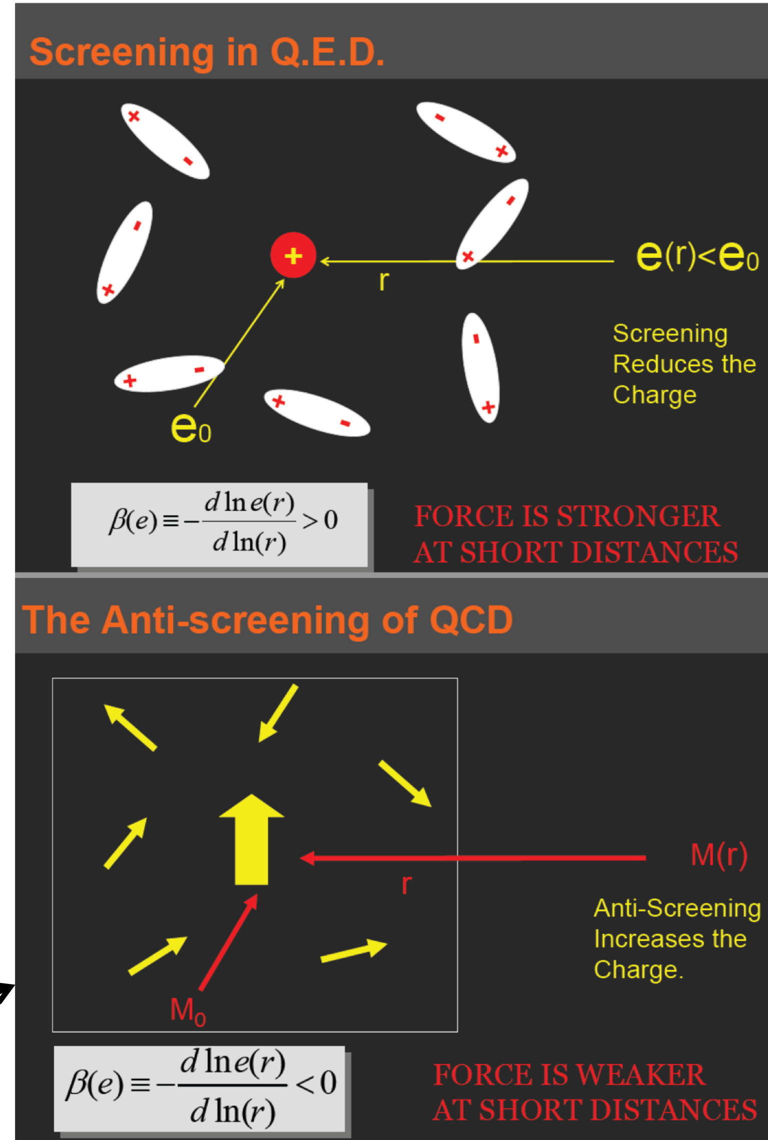

CEBAF @ Jefferson Lab (6 GeV era)

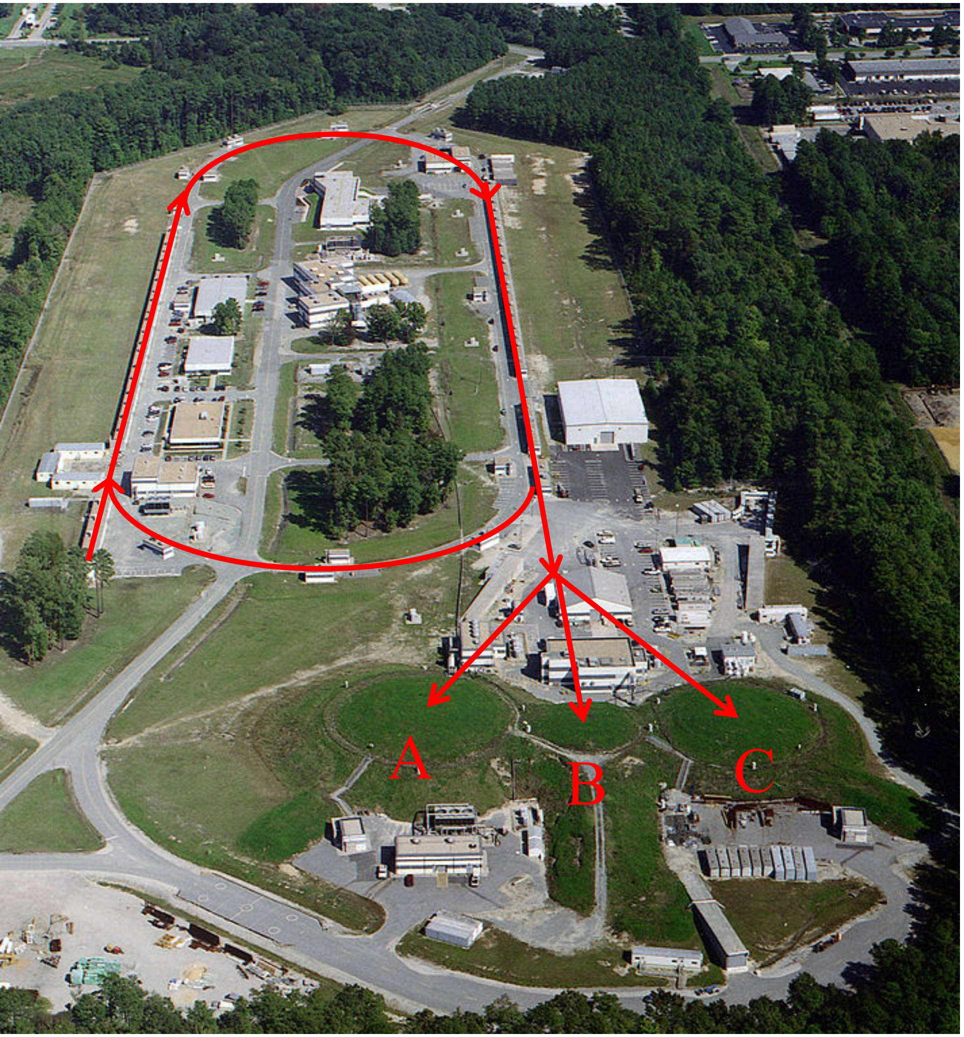

JLab Aerial View

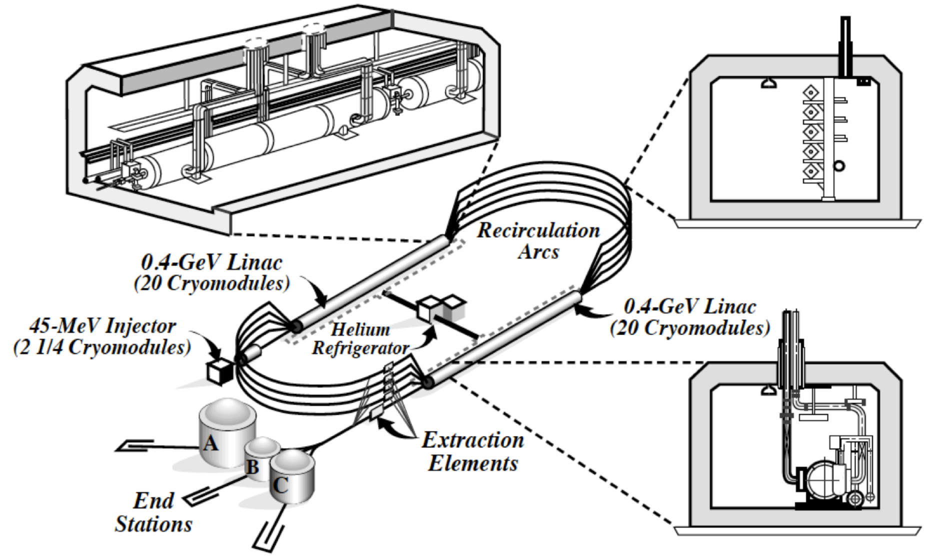

- Superconducting RF electron linacs with up to 5X recirculation
- CW ("100%" duty factor) operation (2 ns bunch period, ~0.3 ps bunch length)
- Polarized source: up to ~90% polarization
- Three experimental Halls
- Energy up to 6 GeV
- Current (up to 180 µA CW)

The 12 GeV Upgrade of CEBAF

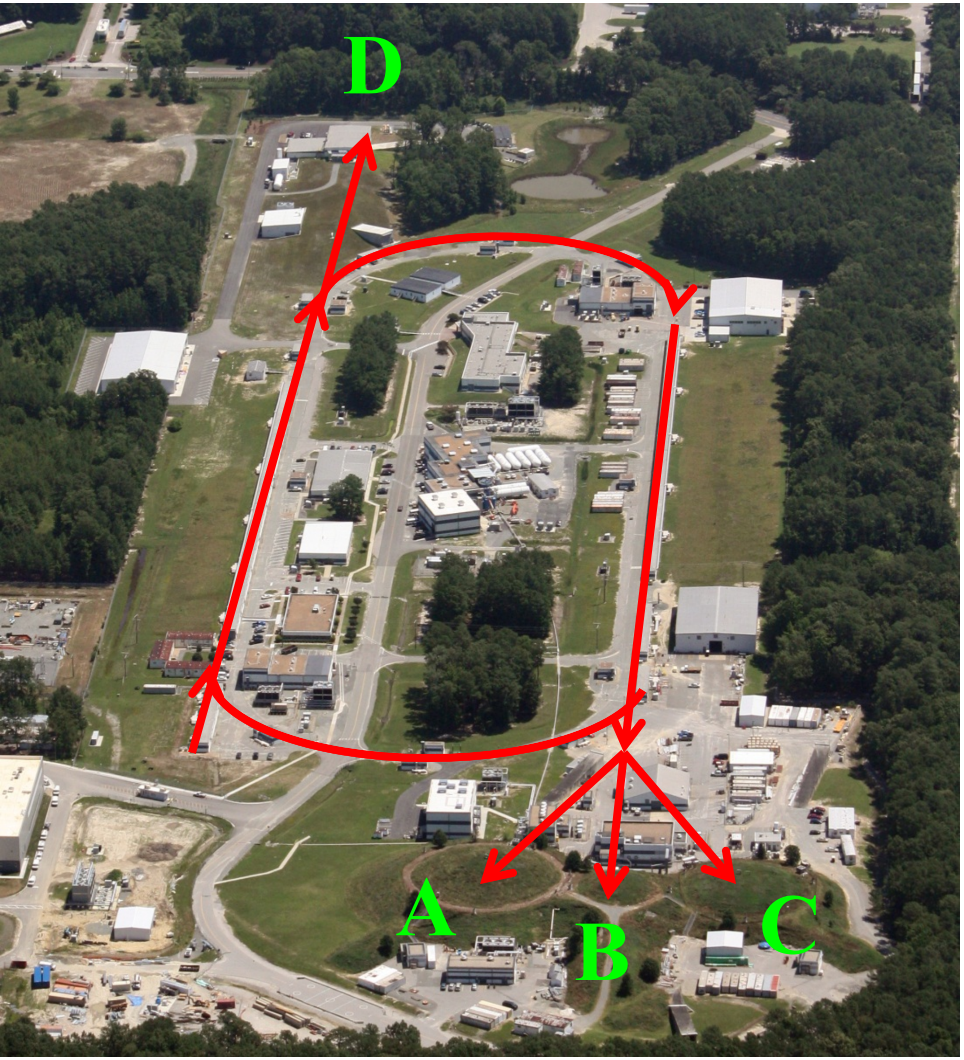

Site Aerial, June 2012

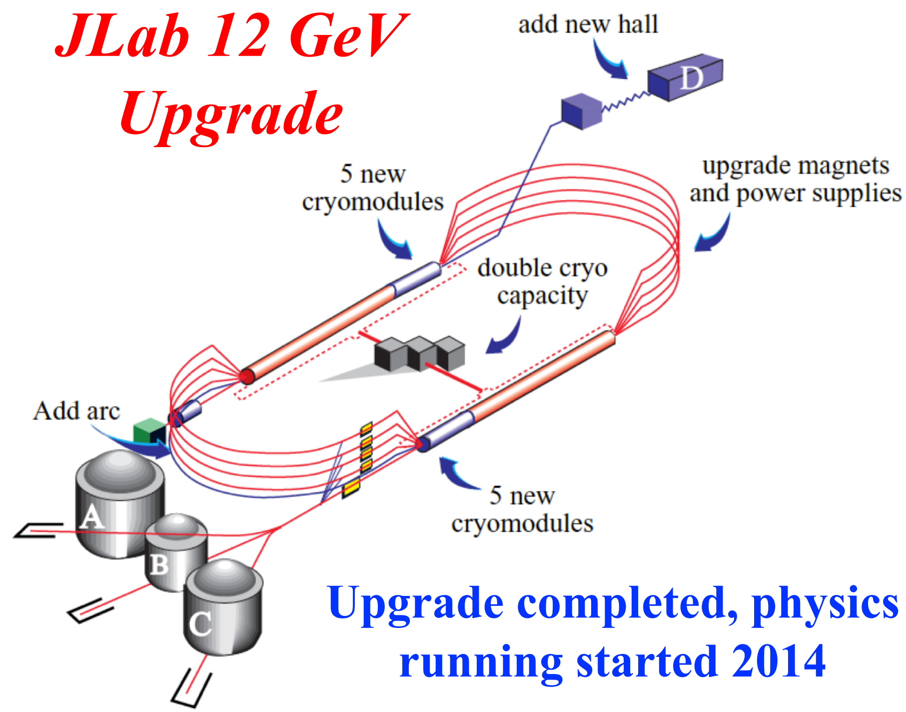

Upgrade completed, physics running started 2014

Seven-cell, High-Gradient Niobium SRF cavity for 12 GeV Upgrade

Proton FFs—Rosenbluth separation data

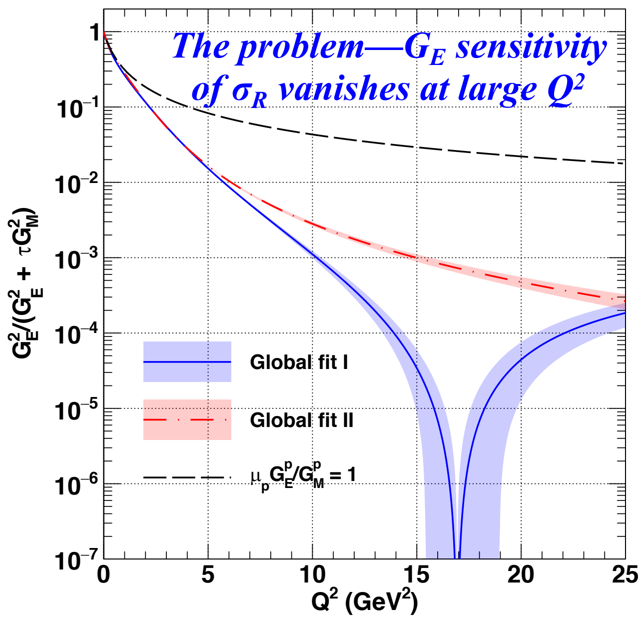

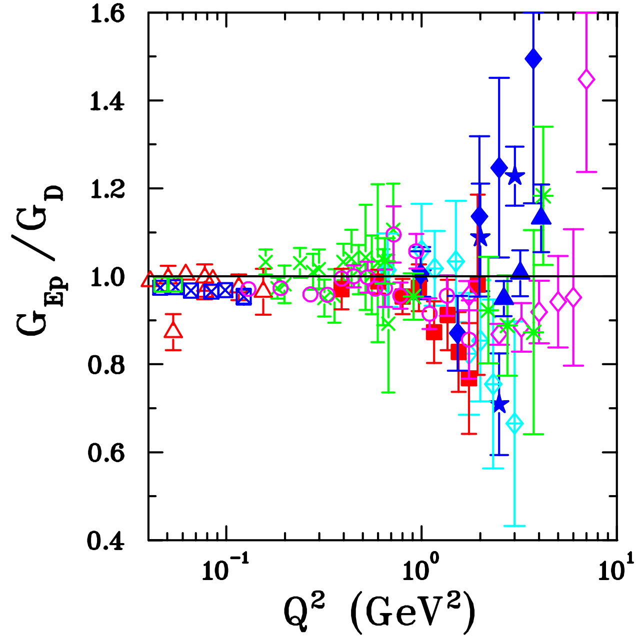

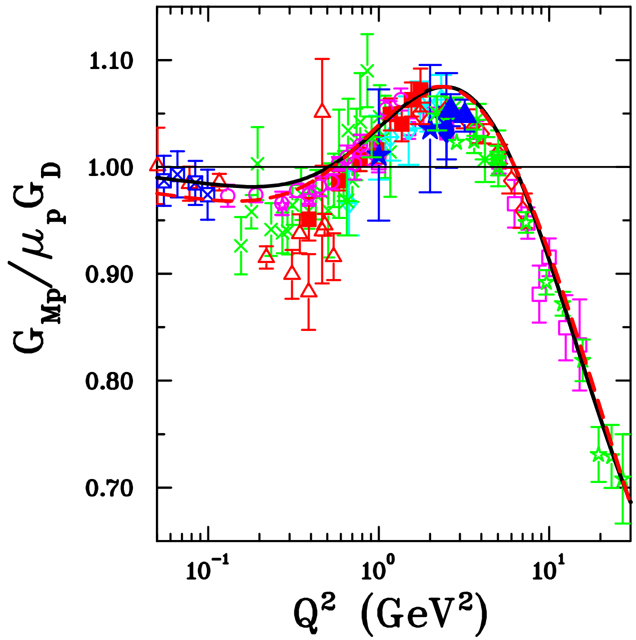

Maximum contribution of G_E^2 term to σ_R vanishes at large τ. Fits to FF data are described in [Phys. Rev. C, 96, 055203 (2017)] (more on these later)

$$\sigma_R = \epsilon G_E^2 + \tau G_M^2$$

G_E^p and G_M^p Rosenbluth Data: $G_E^p \approx \frac{G_M^p}{\mu_p} \approx G_D$

$$G_D \equiv \left(1 + \frac{Q^2}{\Lambda^2}\right)^{-2}$$
$$\Lambda^2 = 0.71 \text{ GeV}^2$$

- Elastic *ep* cross sections have been measured for $\sim 0.003 \le Q^2 \le 31.2$ GeV^2.
- Rosenbluth data for G_E^p and G_M^p are qualitatively described by the “dipole” form factor, which is the Fourier transform of a spherically symmetric, exponentially decreasing radial charge/magnetization density.

Polarization Transfer in Elastic *eN* scattering

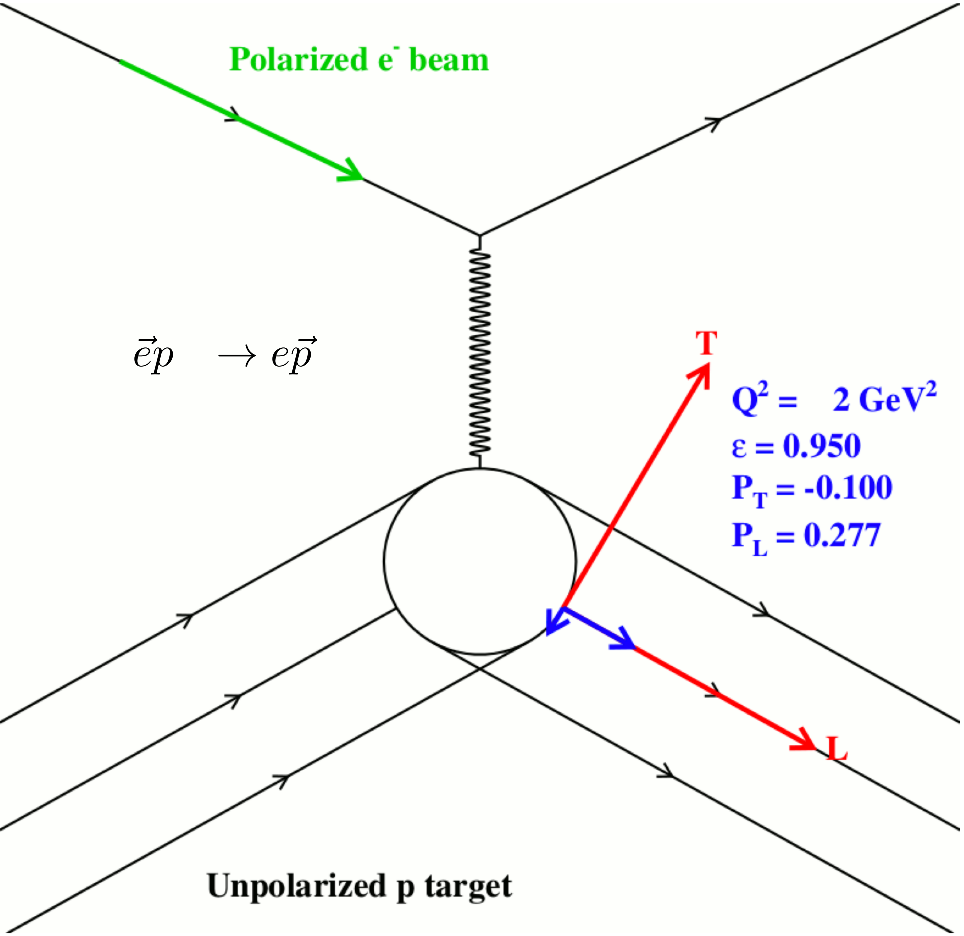

$$P_T = -P_{beam}\sqrt{\frac{2\epsilon(1-\epsilon)}{\tau}}\frac{r}{1+\frac{\epsilon r^2}{\tau}}$$

$$P_L = P_{beam}\frac{\sqrt{1-\epsilon^2}}{1+\frac{\epsilon r^2}{\tau}}$$

$$r \equiv \frac{G_E}{G_M}$$

$$\Longrightarrow R_p \equiv \mu_p \frac{G_E^p}{G_M^p} = -\mu_p\sqrt{\frac{\tau(1+\epsilon)}{2\epsilon}}\frac{P_T}{P_L}$$

$$\tau = \frac{Q^2}{4M_p^2}$$

$$\frac{1}{\epsilon} = 1 + 2(1+\tau)\tan^2\frac{\theta_e}{2}$$

- ***The ratio of transferred polarization components is directly proportional to G_E/G_M, and therefore much more sensitive to G_E at large Q^2 than the cross section***

Recoil Proton Polarimetry: General Principles

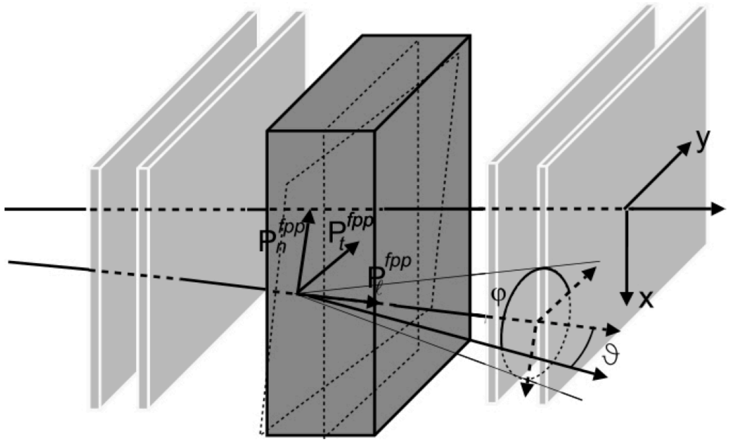

FIG. 9. Principle of the polarimeter, showing a noncentral trajectory through the front chambers, scattering in the analyzer, and a track through the back chambers; ϑ is the polar angle, and φ is the azimuthal angle from the y direction counterclockwise.

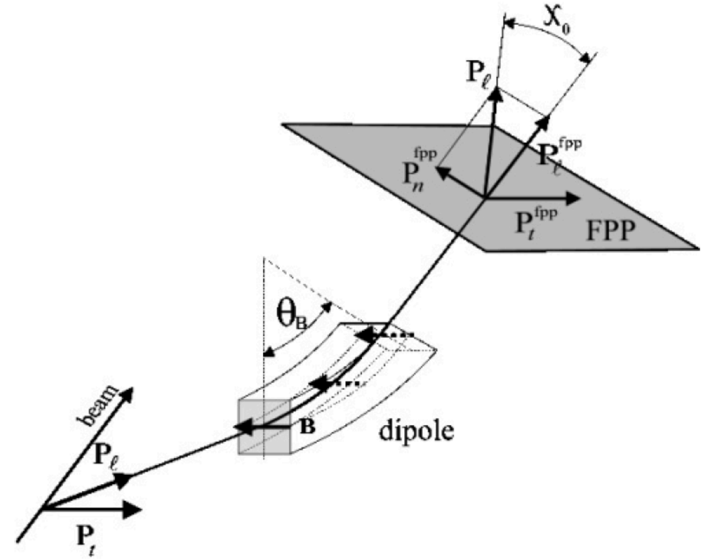

FIG. 15. Precession of the polarization component P_ℓ in the dipole of the HRS by an angle χ_θ.

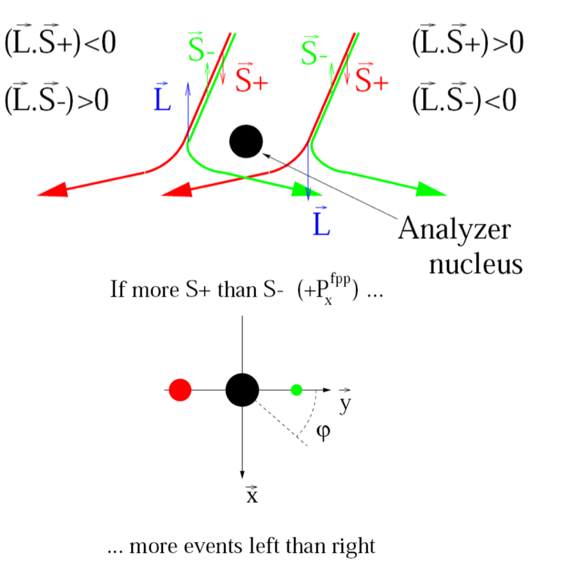

- Proton polarimetry via proton-nucleus scattering is based on the spin-orbit coupling in the nucleon-nucleon force.
- A spin-1/2 particle, such as a proton, is preferentially deflected by a spin-orbit force along the direction of $\vec{p}\times\vec{S}$, where $\vec{p}$ is the incident proton momentum, and $\vec{S}$ is the proton spin.
  - Note that a spin-orbit force is insensitive to longitudinal polarization!
  - Precession in spectrometer dipole field rotates P_L into a transverse component that can be measured
- By tracking the incident and scattered proton and measuring the azimuthal asymmetry in the angular distribution of secondary scatterings, the incident proton's (transverse) polarization can be reconstructed

GEp-I in Hall A: $0.5 \le Q^2 \le 3.5\ GeV^2$

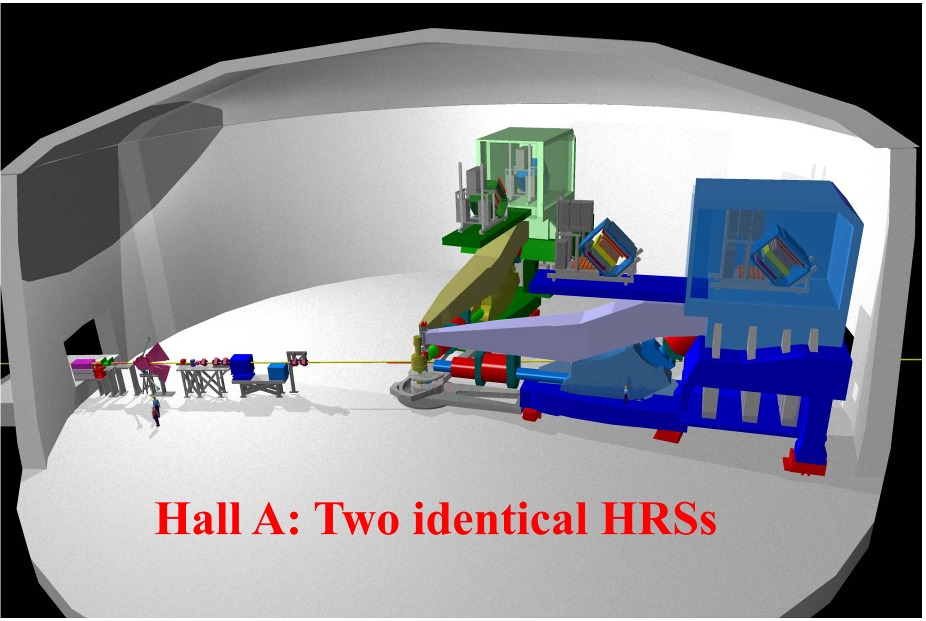

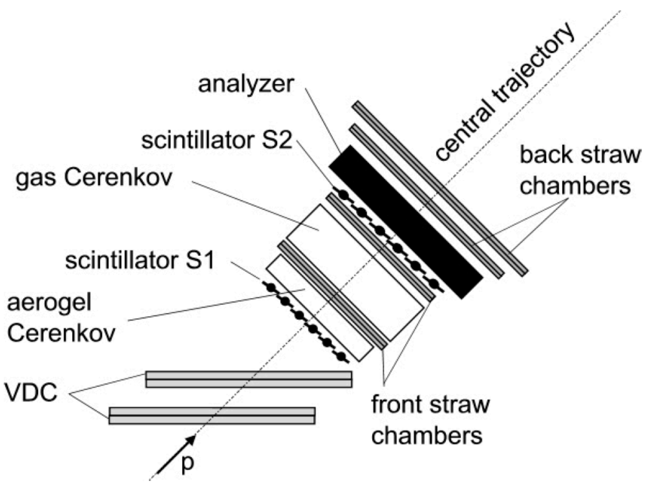

FIG. 2. Side view of the hadron arm detector package including the polarimeter.

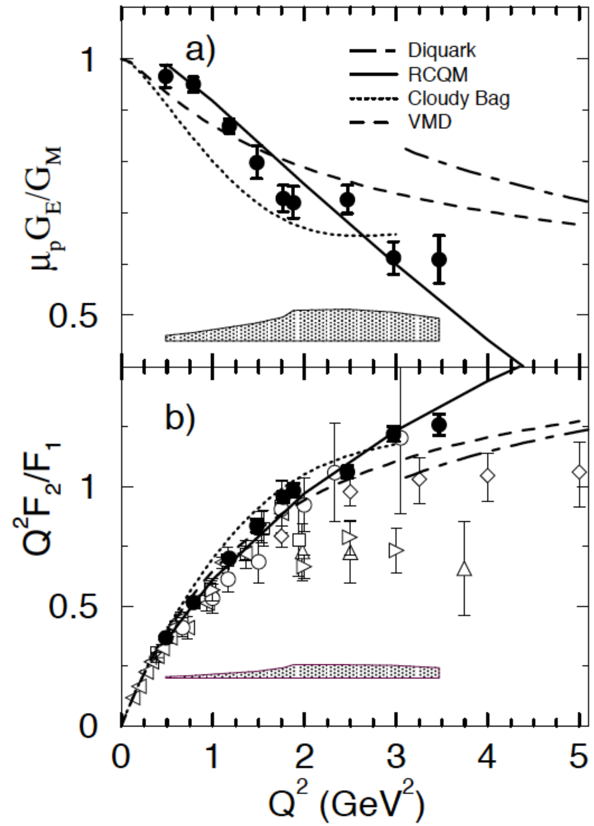

FIG. 2. (a) The ratio $\mu_p G_{Ep}/G_{Mp}$ from this experiment, compared with theoretical calculations. (b) The ratio Q^2F_{2p}/F_{1p} for the same data, compared to the same theoretical models as in (a) and world data; symbols as in Fig. 1. In both (a) and (b) the absolute value of systematic error from this experiment is shown by the shaded area.

Jones *et al.*, Phys. Rev. Lett. 84, 1398 (2000)

GEp-II in Hall A: $3.5 \le Q^2 \le 5.6\ GeV^2$

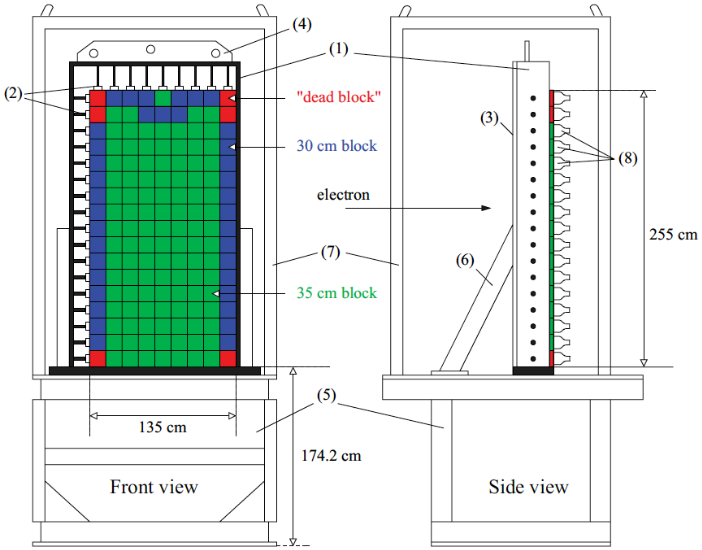

FIG. 4. (Color) Design of the calorimeter used to detect the scattered electron. In the front view, the 2.54-cm-thick aluminum plate in front of the blocks is not shown. See text for details.

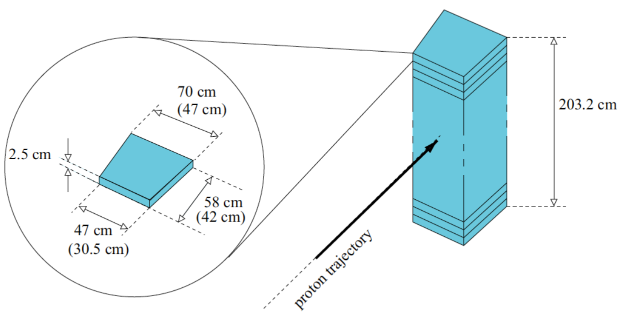

FIG. 3. (Color online) Stack of polyethylene plates for the analyzer. The dimensions shown on the plate are for the 58-cm (42-cm) stack and were chosen to match the envelope of elastically scattered protons in HRSL.

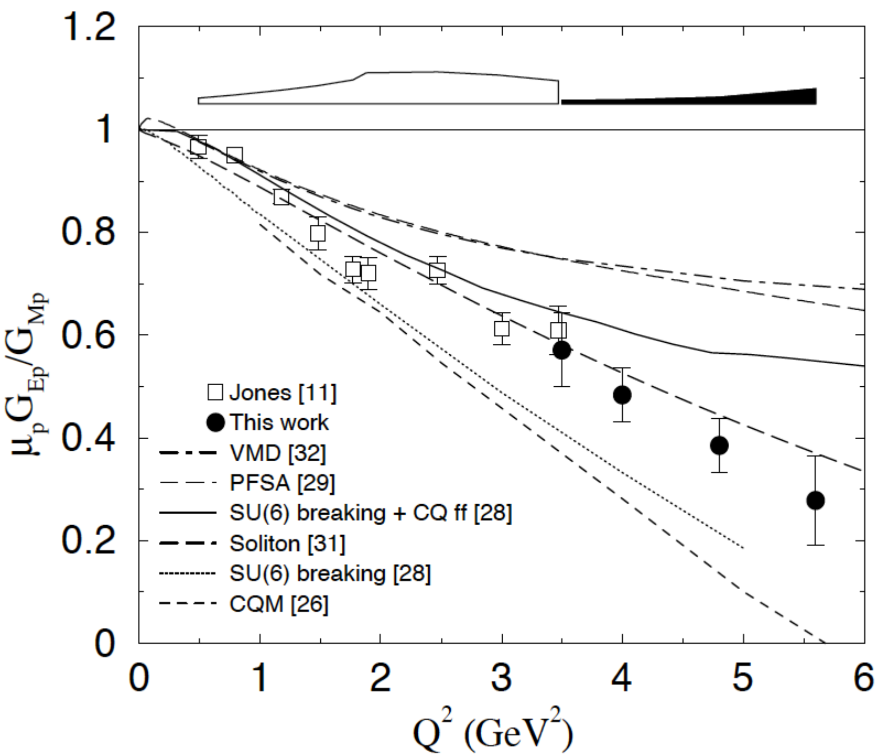

Gayou *et al.*, Phys.Rev.Lett. 88 (2002) 092301

- Relative to GEp-I: increase analyzer thickness, change material from carbon to CH_2 (polyethylene)
- Use large solid-angle lead-glass calorimeter instead of HRS to detect the scattered electron in coincidence

GEp-III and GEp-2γ in Hall C: $2.5 \le Q^2 \le 8.5\ GeV^2$

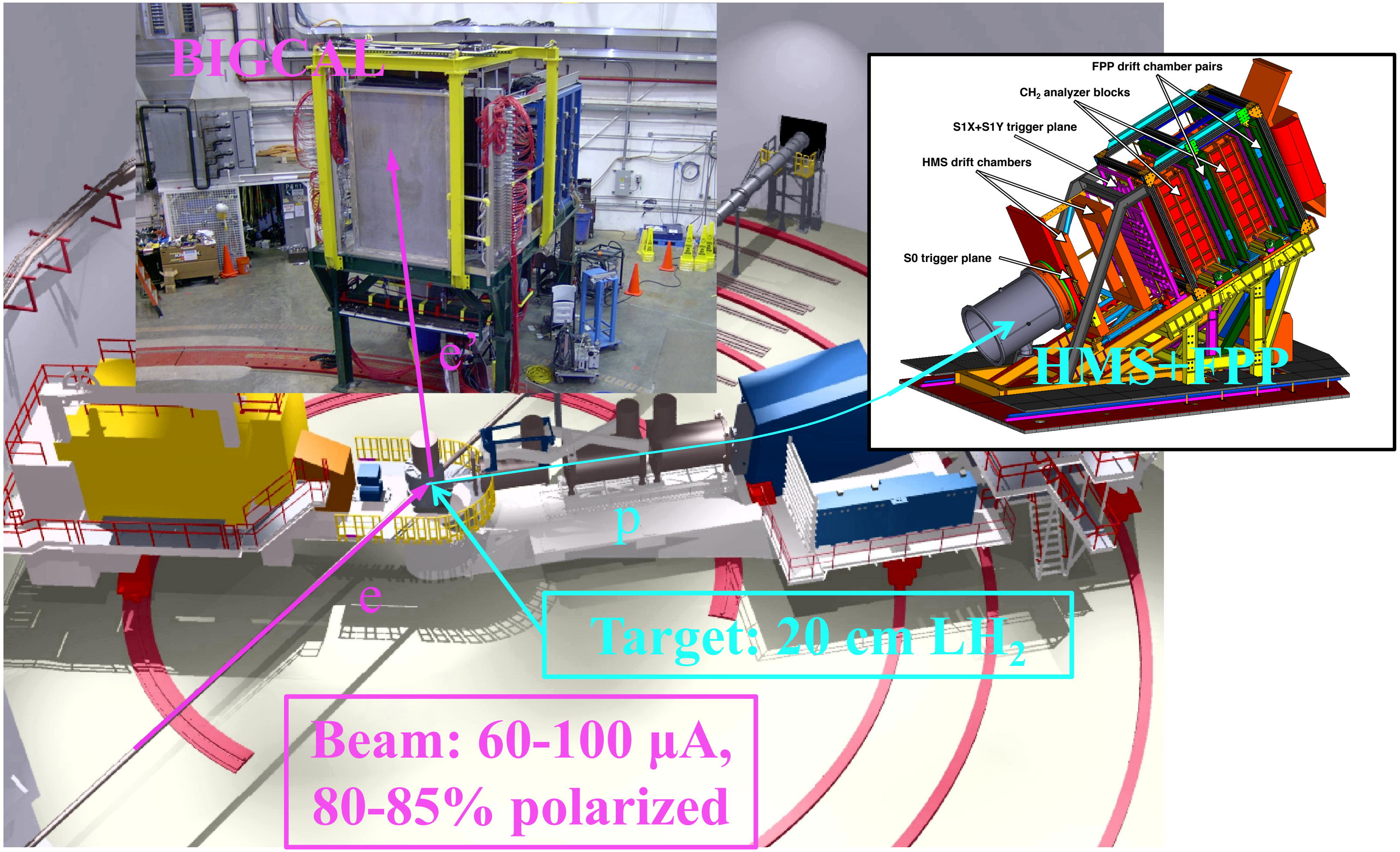

- Polarization transfer in ^{1}H(**e**,e'**p**). Nominal luminosity ~ 4×10^{38} Hz/cm^2
- Changes from Hall A measurements: new double-FPP layout, more finely segmented electron calorimeter, Hall C HMS to detect protons up to p $= 5.41\ GeV$

Hall C GEp results

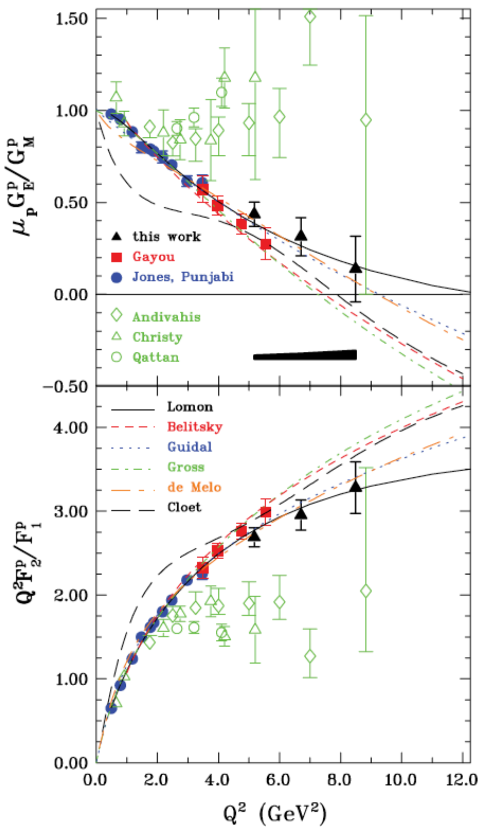

FIG. 3 (color). Upper panel: The proton form factor ratio $\mu_p G_E^p/G_M^p$ from this experiment (filled black triangles), with statistical error bars and systematic error band below the data. Previous experiments are [1] (Jones, Punjabi, Gayou), [3] (Andivahis), [4] (Christy), and [5] (Qattan). Theory curves are [20] (Lomon), [21] (de Melo), [22] (Gross), [23] (Cloët), [24] (Guidal), and [25] (Belitsky). Lower panel: The same data and theory curves as the upper panel, expressed as $Q^2F_2^p/F_1^p$.

Puckett *et al.*, **Phys.Rev.Lett. 104 (2010) 242301**

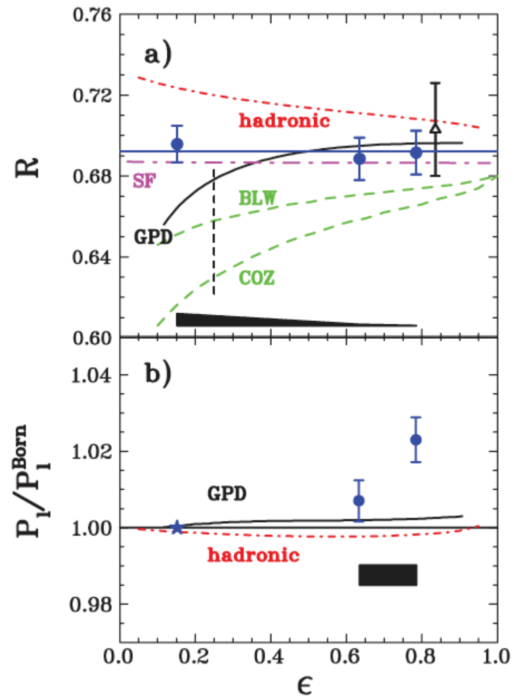

FIG. 2 (color). (a) R as a function of ϵ with statistical uncertainties, filled circles from this experiment and open triangle from [7]. The theoretical predictions are from [14] (hadronic), [13] (GPD), [19] (COZ and BLW), and [17] (SF) offset for clarity by -0.006 with respect to the fit. The one-parameter fit result is $R = 0.6923 \pm 0.0058$. (b) $P_\ell/P_\ell^{\mathrm{Born}}$ as a function of ϵ. The point-to-point systematic uncertainties, shown with a band in both panels, are relative to the largest ϵ kinematic in (a) and relative to the smallest ϵ kinematic in (b). The star indicates the ϵ value at which the analyzing power is determined.

Meziane *et al.*, **Phys.Rev.Lett. 106 (2011) 132501**

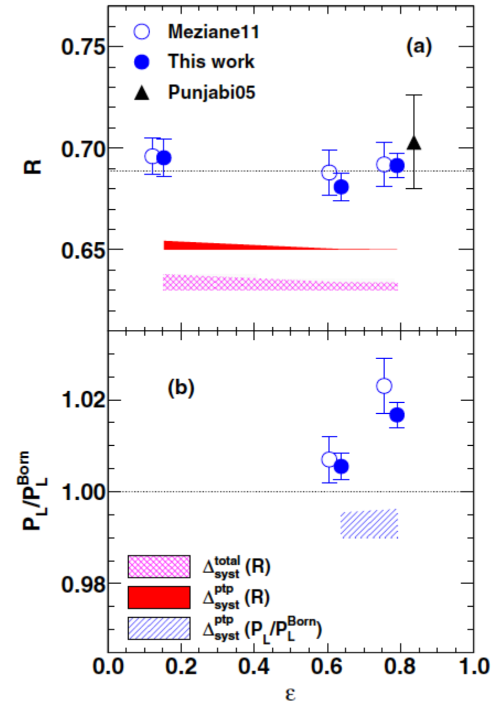

FIG. 19. Final, acceptance-averaged results of the GEp-2γ experiment, without bin-centering corrections, as a function of ϵ, for the ratio $R \equiv -\mu_p \frac{P_t}{P_\ell}\sqrt{\frac{\tau(1+\epsilon)}{2\epsilon}}$ (a), and the ratio $P_\ell/P_\ell^{\mathrm{Born}}$ (b), compared to the originally published results [47] (Meziane11), and the GEp-I result [29] (Punjabi05) at $Q^2 = 2.47$ GeV^2. Error bars on the data points are statistical only. For R, the (one-sided) total and point-to-point (relative to $\epsilon = 0.79$) systematic uncertainty bands are shown, while only the point-to-point (relative to $\langle\epsilon\rangle = 0.153$) systematic errors are shown for $P_\ell/P_\ell^{\mathrm{Born}}$ (also one-sided). The originally published points from Ref. [47] have been offset by -0.03 in ϵ for clarity. Note that $P_\ell/P_\ell^{\mathrm{Born}} \equiv 1$ at $\langle\epsilon\rangle = 0.153$.

Puckett *et al.*, **Phys.Rev. C96 (2017) no.5, 055203**

GEp/GMp polarization transfer data are among the most-cited JLab results: Why?

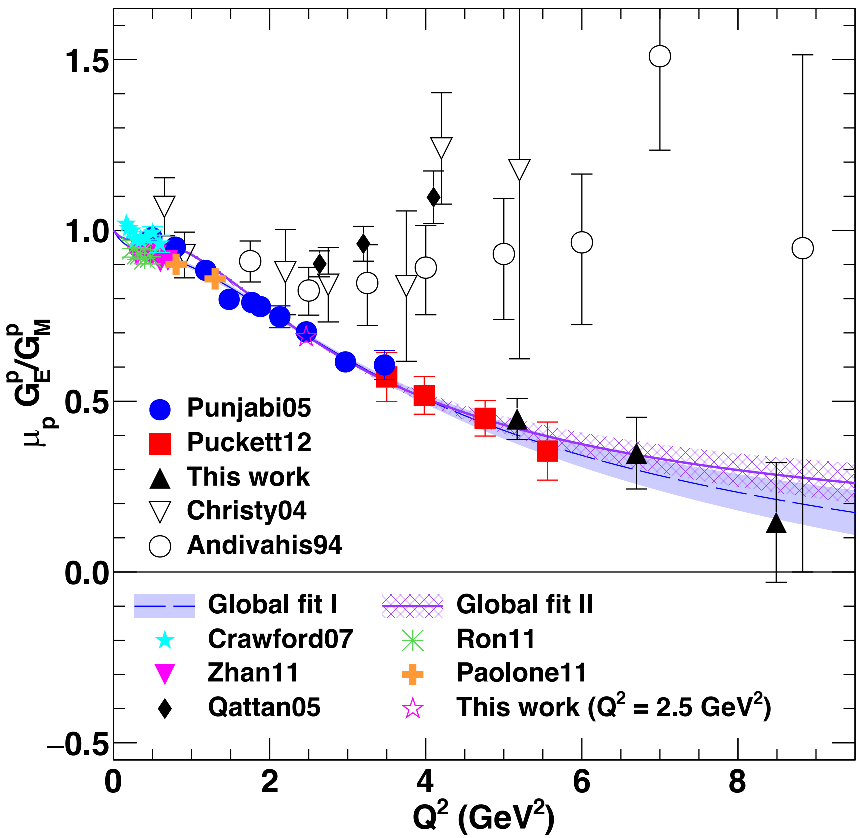

- *Extraction of the same physical property of the proton from different experimental observables yields different results!*
- Guichon and Vanderhaeghen, **PRL** 91, 142303 (2003): *"This discrepancy is a serious problem as it generates confusion and doubt about the whole methodology of lepton scattering experiments."*
- Discrepancy still not yet fully understood

- GEp-I:
  - Jones *et al.,* **Phys. Rev. Lett. 84 (2000) 1398-1402: 855 INSPIRE-HEP citations**
  - Punjabi *et al.*, **Phys.Rev. C71 (2005) 055202: 418 INSPIRE-HEP citations**
- GEp-II:
  - Gayou *et al.*, **Phys.Rev.Lett. 88 (2002) 092301: 779 INSPIRE-HEP citations**
  - Puckett *et al.*, **Phys.Rev. C85 (2012) 045203: 130 INSPIRE-HEP citations**
- GEp-III/GEp-2γ:
  - Puckett *et al.*, **Phys.Rev.Lett. 104 (2010) 242301,** 244 INSPIRE-HEP citations
  - Meziane *et al.,* **Phys.Rev.Lett. 106 (2011) 132501,** 74 INSPIRE-HEP citations
  - Puckett *et al.*, **Phys.Rev. C96 (2017) no.5, 055203,** 13 INSPIRE-HEP citations
- Low-Q^2 data from JLab:
  - Ron *et al.*, **Phys.Rev.Lett. 99 (2007) 202002**, 69 INSPIRE-HEP citations
  - Ron *et al.*, **Phys.Rev. C84 (2011) 055204,** 91 INSPIRE-HEP citations
  - Zhan *et al.*, **Phys.Lett. B705 (2011) 59-64,** 163 INSPIRE-HEP citations
  - Paolone *et al.*, **Phys.Rev.Lett. 105 (2010) 072001**, 84 INSPIRE-HEP citations

2017 Tom W. Bonner Prize in Nuclear Physics Recipient

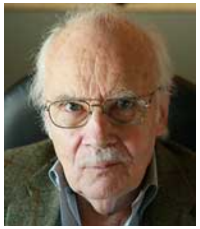

Charles F. Perdrisat
College of William and Mary

Citation:

"*For groundbreaking measurements of nucleon structure, and discovering the unexpected behavior of the magnetic and electric nucleon form factors with changing momentum transfer.*"

Background:

Charles F. Perdrisat, Ph.D., was a professor at the College of William and Mary (Williamsburg, Va.) for the last 50 years having retired earlier this year. Throughout his career, Dr. Perdrisat's research focus included nuclear reactions with proton and deuteron beams, both polarized and unpolarized. He conducted research at SATURNE in Saclay, France, TRIUMF in Vancouver, B.C., LAMPF in Los Alamos, New Mexico, Brookhaven National Laboratory in Upton, N.Y., and JINR in Dubna, Russia. During the last half of his career, he was committed to the investigation of the structure of the proton at Jefferson Laboratory, concentrating in obtaining polarization transfer data in the scattering of polarized electrons on unpolarized protons. These data, from 3 distinct experiments organized in close collaboration with Vina Punjabi, Ph.D., Mark K. Jones, Ph.D., Edward J. Brash, Ph.D., and Lubomir Pentchev, Ph.D., have resulted in a significant change of paradigm in the understanding of the structure of the nucleon. After completing his undergraduate training in physics and mathematics at the University of Geneva in 1956, Dr. Perdrisat became an assistant in the physics department at the Swiss Federal Institute of Technology in Zurich) in Switzerland, under Prof. Paul Scherrer; he received his Ph.D. in 1962. He completed a three-year postdoctoral fellowship at the University of Illinois Urbana-Champaign, before heading to William and Mary in 1966.

Selection Committee:

2017 Selection Committee Members: Rocco Schiavilla (Chair), D. Hertzog, P. Jacobs, Kate Jones, I-Y. Lee

Nucleon "imaging" (traditional): Rest-frame charge and magnetization densities in 3D space

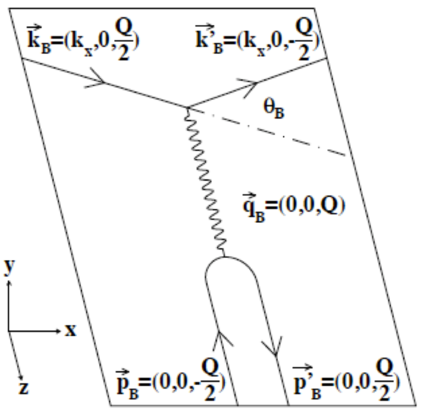

Figure 1-2: Elastic scattering in the Breit frame

$$\lambda_E = \lambda_M = 2$$

$$\tilde{\rho}_{ch}(k) = G_E(Q^2)(1+\tau)^{\lambda_E},$$

$$\mu\tilde{\rho}_m(k) = G_M(Q^2)(1+\tau)^{\lambda_M},$$

$$\rho(r) = \frac{2}{\pi}\int_0^\infty dk\, k^2 j_0(kr)\tilde{\rho}(k).$$

$$k^2 = \frac{Q^2}{1+\tau}$$

$$\tau = \frac{Q^2}{4M^2}$$

$$\rho_{ch}^{NR}(r) = \frac{2}{\pi}\int_0^\infty dQ\, Q^2 j_0(Qr) G_E(Q^2),$$

$$\mu\rho_m^{NR}(r) = \frac{2}{\pi}\int_0^\infty dQ\, Q^2 j_0(Qr) G_M(Q^2),$$

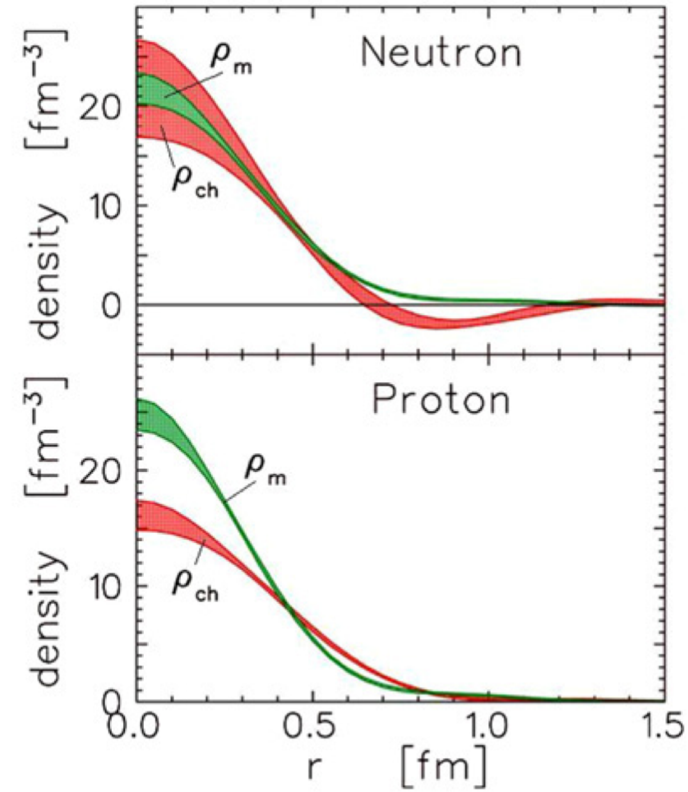

J. J. Kelly: PRC 66, 065203 (2002)

FFs and "imaging": transverse densities, I

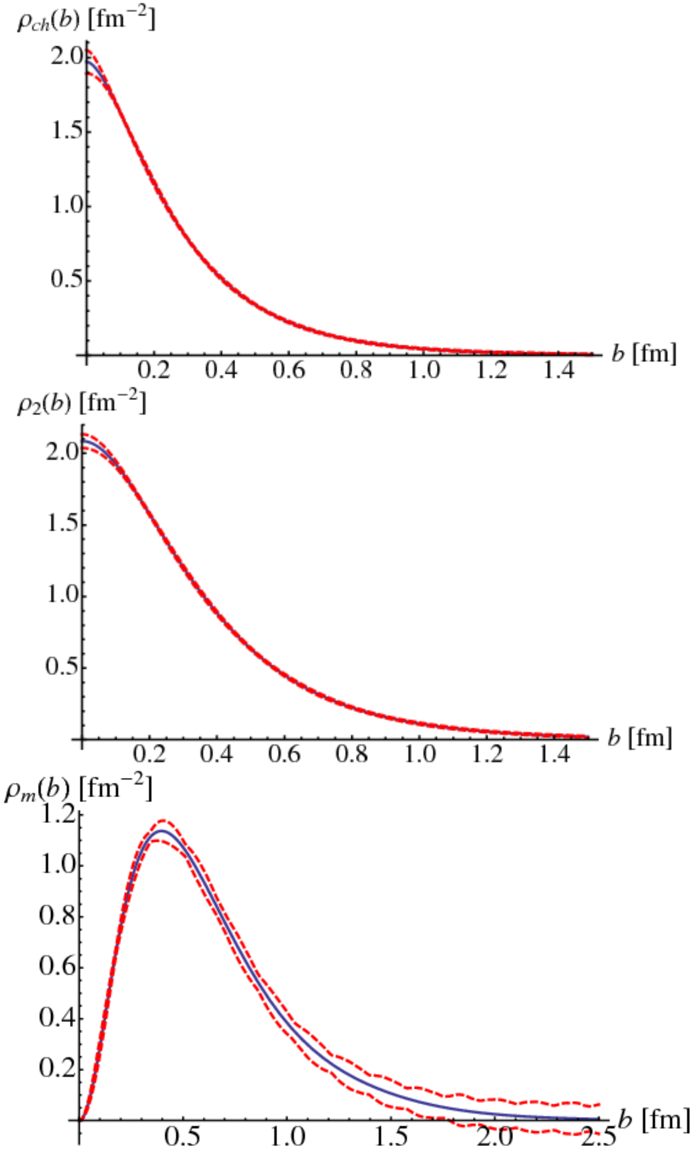

- Miller et al, **Phys. Rev. C, 83, 015203 (2011)**: ***model-independent,*** impact parameter-space charge and magnetization densities in the infinite momentum frame.
- Proton results shown for
  - Charge
  - 2D Fourier transform of F_2 (Pauli FF)
  - Anomalous magnetization density

$$\rho_{ch}(b) = \frac{1}{2\pi}\int QdQ\,J_0(Qb)F_1(Q^2)$$

$$\rho_2(b) = \frac{1}{2\pi}\int QdQ\,J_0(Qb)F_2(Q^2)$$

$$\rho_m(b) = -b\frac{d}{db}\rho_2(b)$$

$$= \frac{b}{2\pi}\int Q^2dQ\,J_1(Qb)F_2(Q^2)$$

FFs and “imaging”: transverse densities, II

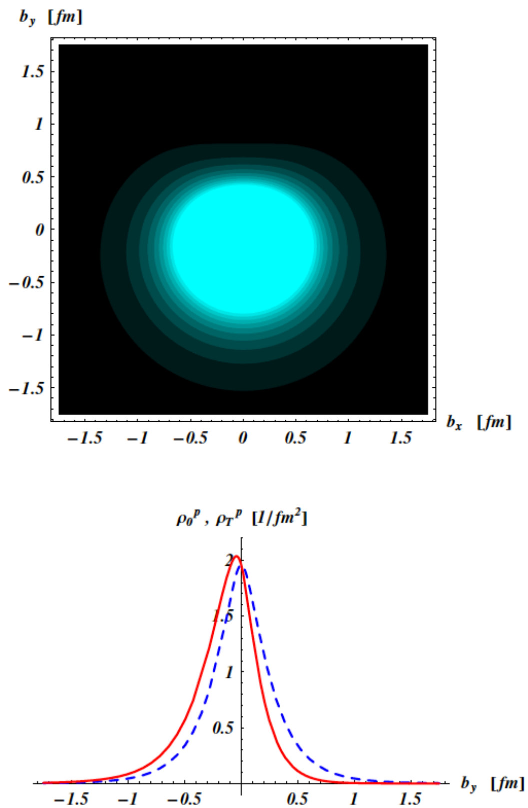

FIG. 1: Quark transverse charge densities in the *proton*. The upper panel shows the density in the transverse plane for a proton polarized along the x-axis. The light (dark) regions correspond with largest (smallest) values of the density. The lower panel compares the density along the y-axis for an unpolarized proton (dashed curve), and for a proton polarized along the x-axis (solid curve). For the proton e.m. FFs, we use the empirical parameterization of Arrington *et al.* [14].

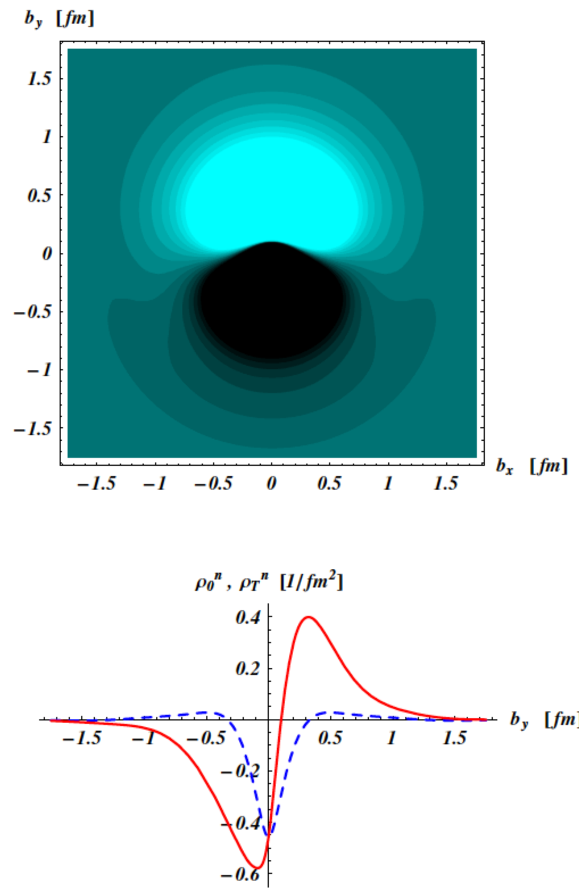

FIG. 2: Same as Fig. 1 for the quark transverse charge densities in the *neutron*. For the neutron e.m. FFs, we use the empirical parameterization of Bradford *et al.* [15].

Proton (left) and neutron (right) 2D polarized transverse charge densities from Carlson and Vanderhaeghen: Phys. Rev. Lett. 100, 032004 (2008)

Polarized Beam-Polarized Target Asymmetry

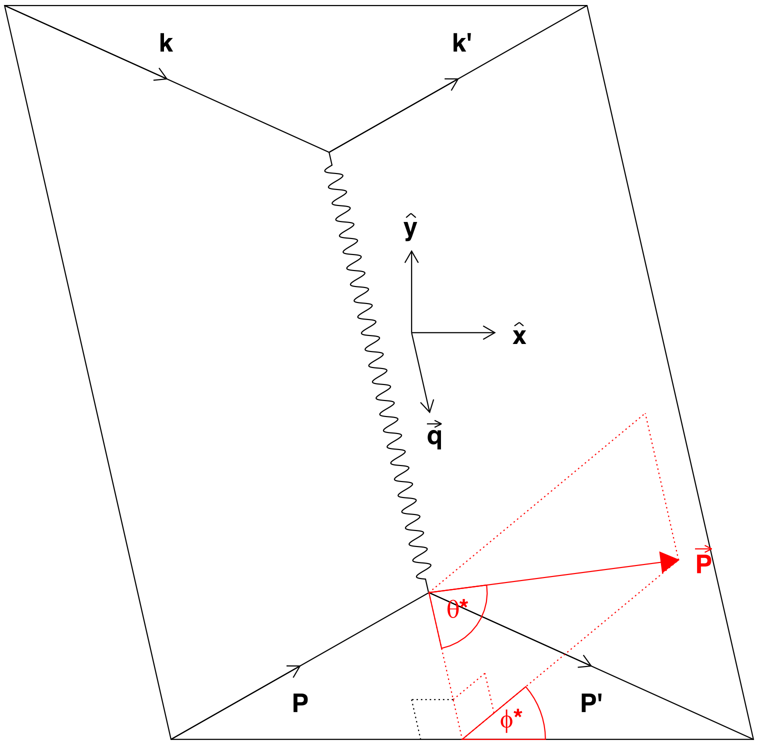

- The beam helicity asymmetry in elastic *eN* scattering from a polarized target is related to the transferred polarization by time reversal symmetry.
- The asymmetry A_t for target polarization perpendicular to the momentum transfer but parallel to the scattering plane ($\theta^* = 90°, \phi^* = 0$) equals the transverse component P_t of the transferred polarization.
- The asymmetry A_ℓ for target polarization along the momentum transfer direction ($\theta^* = 0$) is equal in magnitude but opposite in sign to the longitudinal transferred polarization P_ℓ.
- The sign change between A_ℓ and P_ℓ is due to the proton spin flip required for the absorption of the transversely polarized virtual photon

$$\vec{\mathbf{P}} \equiv \text{Target polarization}$$

$$\begin{aligned}
A_{eN} &= -\frac{P_{beam}P_{target}}{1+\frac{\epsilon}{\tau}r^2}\left[\left(\sqrt{\frac{2\epsilon(1-\epsilon)}{\tau}}\sin\theta^*\cos\phi^*\right)r + \sqrt{1-\epsilon^2}\cos\theta^*\right] \\
&\equiv P_{target}\left[A_t\sin\theta^*\cos\phi^* + A_\ell\cos\theta^*\right] \\
A_t &= P_t \\
A_\ell &= -P_\ell \\
A_n &= P_n = 0
\end{aligned}$$

Neutron electric form factor G_{En}

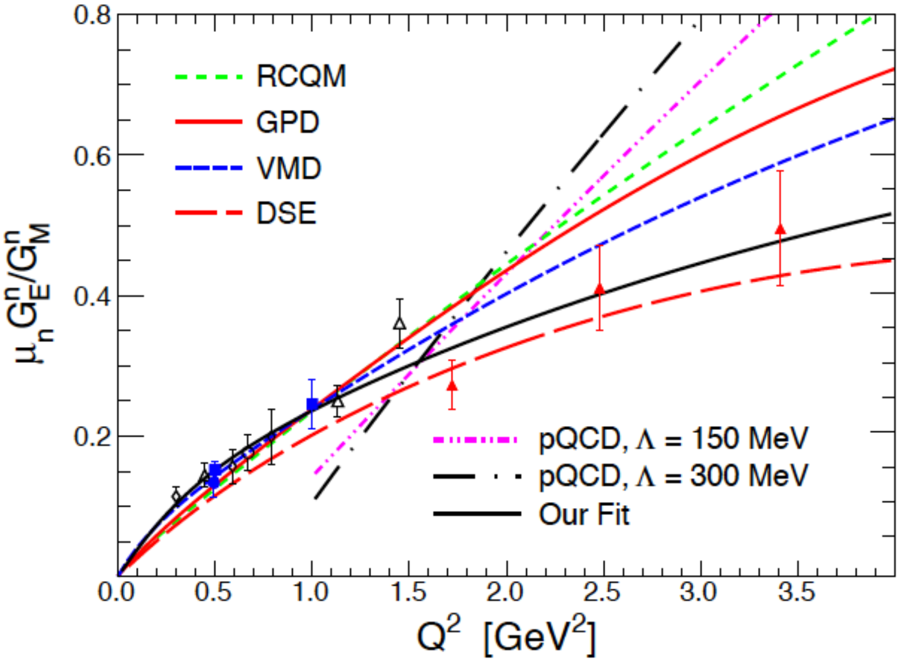

Riordan *et al.*, Phys. Rev. Lett. 105, 262302 (2010)

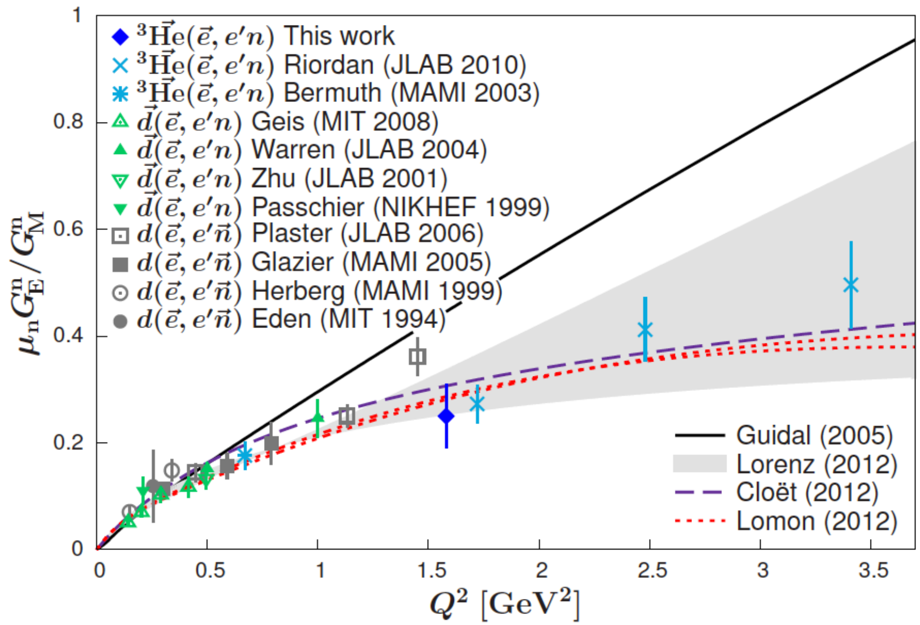

Schlimme *et al.*, Phys.Rev.Lett. 111 (2013), 132504

- G_{En} is the least well-known and most difficult to measure of the nucleon EMFFs:
  - Goes to zero at low Q^2 and cross-section contribution is small at large Q^2
- Existing knowledge (considered reliable) is based on polarization observables:
  - Beam-target double-spin asymmetry in semi-exclusive quasi-elastic ^{3}**He**(**e**,e'n)pp
  - Beam-target double-spin asymmetry in semi-exclusive quasi-elastic ^{2}**H**(**e**,e'n)p
  - Neutron recoil polarimetery: d(**e**,e'**n**)p

Experiment E02-013 (G_E^n-I) in Hall A

Screenshot is from GEANT4-based Monte Carlo Simulation

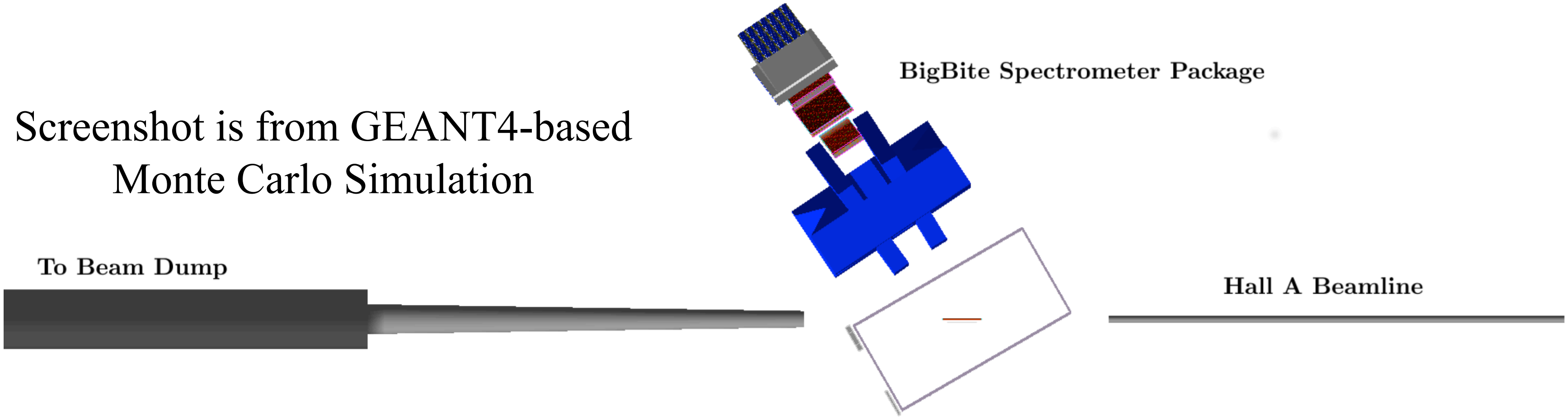

Neutron Detector

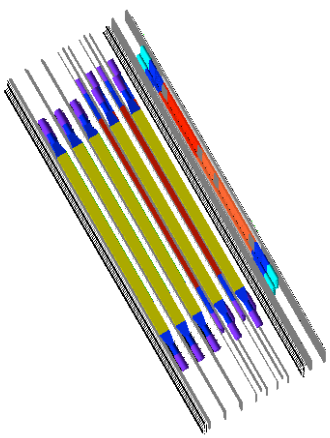

Q^2 [GeV^2]	Days	E_b [GeV]	θ_{BB} [deg]	θ_{NA} [deg]
1.16	8	1.519	-56.3	35.74
1.72	9	2.079	-51.6	35.74
2.48	19	2.640	-51.6	30.25
3.41	33	3.291	-51.6	25.63

E02-013 Kinematics: lowest Q^2 not included in PRL 2010 publication

Polarized ^{3}He Target

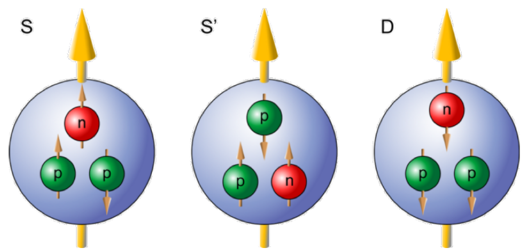

- Polarized ^{3}He as effective polarized neutron target:
- Ground state wavefunction dominated by S-state, with unpaired neutron carrying the nuclear spin

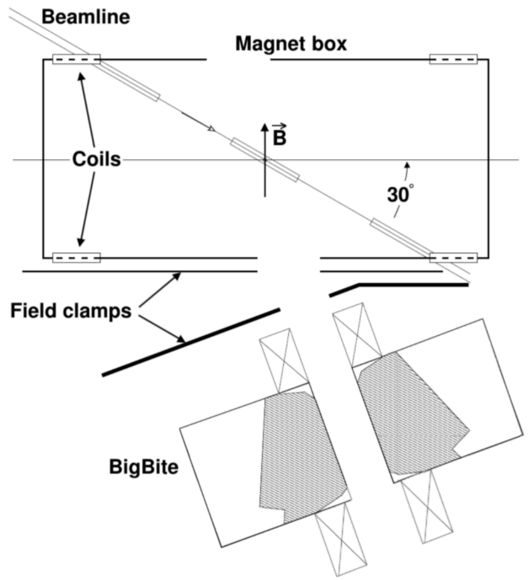

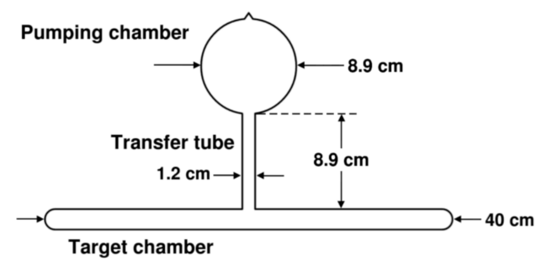

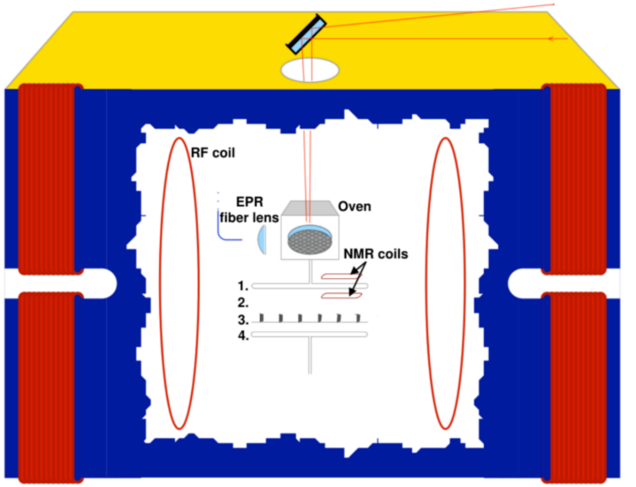

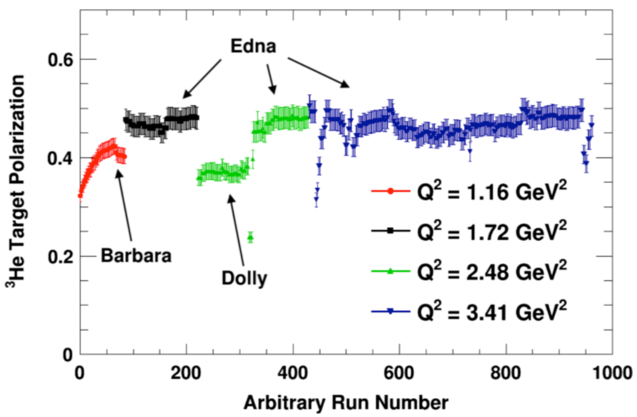

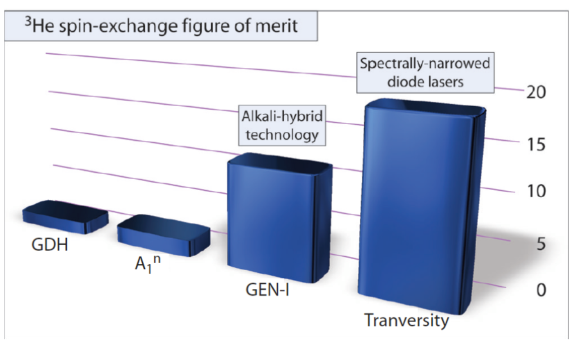

- GEN-I (2006) was the first electron-polarized ^{3}He scattering experiment to utilize the alkali-hybrid spin-exchange optical pumping technique to increase figure-of-merit.

GEN-I results

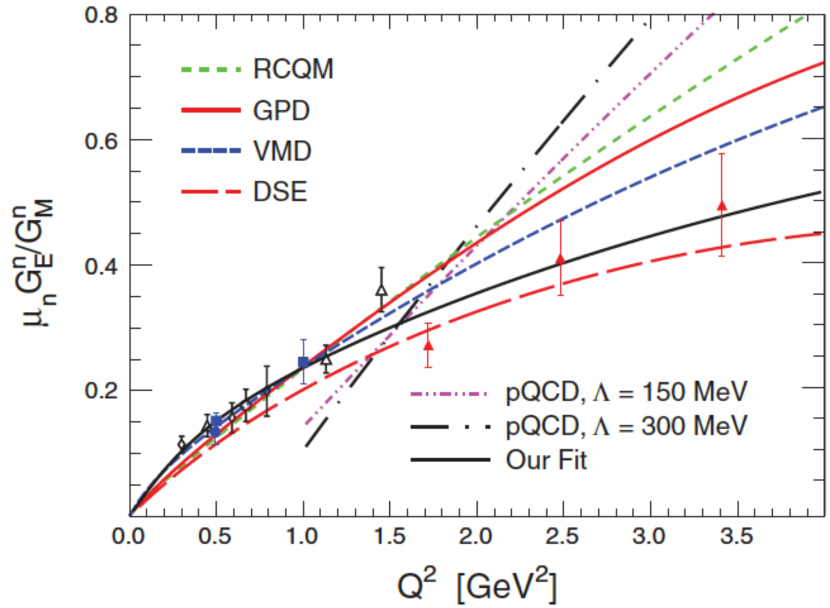

FIG. 1 (color). The ratio of $\mu_n G_E^n/G_M^n$ vs the momentum transfer with results of this experiment (solid triangles) and selected published data: diamonds [5], open triangles [6], circles [7], squares [8], open circles [12], and calculations: pQCD [28], RCQM [29], DSE [30], GPD [31], and VMD [32]. The curves labeled pQCD present pQCD-based scaling prediction [28] normalized to 0.3 at $Q^2 = 1.5$ GeV^2. The error bars for our data points show the statistical and the systematic uncertainties added in quadrature. Our fit is also shown; see parameterization in the text.

Riordan *et al.*, Phys. Rev. Lett. 105, 262302 (2010)

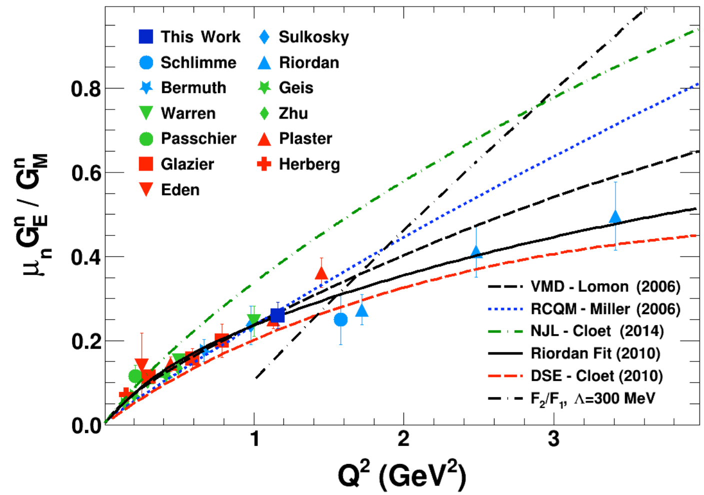

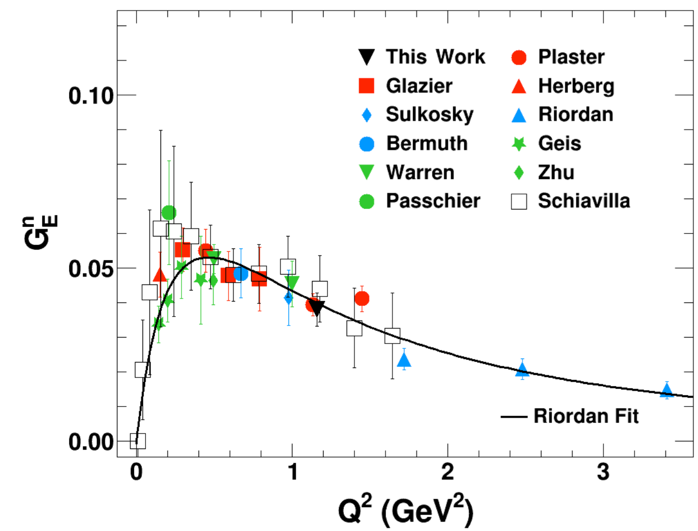

Obrecht *et al.*, Phys. Rev. C, in preparation (unpublished lowest-Q^2 analysis completed, high-Q^2 points reanalyzed)

Pushing Nucleon FFs to the highest possible Q^2 with 11 GeV CEBAF

New precision elastic ep cross sections in Hall A

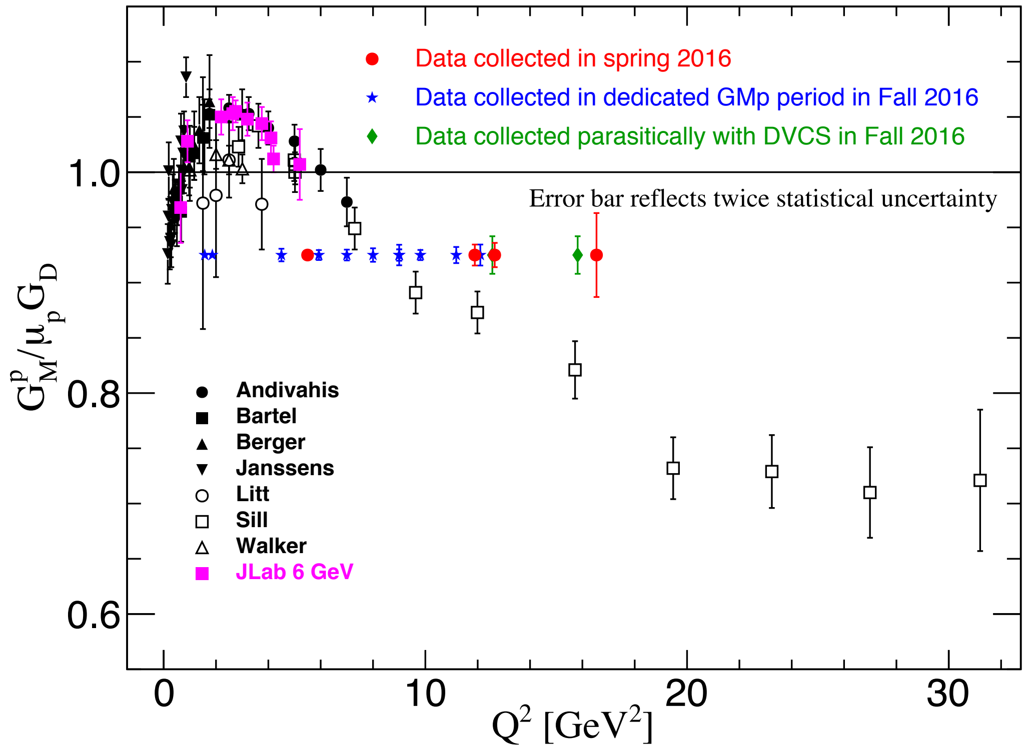

Projected uncertainties from recently completed Hall A high-Q^2 G_{Mp} run: 2018 publication anticipated

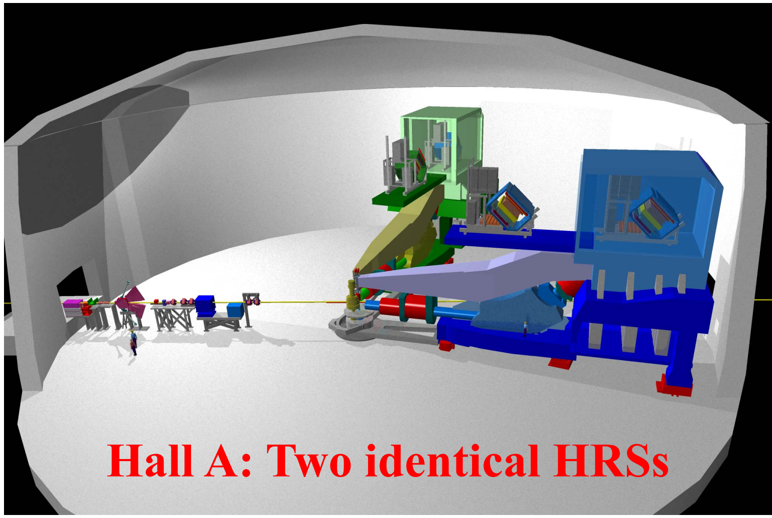

- Elastic ep → ep cross section at large Q^2 is dominated by G_{Mp}.
- Existing data for $Q^2 \geq 10$ GeV^2 come from two SLAC experiments (Kirk *et al.*, Phys. Rev. D **8**, 63 (1973) and Sill *et al.*,Phys. Rev. D, 48(1), 29 (1993)) with large uncertainties
- The absolute elastic *ep* cross section data serve as the "anchor" for the determination of all four nucleon EMFFs

GMp - E012-07-108 results

- Cross-section results presented below with ~1.25-1.6 %(pt-pt), 1.5%(norm)

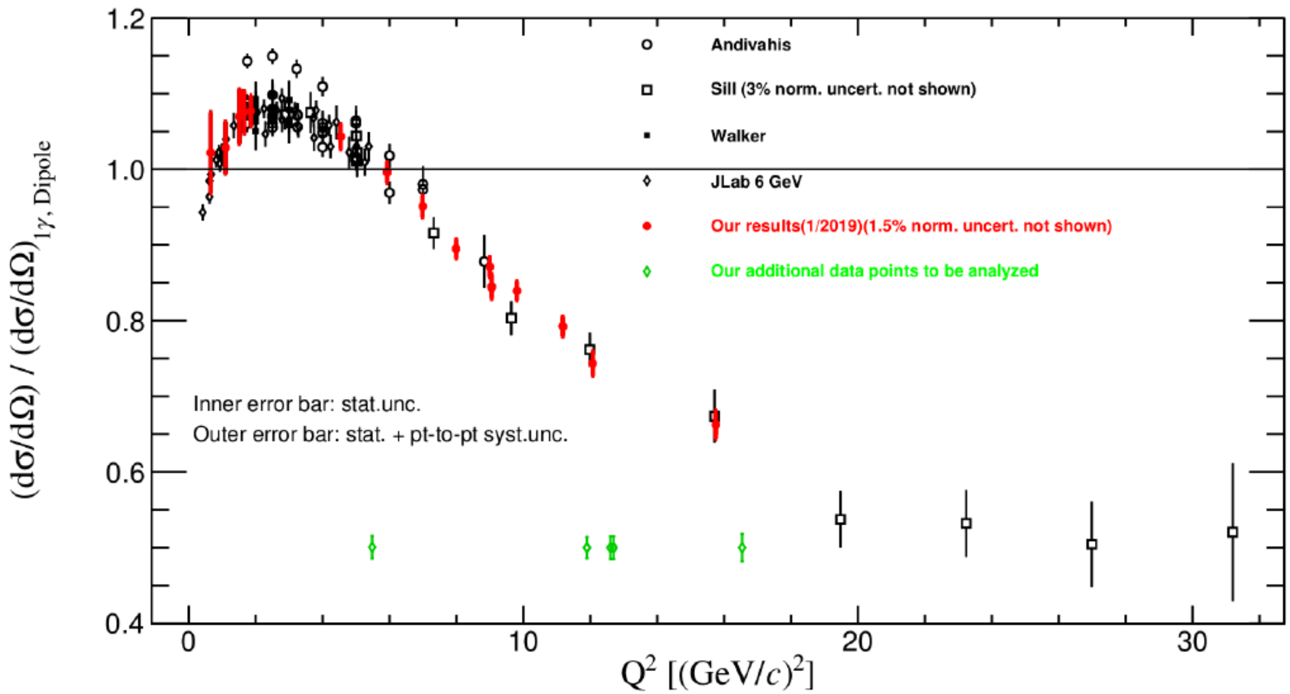

1γ refers to single photon approximation and Dipole corresponds to both form factor

28

PRELIMINARY results from GMP collaboration: Presented by Thir Gautam at recent Hall A Collaboration Meeting

Statistical requirements: asymmetries vs. cross section measurements

Cross sections:

$$\sigma \propto N$$

$$\Longrightarrow \frac{\Delta\sigma}{\sigma} = \frac{1}{\sqrt{N}}$$

To measure a cross section with a relative statistical precision of 1%, you need 10,000 events.

Asymmetries:

$$\Delta A = \sqrt{\frac{1-A^2}{N}}$$

$$\frac{\Delta A}{A} = \sqrt{\frac{1-A^2}{NA^2}}$$

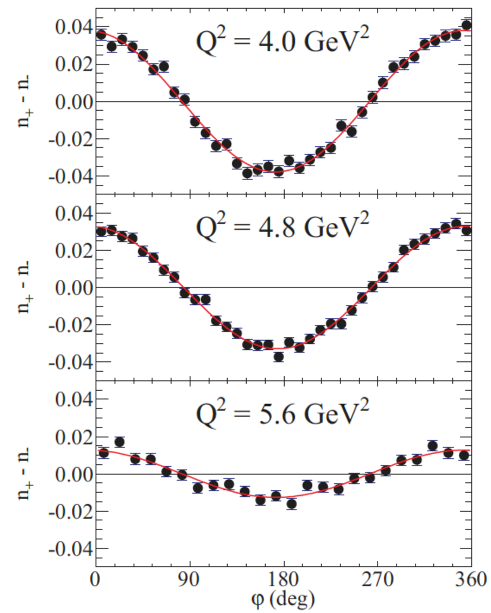

FIG. 6. (Color online) Focal-plane helicity-difference asymmetry $n_+ - n_- \equiv (N_{\rm bins}/2)[N^+(\varphi)/N_0^+ - N^-(\varphi)/N_0^-]$, where $N_{\rm bins}$ is the number of φ bins and $N^\pm(\varphi)$, $N_0^\pm$ are defined as in Eq. (4), for the three highest Q^2 points from GEp-II. Curves are fits to the data. See text for details.

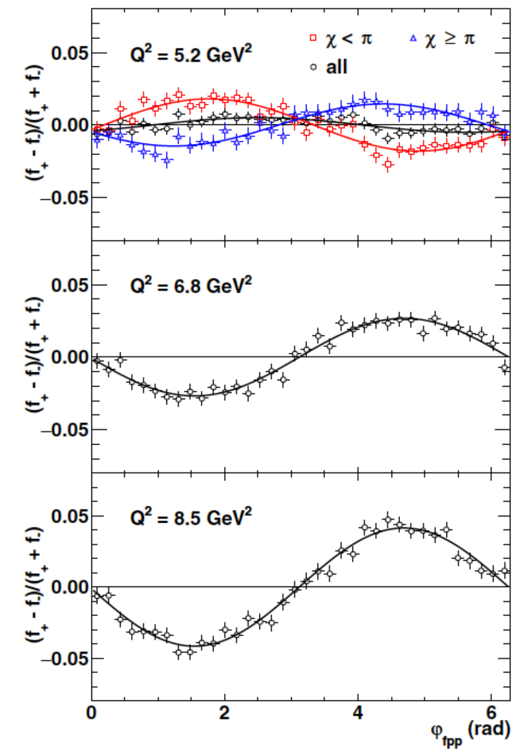

FIG. 10. Focal plane helicity difference/sum ratio asymmetry $(f_+ - f_-)/(f_+ + f_-)$, defined as in Eq. (20), for the GEp-III kinematics, for FPP1 and FPP2 data combined, for single-track events selected according to the criteria discussed in Sec. III B 2. Asymmetry fit results are shown in Table V. The asymmetry at $Q^2 = 5.2$ GeV^2 is also shown separately for events with precession angles $\chi < \pi$ and $\chi \geqslant \pi$, illustrating the expected sign change of the $\sin(\varphi)$ term.

- Typical asymmetry magnitude in a recoil proton polarimeter at "high" momentum is ~few percent.
- For example: to measure a 5% asymmetry with a relative precision of 1%, one needs $N = 10{,}000 \times \frac{1-A^2}{A^2} \approx 4 \times 10^6$ events!

→ Asymmetry measurement must maximize beam and/or target polarization, and luminosity × acceptance!

How to reach higher Q^2?

- Elastic ep cross section scales as $\sigma \approx E^2/Q^{12}$
- FPP efficiency is roughly Q^2-independent
- FPP analyzing power scales roughly as $1/p_p \sim M/Q^2$
- Statistical FOM scales as $NA_y^2 \sim E^2/Q^{16}$
- Increase beam polarization? 80%→100% would only increase FOM by 1.6
- Increase luminosity? Best possible at JLab 12 GeV ~ 10^{39} cm^{-2} s^{-1}; ~factor of 2 above 6 GeV expt's.
- Most room for growth? →***Increase solid angle/Q^2 acceptance!***
  - **2X increase in target thickness and solid angle from 6→35 msr leads to ~30X gain in figure-of-merit**
- JLab PAC-approved G_E^p experiment: E12-07-109; 45 days in Hall A
  - $\Delta(\mu G_E/G_M) \sim 0.07$ @$Q^2 = 12$ GeV^2

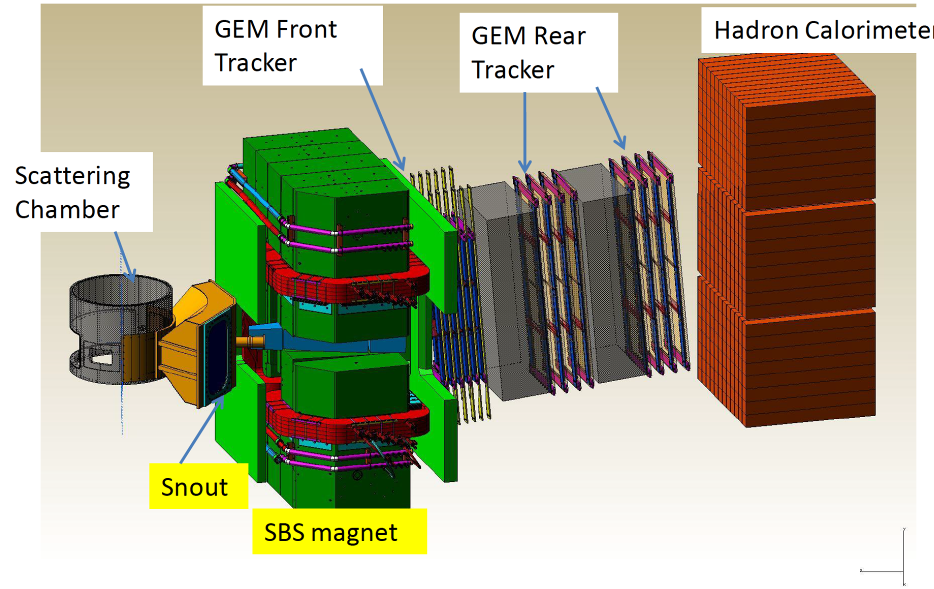

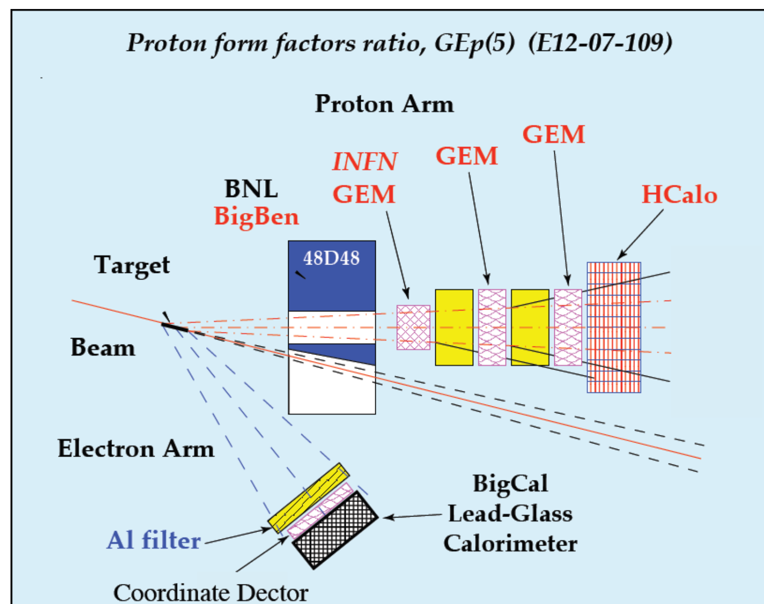

The Super BigBite Spectrometer in Hall A

Proton form factors ratio, GEp(5) (E12-07-109)

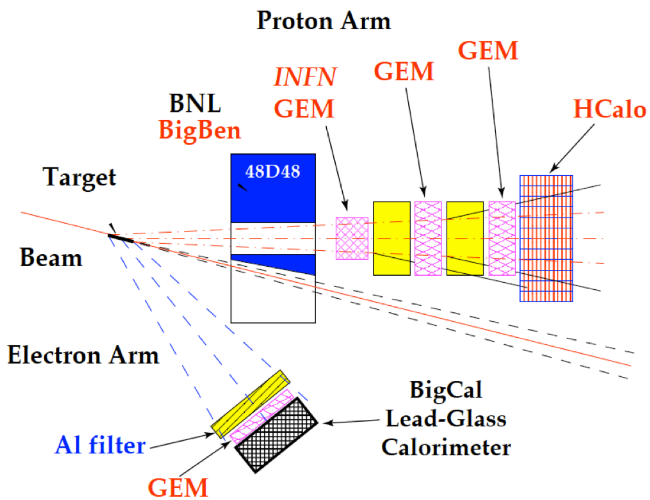

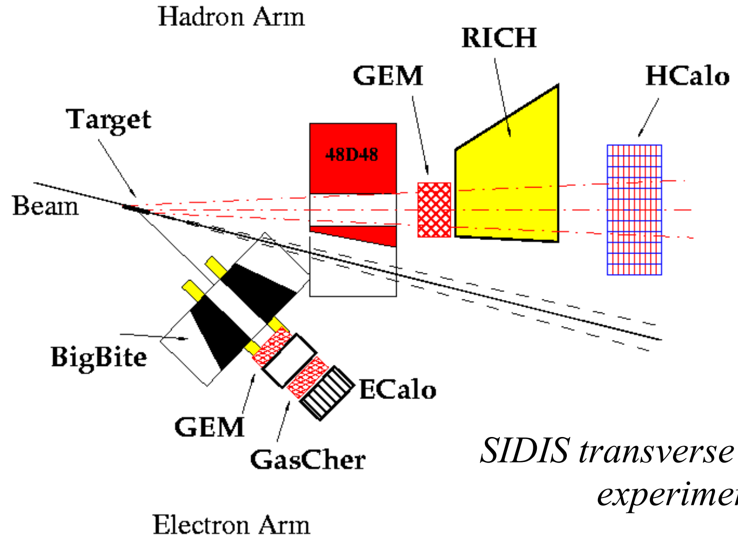

SIDIS transverse single-spin asymmetry experiment: E12-09-018

Neutron form factors, E12–09–016 and E12–09–019

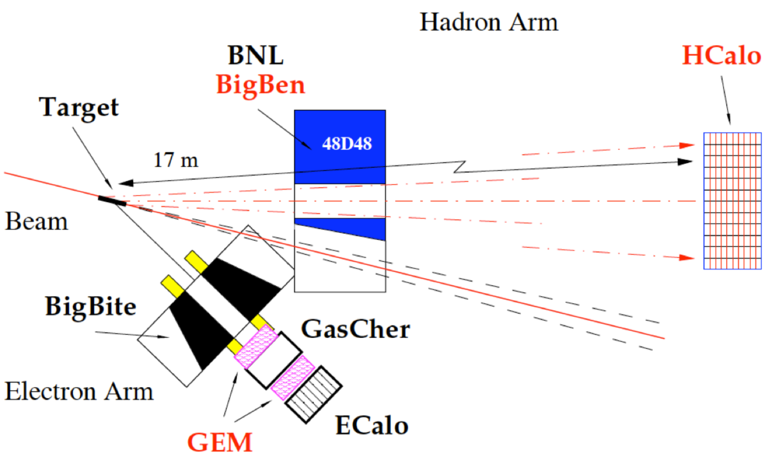

- What is SBS? → A 2.5 T*m dipole magnet with vertical bend, a cut in the yoke for passage of the beam pipe to reach forward scattering angles, and a flexible/modular configuration of detectors.
- Designed to operate at luminosities up to 10^{39} cm^{-2} s^{-1} with large momentum bite, moderate solid angle
- Time-tested "Detectors behind a dipole magnet", two-arm coincidence approach—historically most productive in fixed-target expts.
- ***Large solid-angle + high luminosity @ forward angles = most interesting physics!***

Gas Electron Multipliers (GEMs): High-Rate, High Resolution Charged-Particle Tracking

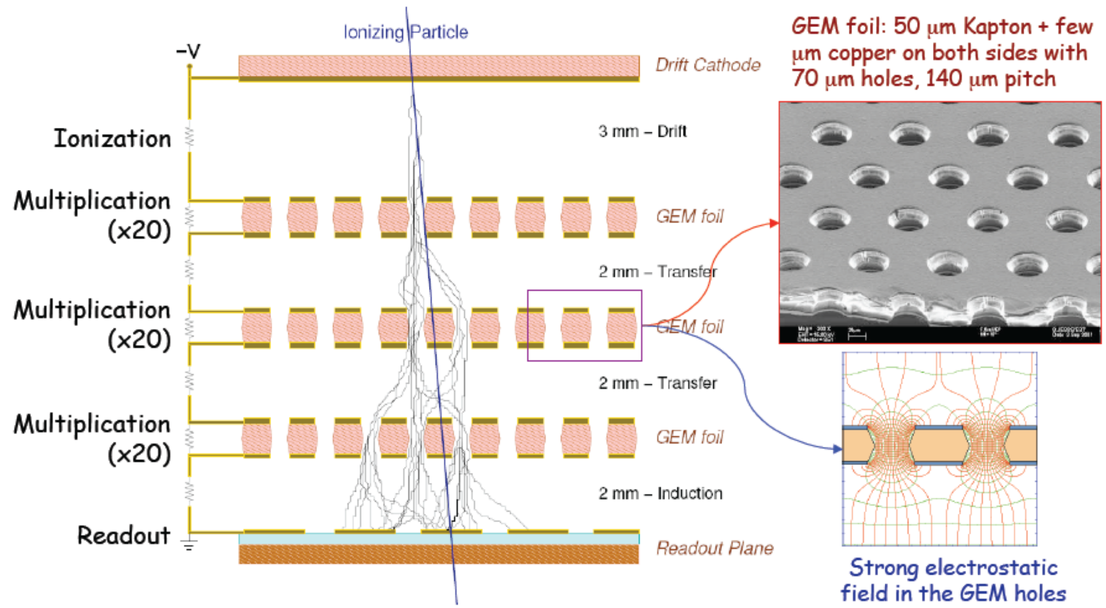

Recent technology: F. Sauli, NIM A 386, 531 (1997)

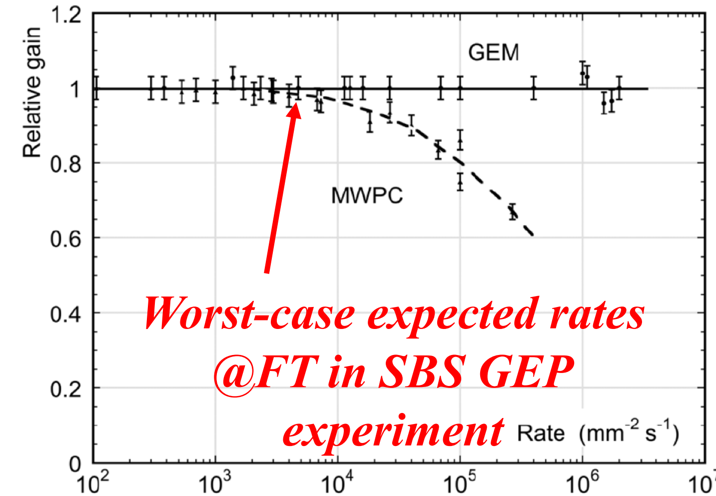

Figure 28.9: Normalized gas gain as a function of particle rate for MWPC [70] and GEM [84].

Stable gain up to very high rates

- High spatial granularity
- Ability to cascade several foils: higher gain at lower voltage, reduced discharge risk
- Readout and amplification stages decoupled
- Excellent spatial resolution ~70 μm
- Fast signals: intrinsic time resolution <10 ns
- **Enabling technology for SBS physics program!**

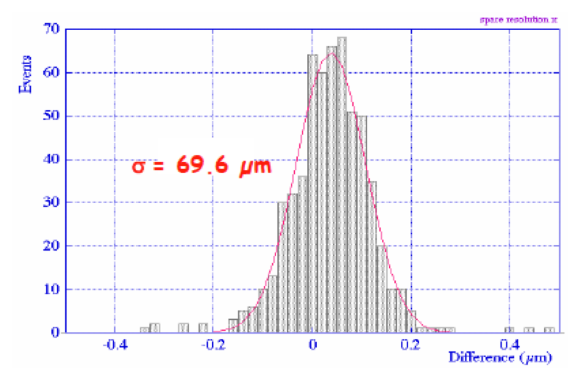

Space resolution

The tracking challenge in high-luminosity, open geometry: a taste

Presented at Nov Review

GEM Tracking Software

- Primary deployed algorithm using recursive TreeSearch (Raw combinatorics also employed for some analyses)
- GEMs provide six time samples over 25ns bins with jitter
- Hits are differentiated by fitting to spatial and temporal components
- Require amplitude matching between x-y components to obtain full 3D
- General restrictions are placed on search areas based on other detector knowledge]
- Basic multithreading implemented

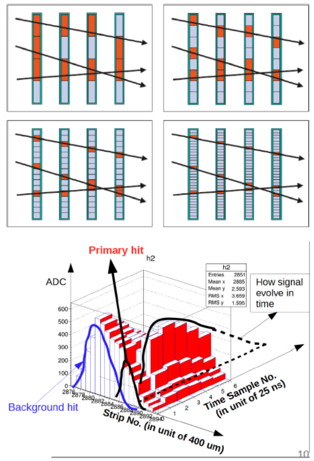

10

Seamus Riordan (ANL) Software and Tracking Feb 27, 2019 10 / 14

Presented at Nov Review

GEM Tracking – GMn

- Since 2016
  - Improved GEM response and validation based on data from constructed GEMs
  - Observe larger and wider background response
- Event reconstruction at
  - 70% tracking efficiency (2020 goal 80%)
  - 3 Hz (2020 goal 8Hz)
- Continuing to evaluate better separation of broad ADC clusters

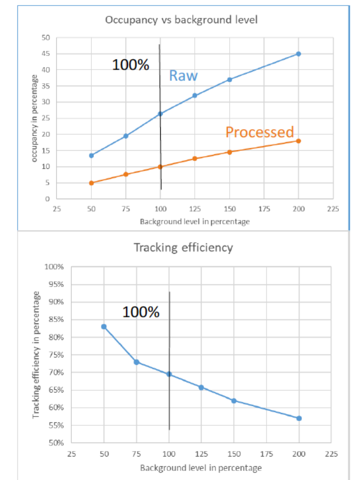

11

Seamus Riordan (ANL) Software and Tracking Feb 27, 2019 11 / 14

- In all the SBS experiments, detectors are located in field-free regions behind large dipole magnets with vertical bend*.
- Magnets shield detectors from low-energy *charged* backgrounds, BUT:
- Large flux of low-energy photons into GEMs—can convert in GEMs via Compton/photoelectric effects, pair production.
  - Secondary electrons from soft photon ionize GEM gas, give high rate of background hits: ~0.5 MHz/cm^2 at $Q^2 = 12\ GeV^2$ in the GEP measurement
- *--except GEP electron calorimeter, which is mainly sensitive to high-energy particles

E12-09-019—Neutron Magnetic FF G_M^n to $Q^2 = 13.5\ GeV^2$

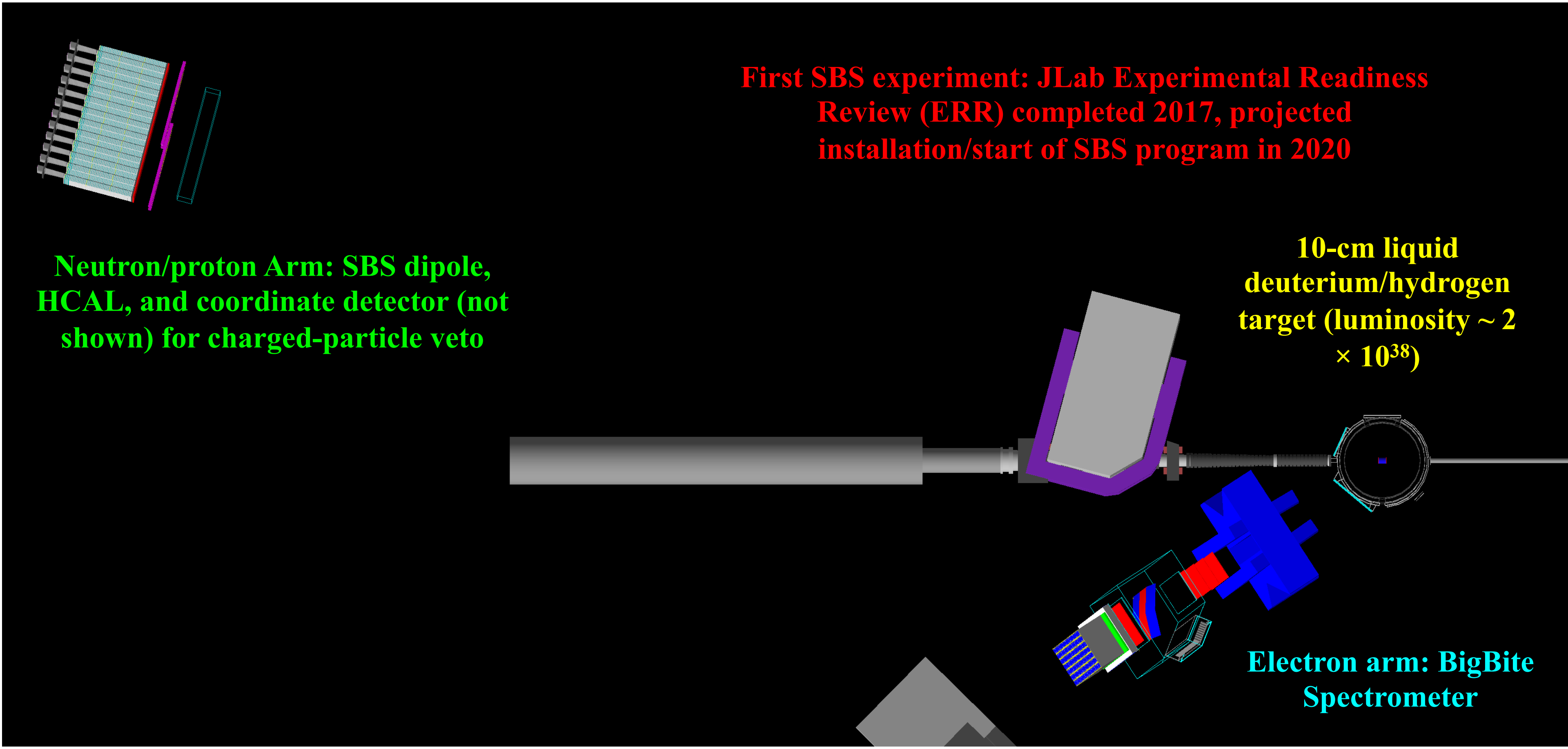

- Neutron magnetic form factor at large Q^2 is obtained from the ratio of quasi-elastic d(e,e'n)p/d(e,e'p)n cross sections on a deuterium target and precise knowledge of elastic ep cross section
- SBS dipole deflects protons to separate from neutrons (relative to $\vec{q}$ vector); nucleon momentum is measured using time-of-flight method to separate quasi-elastic/inelastic channels.
- Existing BigBite spectrometer with upgraded detector package detects the scattered electron.

SBS G_{Mn} projected Results

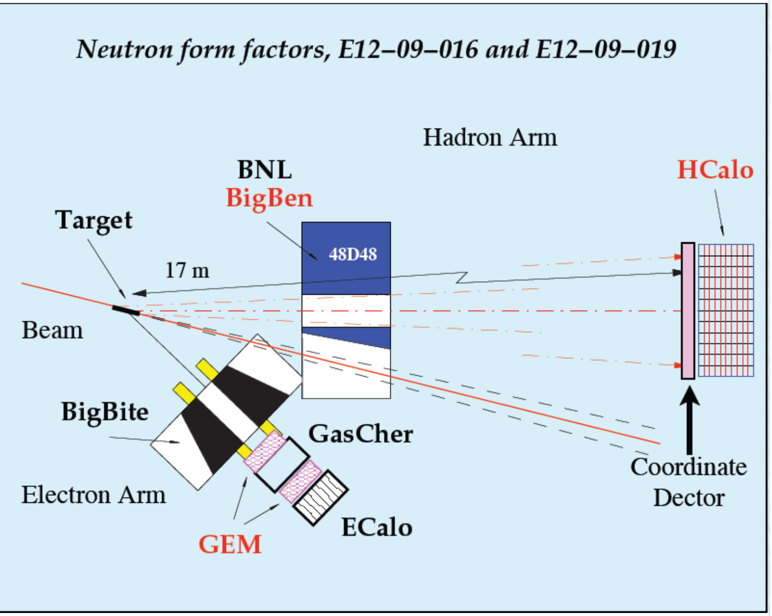

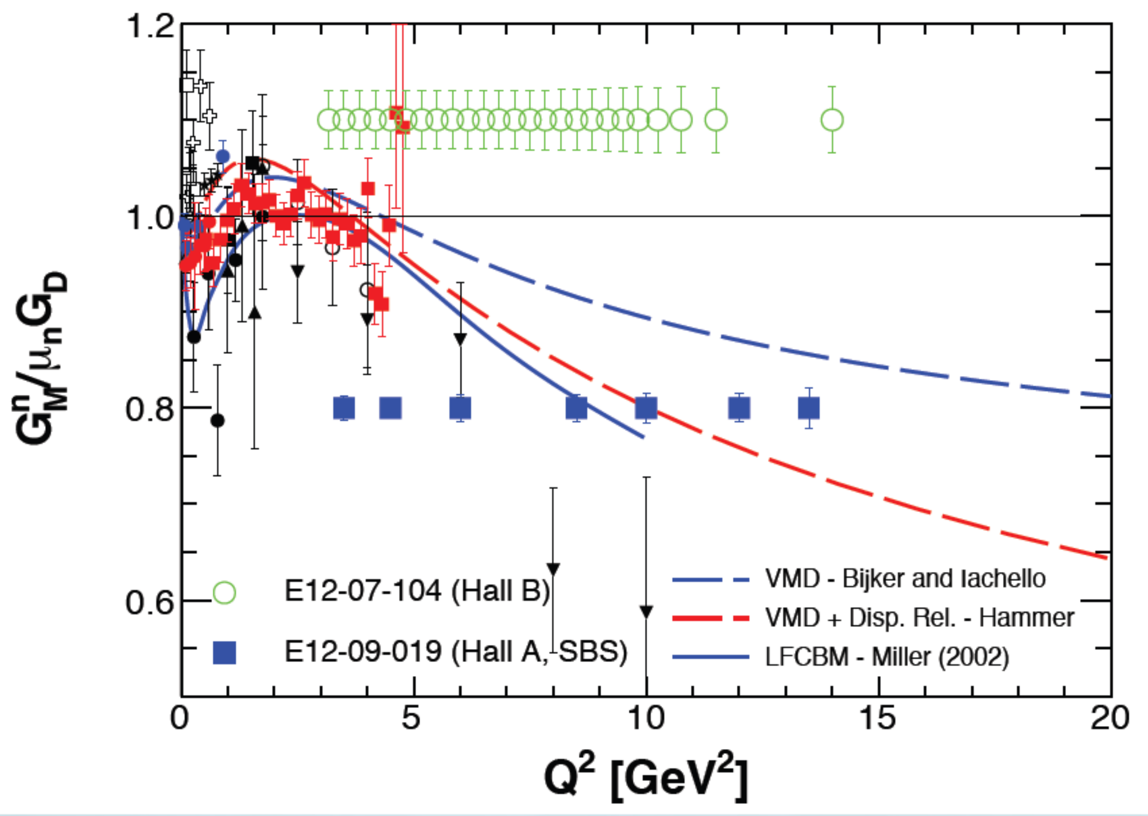

- SBS as neutron arm w/48D48 + HCAL
- Magnet sweeps charged particles out of acceptance, limiting backgrounds and "CDet" acts as charged-particle veto
- BigBite as electron arm w/upgraded 12 GeV detector package (including re-use of GEMs, built for GEP, not otherwise in use during BigBite expt's.)
- Standard LH2/LD2 target
- Different detection method—different (and smaller) systematics; complementary to CLAS12 G_{Mn} measurement
    - Overlapping collaborations between CLAS12 and SBS experiments.

Experiment E12-09-016 (G_{En} at large Q^2)

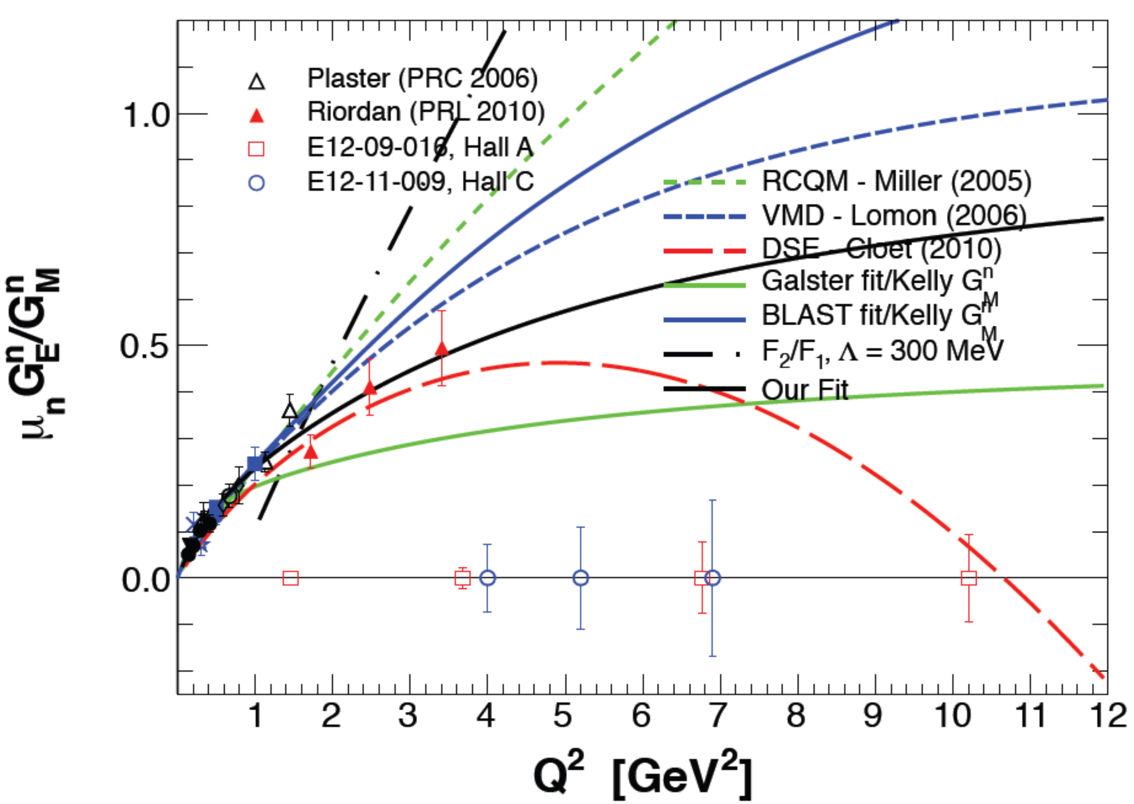

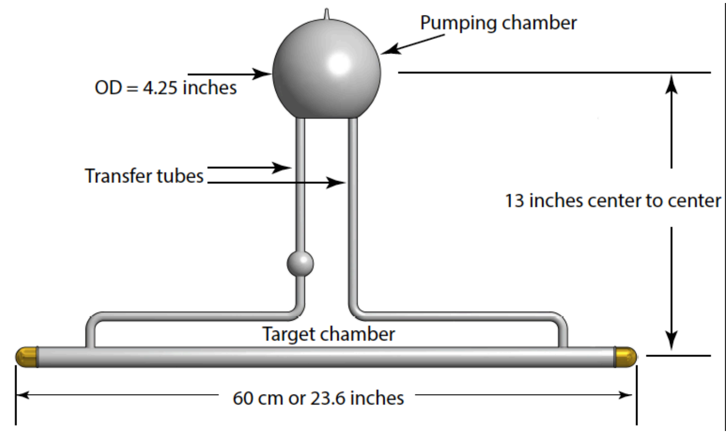

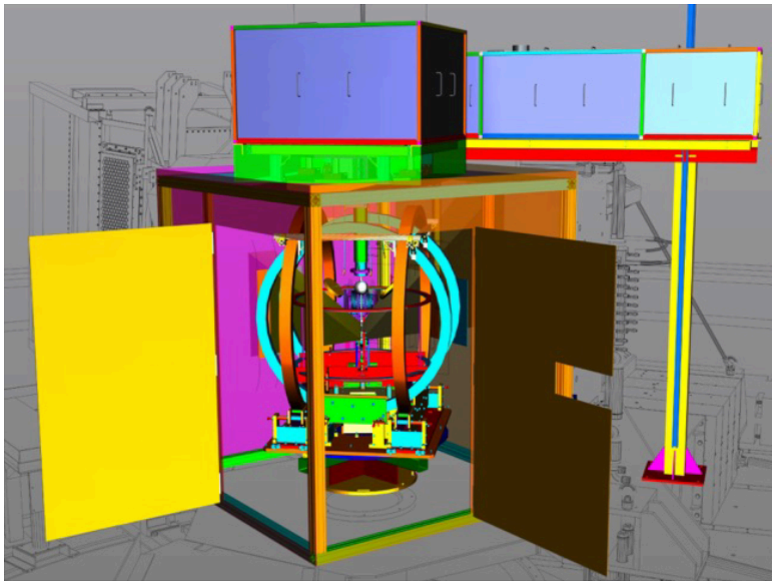

- Detector configuration same as GMN experiment
- Upgraded, high-luminosity polarized ^{3}He target based on spin-exchange optical pumping and convection-driven circulation of polarized gas between optical pumping chamber and target chamber.
- Will reach $Q^2 = 10$ GeV^2 in 50 days (approximately tripling Q^2 reach of the data)

Conceptual and Engineering Designs of Polarized ^{3}He target

Experiment E12-07-109 (G_{Ep}/G_{Mp} at large Q^2)

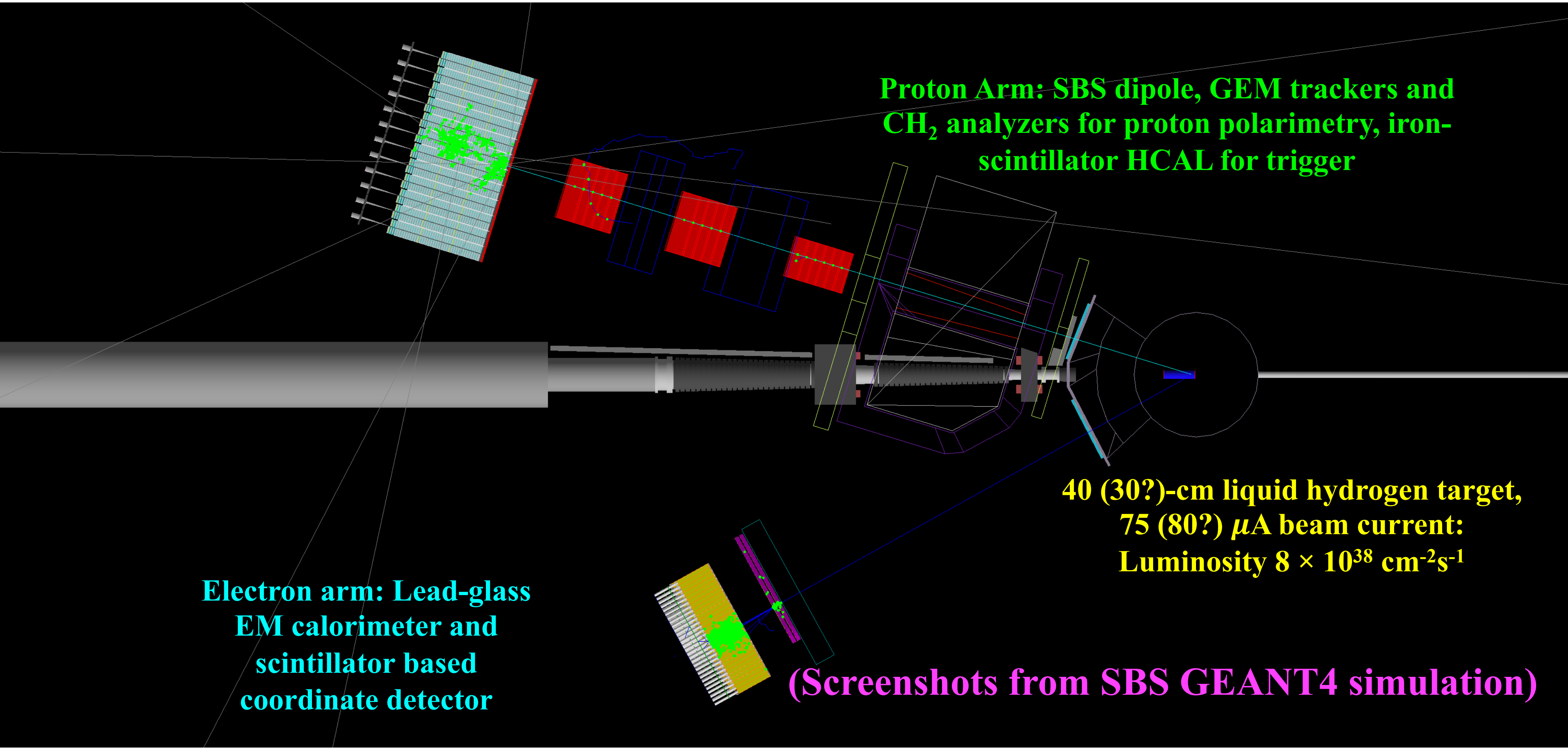

- Original motivation for SBS concept. Need large solid angle to overcome rapidly falling cross section at large Q^2 in elastic *ep* scattering. New double proton polarimeter with GEM-based tracking and hadronic calorimeter-based trigger
- Lead-glass electromagnetic calorimeter to detect the scattered electron in coincidence (using two-body kinematic correlations to aid tracking in high-rate environment and reject inelastic background events); also provides a selective trigger for high-energy electrons.

SBS G_E^p Projected Results

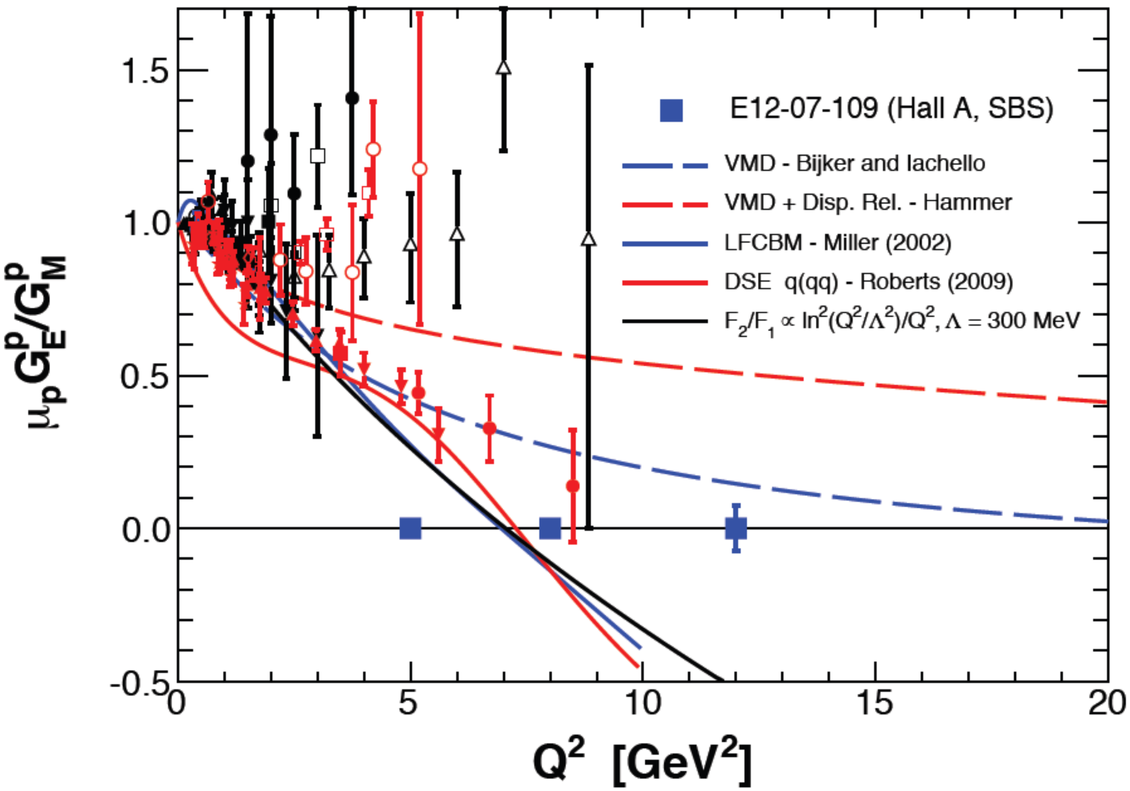

- The SBS GEP experiment in ~11 days running will dramatically improve the statistical precision in $\mu G_E/G_M$ at Q^2 in the range overlapping GEp-II/III, and in 30 days will reach comparable precision at 12 GeV^2 to that of GEp-II/III at 5-6 GeV^2
- Data of such precision carry significant discovery potential and may (or may not) settle the questions of a zero crossing of G_E^p and the onset (or lack thereof) of dimensional scaling.

- Combined with GEN, GMN, GMP experiments, full flavor decomposition of F_1 and F_2 becomes possible up to 10 GeV^2

Kinematics and expected accuracy							
E (GeV)	Q^2 (GeV^2)	θ_E (deg)	P_e (GeV)	Θ_p (deg)	P_p (GeV)	Days	$\Delta\mu G_E/G_M$
6.6	5.0	25.3	3.94	29.0	3.48	1	0.023
8.8	8.0	25.9	4.54	22.8	5.12	10	0.032
11.0	12.0	28.2	4.60	17.4	7.27	30	0.074

GEN via Recoil Polarization—E12-17-004

University of Glasgow

Recoil Neutron Polarimetry at High Momentum

- Until recently no data on n+C→n+p+X at several GeV/c (nor any nucleus)

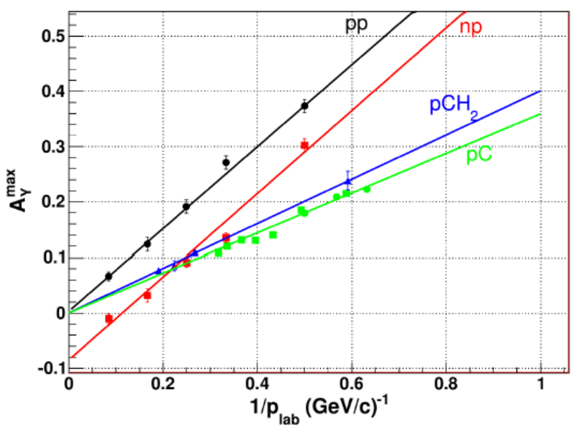

- A_y for np→np falling rapidly with increasing neutron momentum
- A_y for charge-exchange np→pn large at sufficiently large t (θ_p ~ few deg.)
- $\sigma_{np\to np}$ factor ~10 higher than $\sigma_{np\to pn}$

Diebold et al., PRL 35,(1975),632
Fits: Ladygin JINR E13-99-123 (1999)

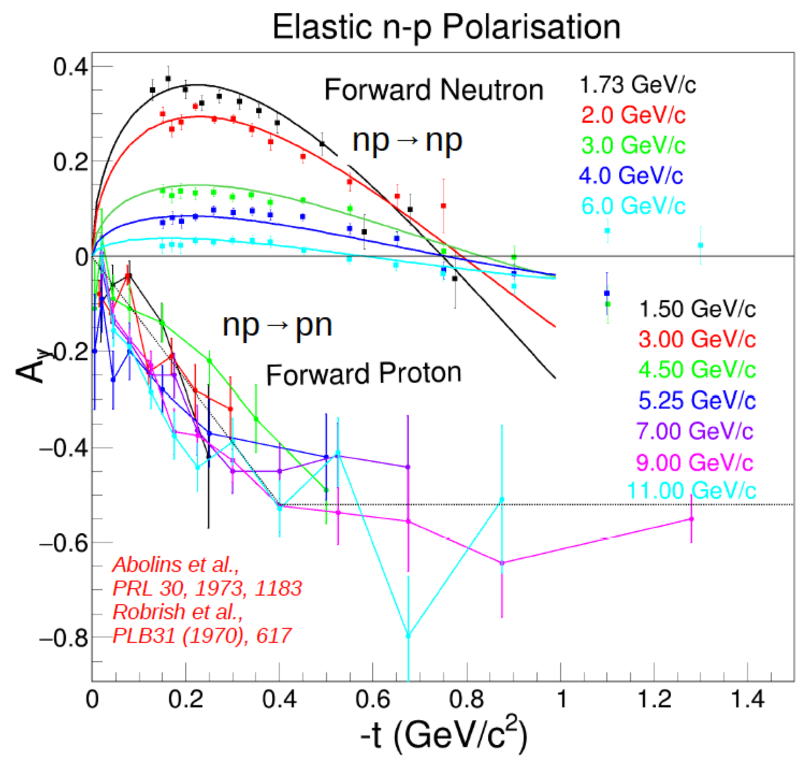

E12-17-004 (Continued)

University of Glasgow

GEn-Recoil Experimental Layout

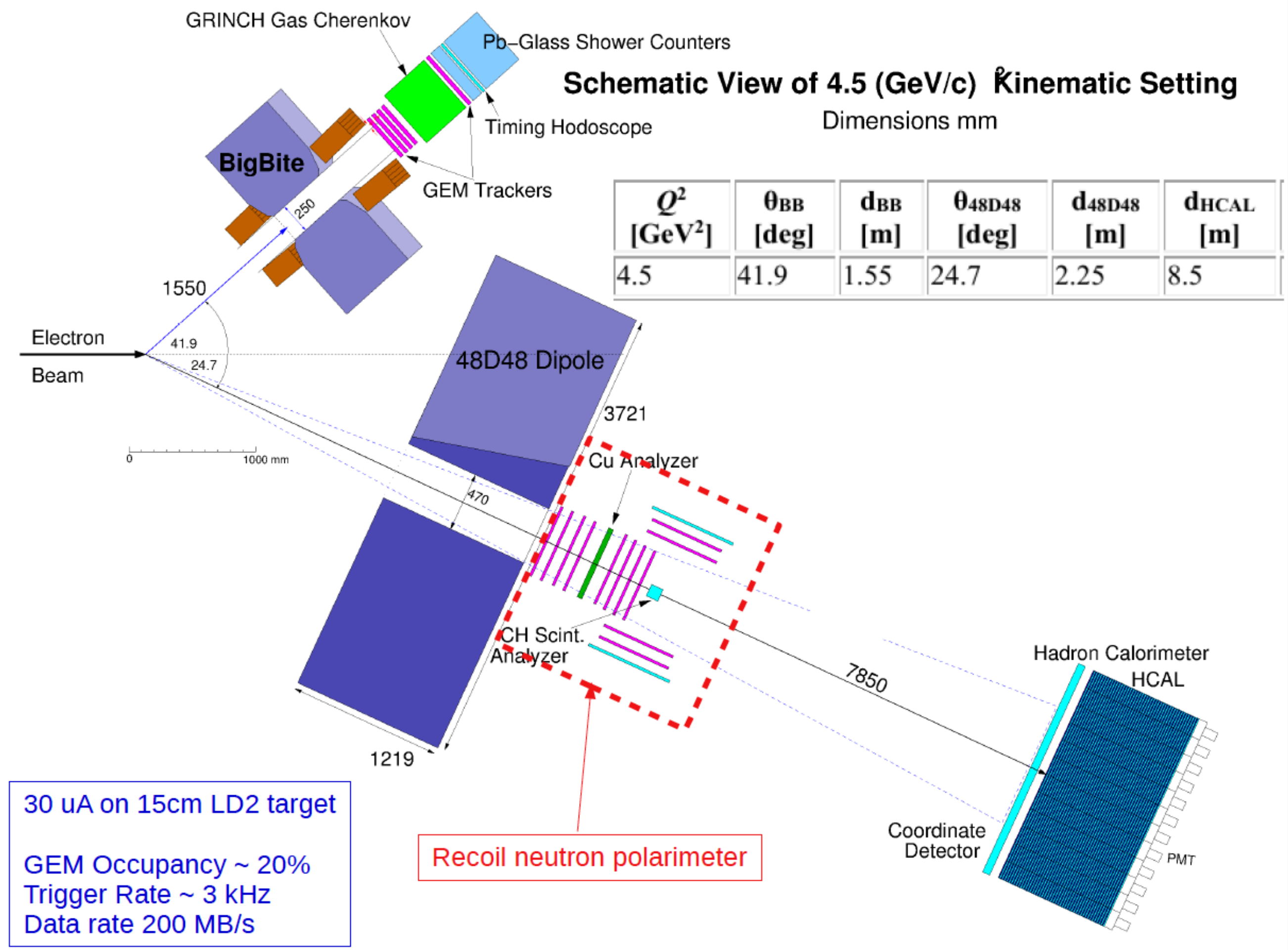

Schematic View of 4.5 (GeV/c)^2 Kinematic Setting

Dimensions mm

Q^2 [GeV^2]	θ_{BB} [deg]	d_{BB} [m]	θ_{48D48} [deg]	d_{48D48} [m]	d_{HCAL} [m]
4.5	41.9	1.55	24.7	2.25	8.5

30 uA on 15cm LD2 target

GEM Occupancy ~ 20%
Trigger Rate ~ 3 kHz
Data rate 200 MB/s

31st Jan 2019 GMn & GEn-Recoil Status Update 14

E12-17-004 Projected Results: Slide Credit to David Hamilton, Glasgow U.

University of Glasgow

Proposed Measurement

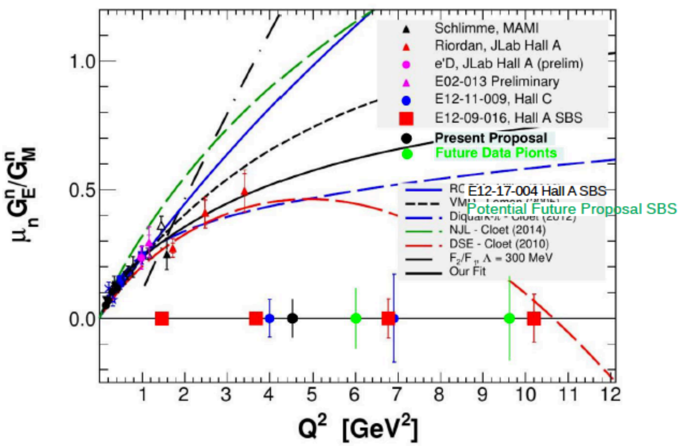

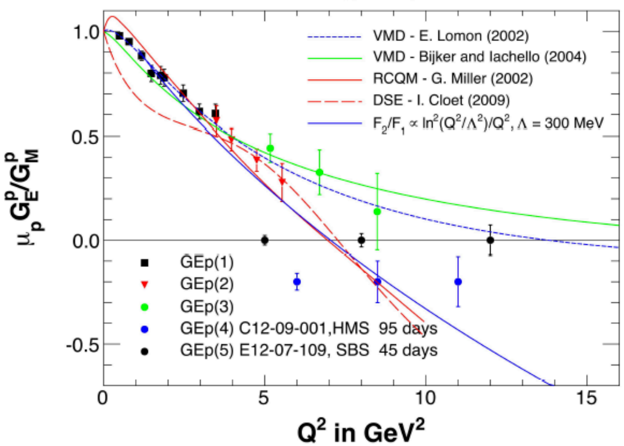

G_E^n/G_M^n 17004 Hydrogen/Deuterium

Experimental Points

10cm Hydrogen/Deuterium

Q^2 [GeV^2]	θ_{BB} [deg]	d_{BB} [m]	θ_{48D48} [deg]	d_{48D48} [m]	d_{HCAL} [m]	Beam Line Configuration #
4.5	41.9	1.55	24.7	2.25	8.5	3

With 5 PAC days (4.4 GeV polarized electron beam on a deuterium target) E12-17-004 will measure:

- G_{En}/G_{Mn} via charge exchange polarimetry;
- G_{En}/G_{Mn} via large angle recoil proton polarimetry;
- G_{Ep}/G_{Mp} via standard (forward) recoil polarimetry;
- G_{Ep}/G_{Mp} via charge exchange polarimetry.

It is anticipated that these measurements will have a large impact on future Halls A and C recoil polarization experiments.

27th February 2019 GEn-RP ERR Preparation 9

The SBS Form Factor Program—Summary

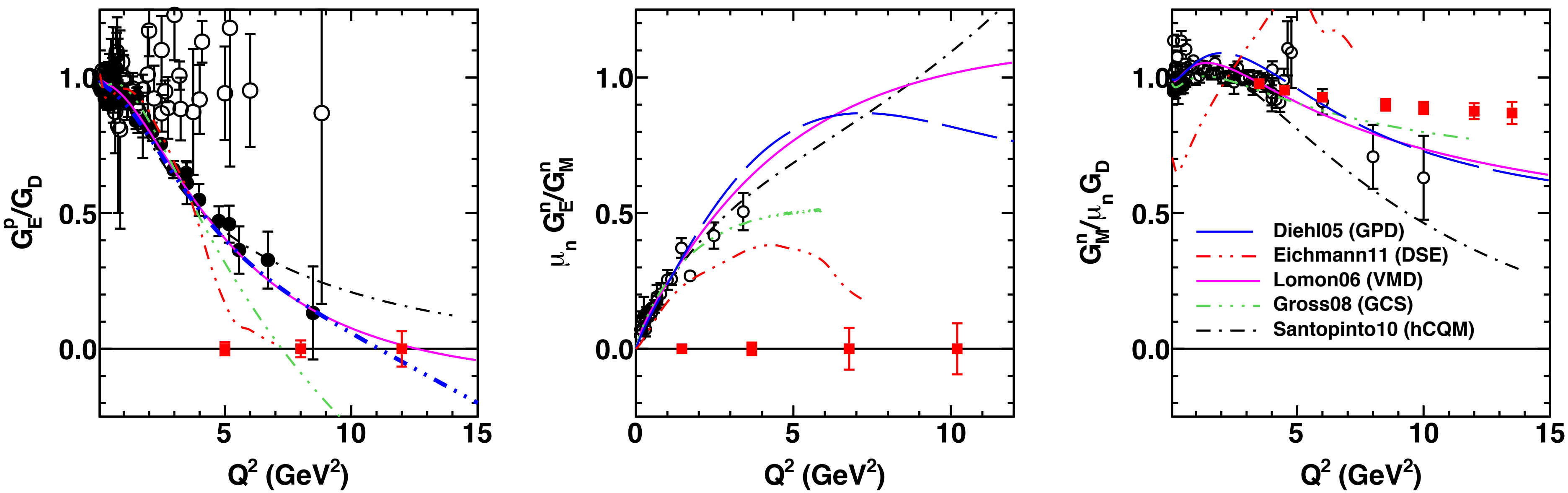

- SBS high-Q^2 form factor program:
  - Map transition to perturbative regime—running of dressed quark mass function
  - Imaging of the nucleon charge and magnetization densities in impact-parameter space in the infinite momentum frame.
  - Precision high-Q^2 form factors have significant impact on GPD program; proton spin decomposition
- GEP: Proton electric form factor, increase Q^2 range from 8.5 → 12 GeV^2
- GEN: Neutron electric form factor, increase Q^2 range from 3.4 → 10 GeV^2
- GMN: Neutron magnetic form factor, increase Q^2 range from 5 → 13.5 GeV^2

SBS Program Status and Tentative Schedule

- GMN ("easiest" SBS experiment) passed readiness review 2017
  - GEN-RP as add-on, proof-of-principle measurement with large impact to future polarization transfer expt's.
- SBS installation 2020, coinciding with long CEBAF shutdown for machine improvements
- GMN spring 2021
- GEN/Transversity 2021-2022
- GEP 2022/23
- The SBS family comprises 5 fully JLab PAC-approved (+1 conditionally approved) experiments, representing more than 200 beam-days in Hall A.
- Form factors are the main program (and subject of this talk), but additional SIDIS physics (E12-09-018, not discussed) is of potentially even broader interest.
- These are highly technically challenging experiments that will produce world-class science in the next five years
- Currently active collaboration of SBS is relatively small for a program of this scope. As such, we are seeking and welcoming new collaborators and *especially* new Ph.D. students

Thank You!

See pretty pictures of the apparatus below, time permitting…

Setup of UVa GEMs in the EEL Clean Room 124

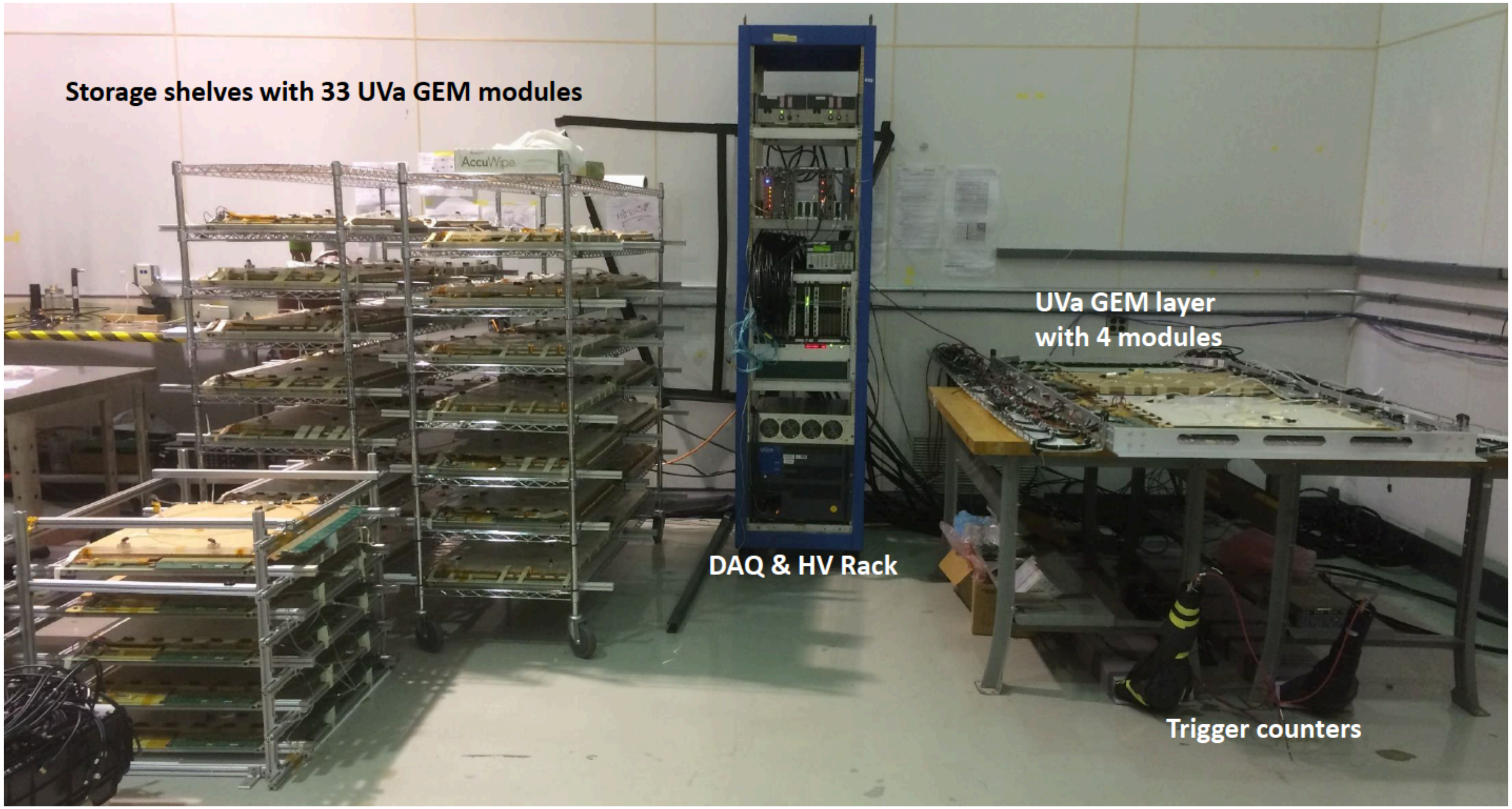

9/19/2018 SBS weekly Meeting 10

BigBite Spectrometer Status

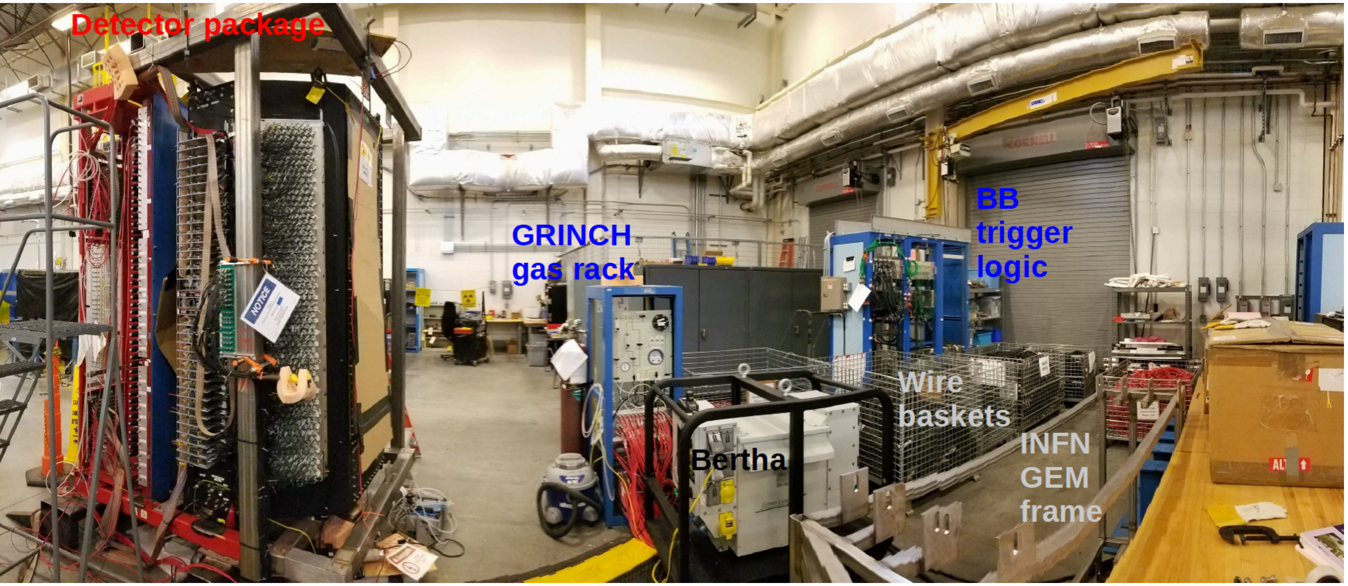

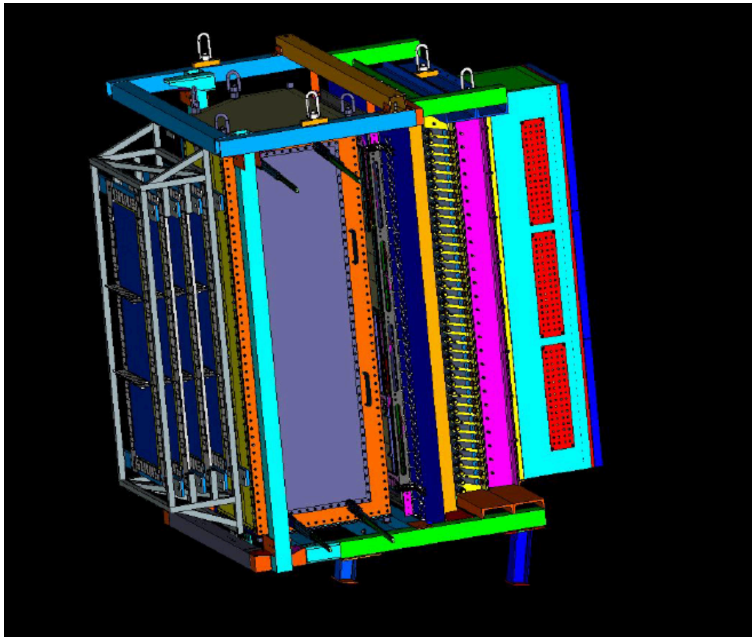

- Above: Assembled BigBite detector package, ex-GEMs
- Right: CAD layout of final BigBite detector package
- Institutions: Jefferson Lab, William and Mary, UConn, INFN, UVA, Glasgow U, others

- Above: the BigBite dipole magnet yoke and coils

Hadron Calorimeter—Carnegie Mellon University and INFN

Images of HCAL setup in TestLab (as of today)

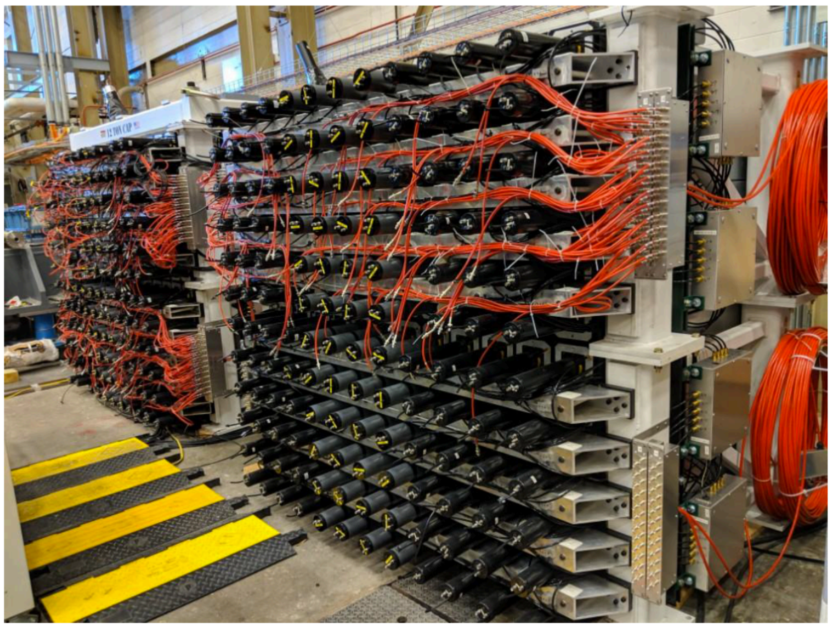

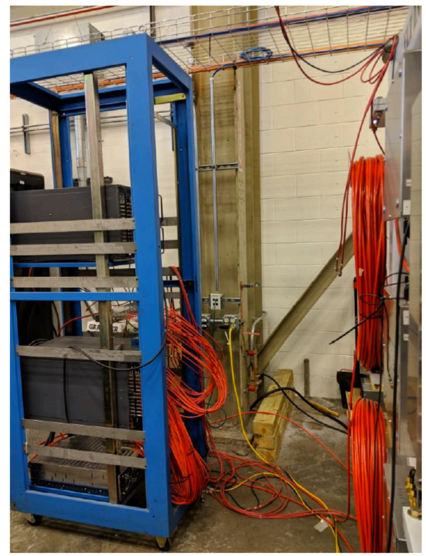

10

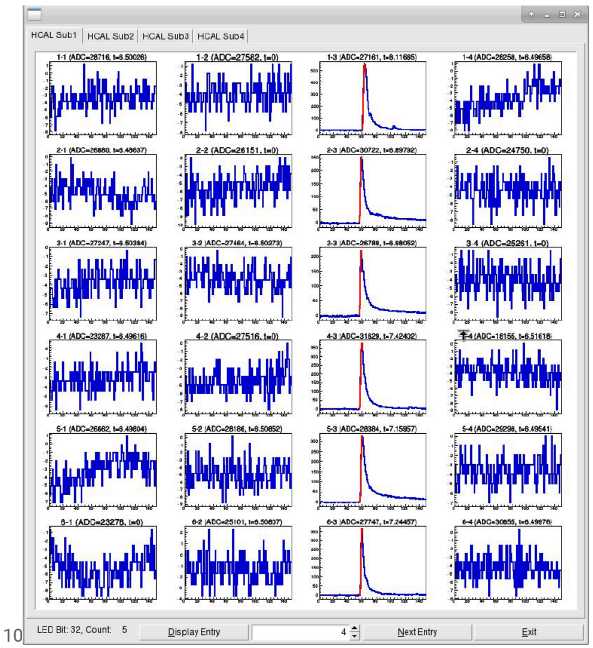

Above: Cosmic test data

Figure credit: J. C. Cornejo, CMU. “TODAY” here means Feb. 26

Polarized ^{3}He target status—UVA (Gordon Cates)

Target cell savior

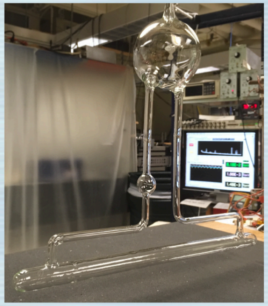

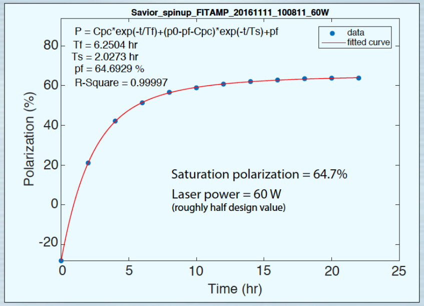

- ✦ Stage-I target cell (3 liter all glass) for A_1^n
- ✦ Excellent performance - important proof of principle
- ✦ Filled in October 2016, Delivered to JLab January 2018

11

The SBS G_E^n (Stage-II) target cell design

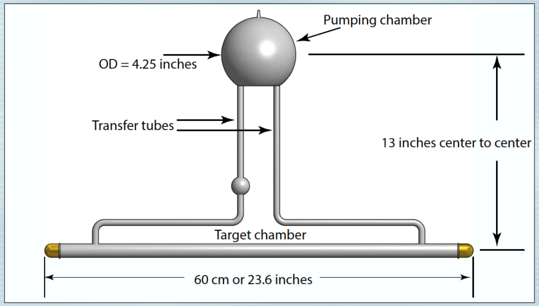

Predominantly three differences with Stage-I target cells:

- Contains <u>6</u> STP liters of He^3 instead of 3 STP liters
- Metal end windows on the target chamber
- 60 cm target chamber instead of 40 cm

24

SBS G_E^n Polarized ^{3}He system - focusing on the target ladder

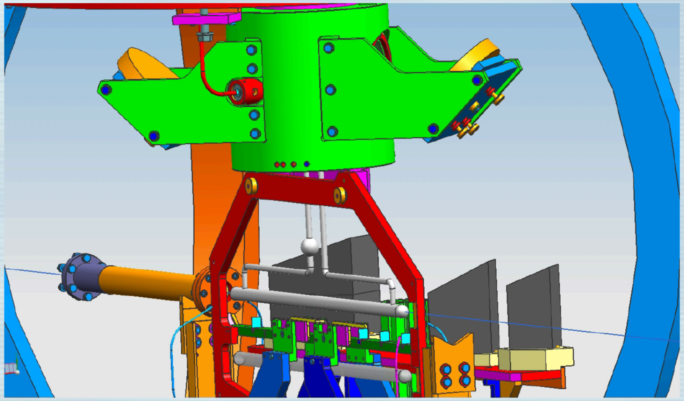

6

SBS G_E^n Polarized ^{3}He system - inside the magnetic shielding

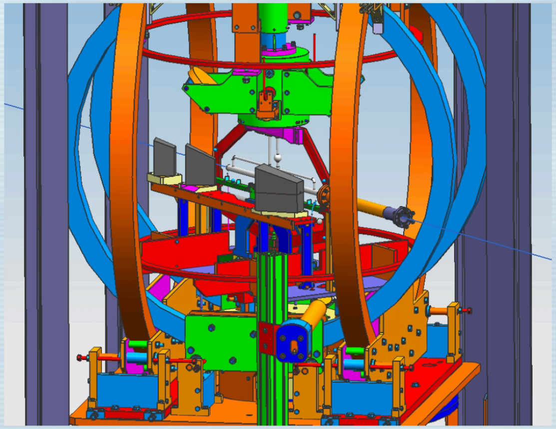

5

Backup Slides

“Role of diquark correlations and the pion cloud in nucleon elastic form factors”

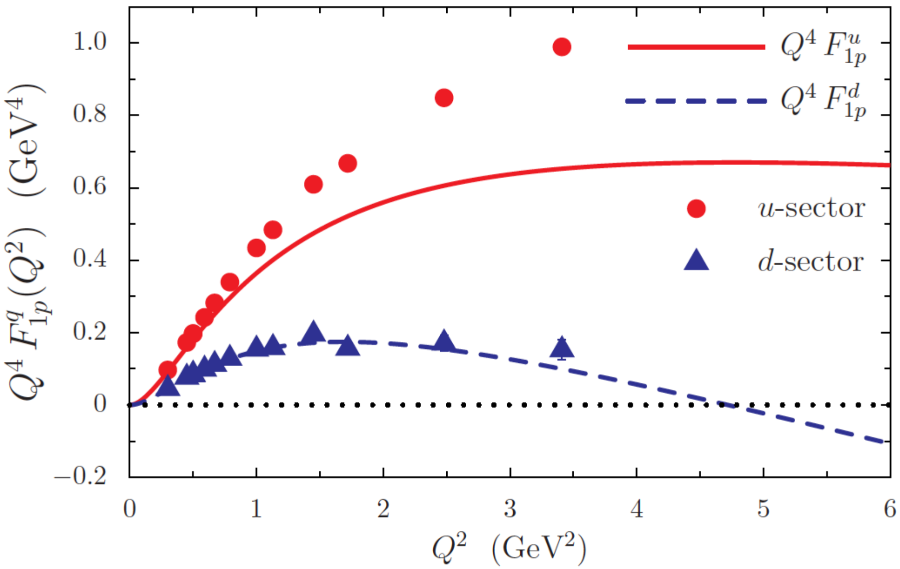

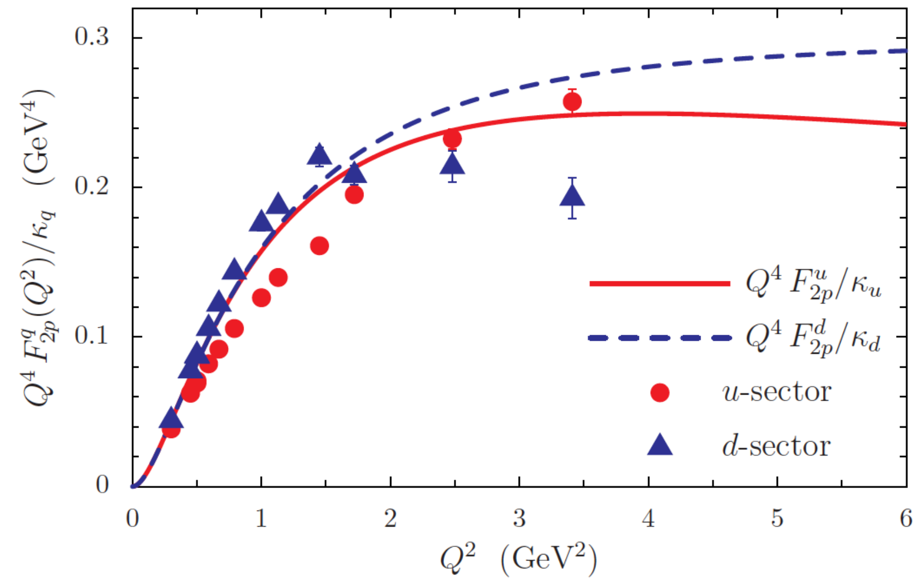

I. Cloet, W. Bentz and A. Thomas: Phys. Rev. C 90, 045202 (2014)

- Nucleon EMFF calculation in covariant, confining NJL model
- Parameter-free calculation (no fit to form factors)
- Softness of d-quark Dirac FF a consequence of dominance of scalar diquark correlations in nucleon wavefunction
- Axial vector diquark correlations and pion cloud effects play a more significant role in the Pauli form factors

Dyson-Schwinger Equations, diquark correlations, and zero crossings of G_{Ep}, G_{En}

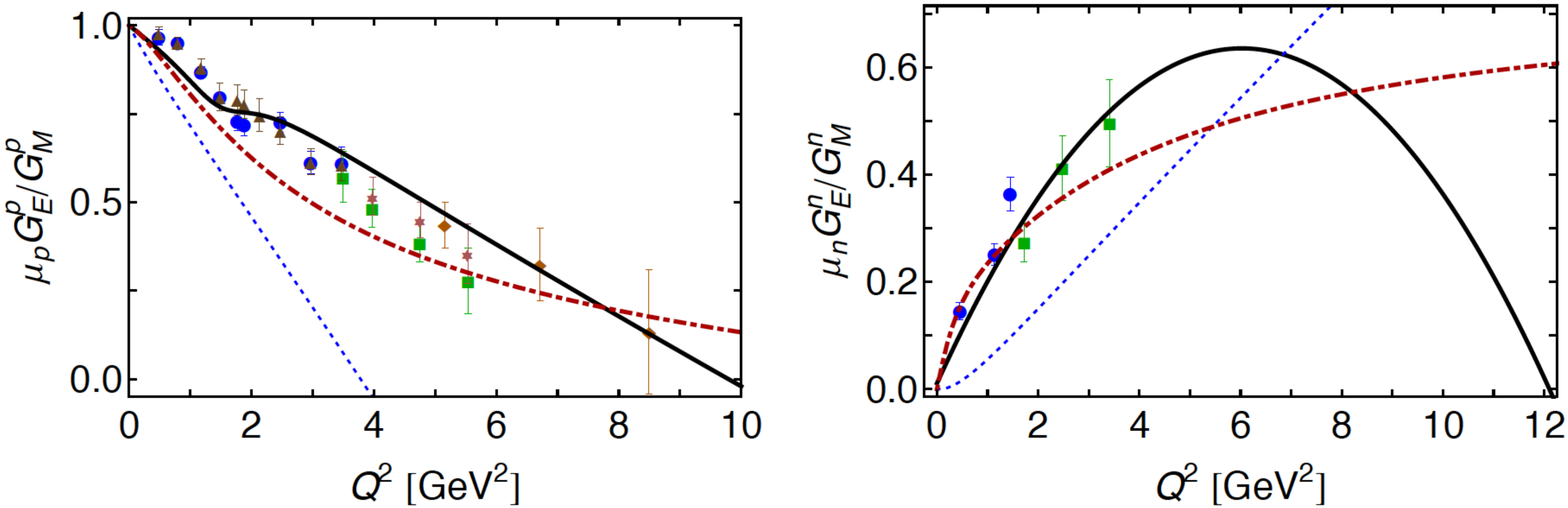

Fig. 3 *Left panel*: normalised ratio of proton electric and magnetic form factors. Curves: *solid, black* – result obtained herein, using our QCD-kindred framework; *Dashed, blue* – CI result [18]; and *dot-dashed, red* – ratio inferred from 2004 parametrisation of experimental data [65]. Data: blue circles [68]; green squares [69]; brown triangles [70]; purple asterisk [71]; and orange diamonds [72]. *Right panel*: normalised ratio of neutron electric and magnetic form factors. Curves: same as in left panel. Data: blue circles [73]; and green squares [74].

J. Segovia, I. Cloet and C. Roberts: [Few-Body Syst. 55, 1185 (2014)]

Quote from the abstract:

of dynamical chiral symmetry breaking in the bound-state problem. Amongst the results we describe, the following are of particular interest: $G_E^p(Q^2)/G_M^p(Q^2)$ possesses a zero at $Q^2 = 9.5\,\text{GeV}^2$; any change in the interaction which shifts a zero in the proton ratio to larger Q^2 relocates a zero in $G_E^n(Q^2)/G_M^n(Q^2)$ to smaller Q^2; there is likely a value of momentum transfer above which $G_E^n > G_E^p$; and the presence of strong diquark correlations within the nucleon is sufficient to understand empirical extractions of the flavour-separated form factors. Regarding the $\Delta(1232)$-baryon, we find that, *inter*

Proton FFs compared to data: “Global Fit II”

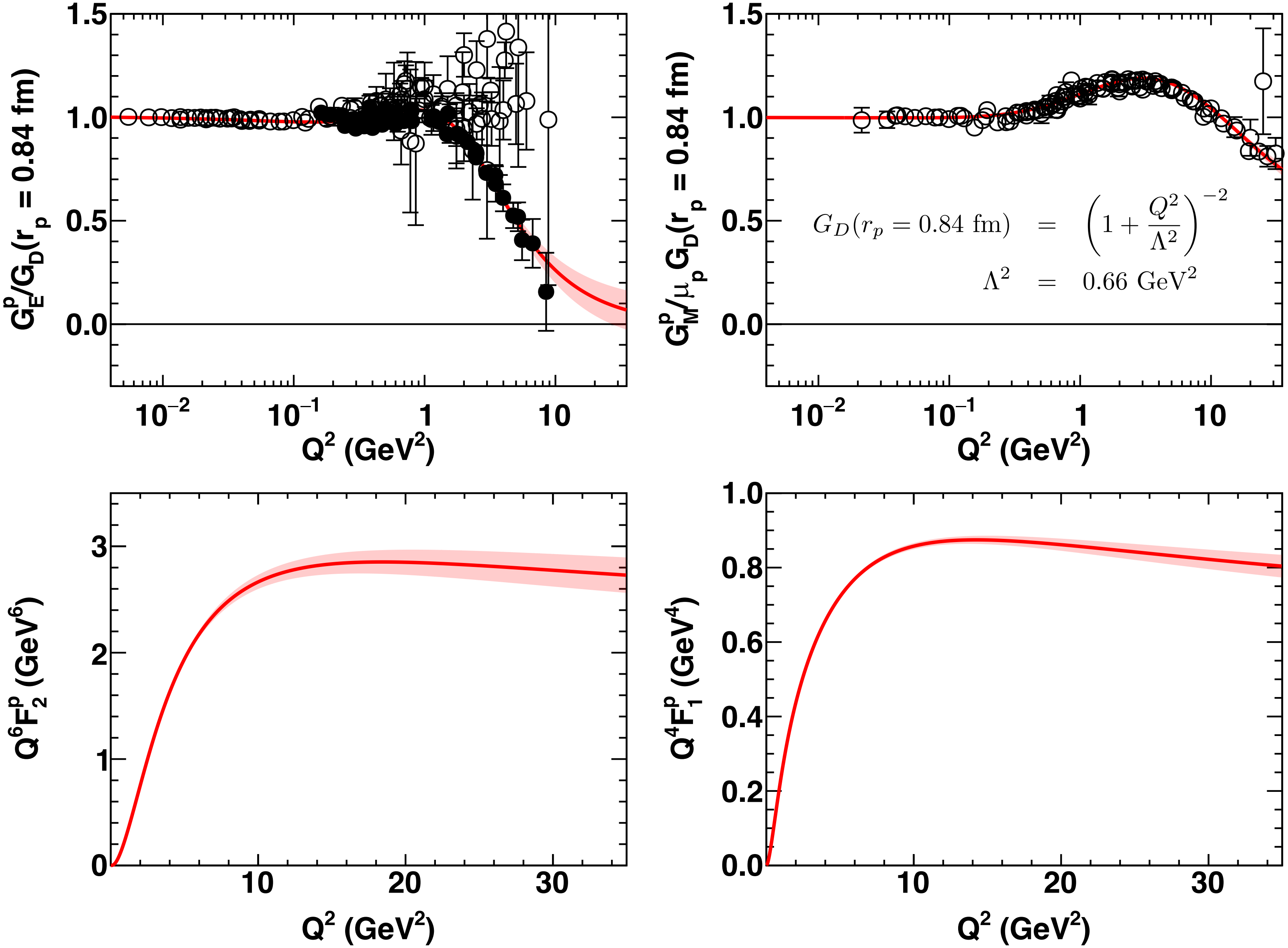

Parton Model—The Physical Meaning of Scaling

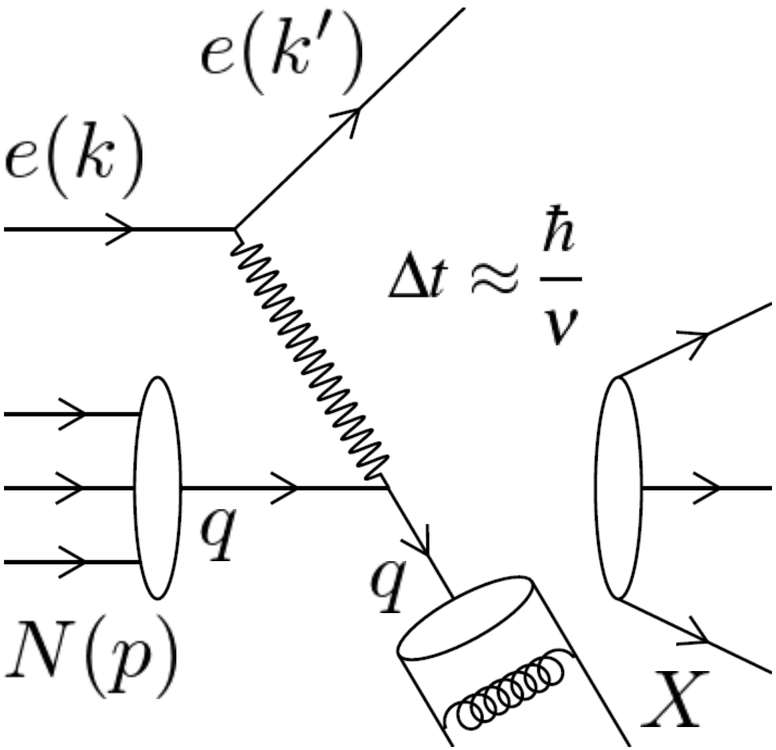

$$p_q = zp$$

$$\frac{Q^2}{2p_q \cdot q} \equiv y = \frac{x}{z} = 1$$

$$(F_2)_{eq\to eq} \Rightarrow \delta\left(1 - \frac{x}{z}\right) = x\delta(z-x)$$

$$(F_1)_{eq\to eq} \Rightarrow \frac{1}{2x}\delta(1-\frac{x}{z}) = \frac{F_2}{2x}$$

$$F_{1,2}^{ep\to eX} \to \sum_i e_i^2 \int_0^1 dz q_i(z) F_{1,2}^{eq_i\to eq_i}$$

$$F_2^{ep}(x) = \sum_i e_i^2 x q_i(x) = 2xF_1^{ep}(x)$$

- Imagine the proton as a collection of quasi-free, non-interacting spin-1/2 constituents moving collinearly with "infinite" momentum.
  - **Then *inelastic* ep→eX becomes *elastic* eq→eq.**

- The *ep* inelastic structure functions become incoherent, charge-squared-weighted sums over quark flavors of *Parton Distribution Functions (PDFs)* representing the number density of quarks carrying fraction *x* of the nucleon momentum
- ***Structure functions become Q^2-independent (for fixed x) due to energy-momentum conservation***
- ***Callan-Gross relation:*** **$F_2 = 2x\ F_1$ (consequence of partons having spin-1/2)**

High-Q^2 Nucleon Form Factors, GPDs and Spin

Flavor decomposition of nucleon EMFFs (neglecting strangeness):

$$F_{1,2}^p \approx e_u F_{1,2}^u + e_d F_{1,2}^d$$

$$F_{1,2}^n \approx e_u F_{1,2}^d + e_d F_{1,2}^u$$

Quark flavor FFs are integrals of valence quark GPDs H and E at zero skewness :

$$F_1^q(t) = \int_0^1 H_v^q(x,t)dx$$

$$F_2^q(t) = \int_0^1 E_v^q(x,t)dx$$

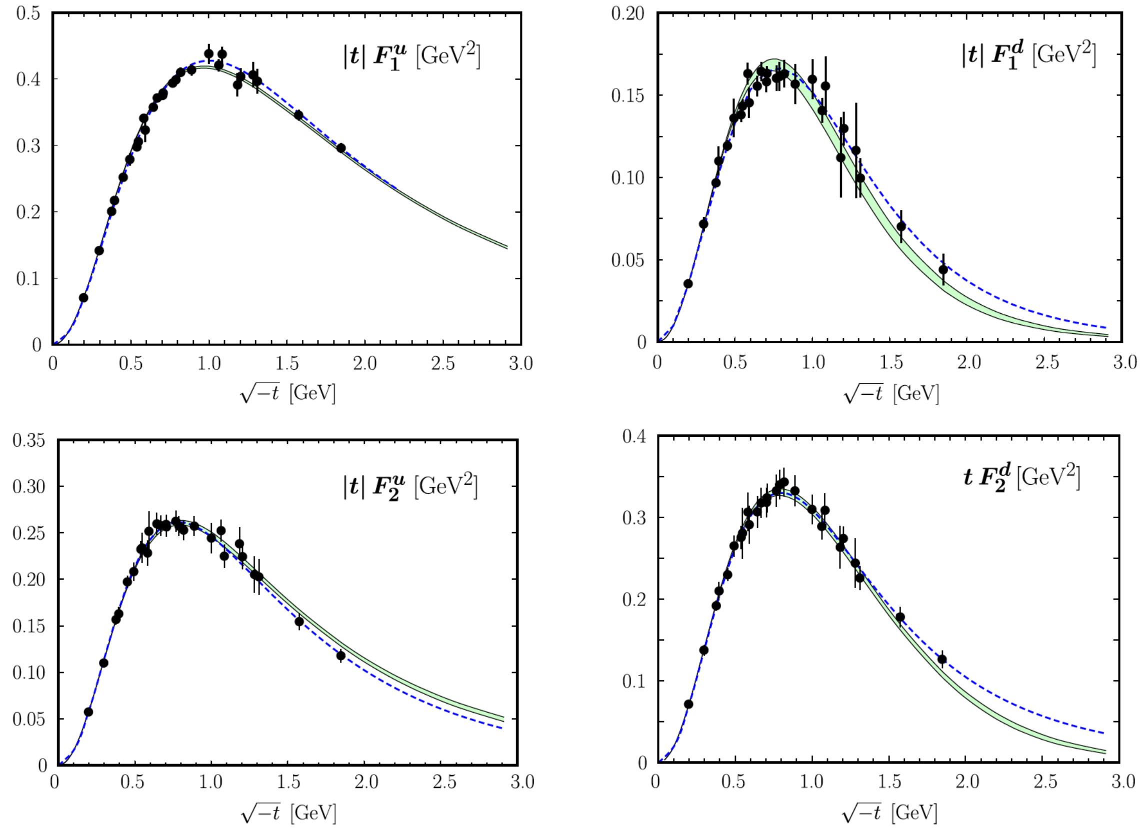

Phys.Rev.Lett. 78 (1997) 610-613: Ji sum rule for total angular momentum

$$J_q = \frac{1}{2}\int_{-1}^{+1} dx\,x[H^q(x,\xi,t=0) + E^q(x,\xi,t=0)].$$

Diehl, Kroll. Eur. Phys. J. C (2013) 73:2397

- FF data + forward PDFs from global DIS fits → model-dependent extraction of GPDs
- Compute valence-quark contributions to the Ji sum rule:

$$J_v^u = 0.230^{+0.009}_{-0.024}, \qquad J_v^d = -0.004^{+0.010}_{-0.016}$$

Exposing the dressed-quark mass function

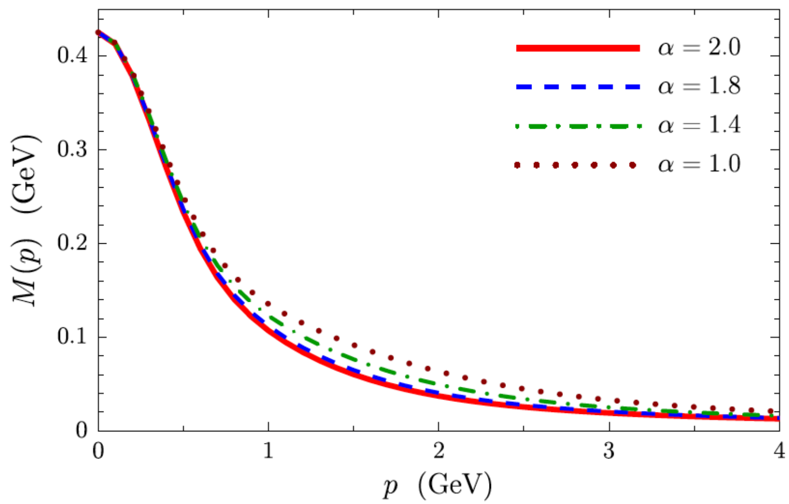

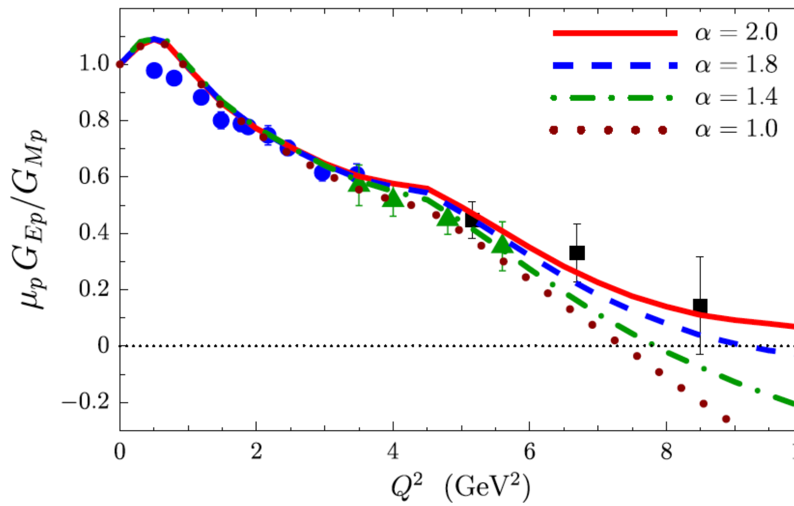

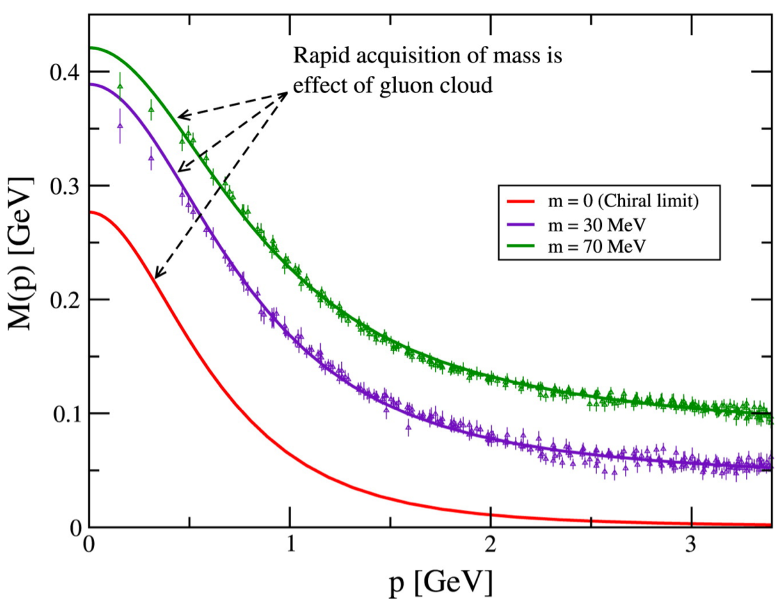

In the framework of Dyson-Schwinger equations, the high-Q^2 nucleon FFs ($Q^2 > 5$ GeV^2) are especially sensitive to momentum-dependent dressed-quark mass function in the few-GeV region, see e.g.,:

- I. Cloet, C. Roberts, A. Thomas: "Revealing Dressed Quarks via the Proton's Charge Distribution", **PRL 111, 101803 (2013)**
- I. Cloet and C. Roberts: "Explanation and Prediction of Observables Using Continuum Strong QCD", arxiv:1310.2651v2 (2013), **PPNP 77 (2014), 1-69**

Dyson-Schwinger Equations, diquark correlations, and zero crossings of G_{Ep}, G_{En}

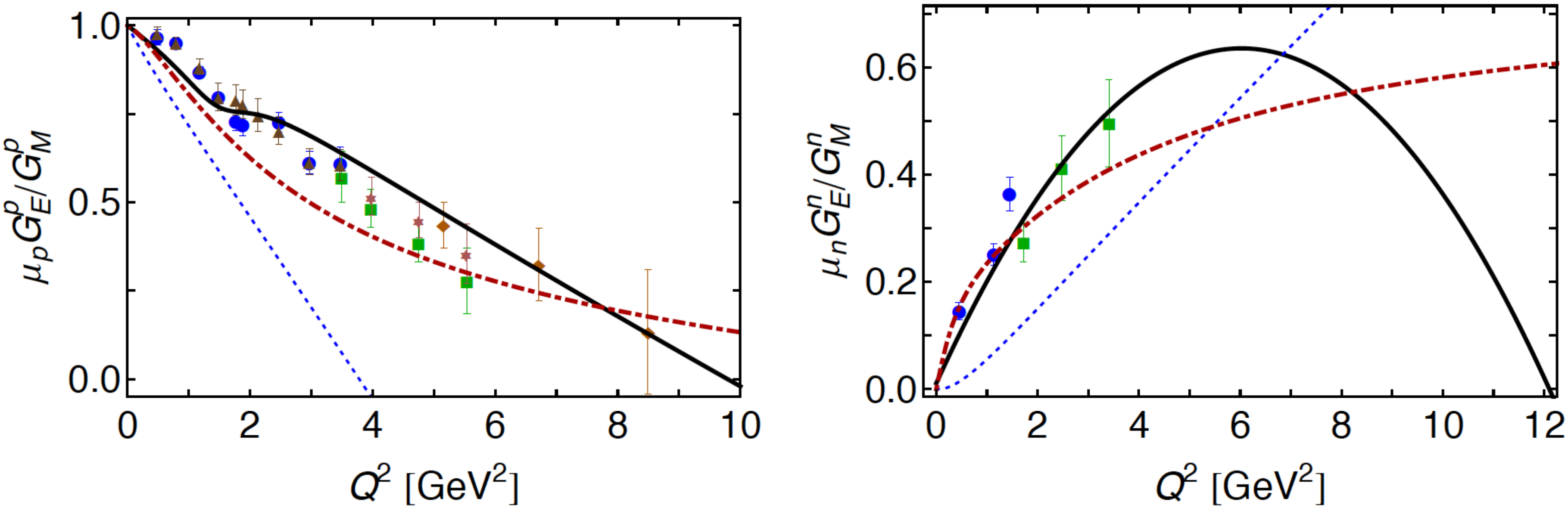

Fig. 3 *Left panel*: normalised ratio of proton electric and magnetic form factors. Curves: *solid, black* – result obtained herein, using our QCD-kindred framework; *Dashed, blue* – CI result [18]; and *dot-dashed, red* – ratio inferred from 2004 parametrisation of experimental data [65]. Data: blue circles [68]; green squares [69]; brown triangles [70]; purple asterisk [71]; and orange diamonds [72]. *Right panel*: normalised ratio of neutron electric and magnetic form factors. Curves: same as in left panel. Data: blue circles [73]; and green squares [74].

J. Segovia, I. Cloet and C. Roberts: [Few-Body Syst. 55, 1185 (2014)]

Quote from the abstract:

of dynamical chiral symmetry breaking in the bound-state problem. Amongst the results we describe, the following are of particular interest: $G_E^p(Q^2)/G_M^p(Q^2)$ possesses a zero at $Q^2 = 9.5\,\mathrm{GeV}^2$; any change in the interaction which shifts a zero in the proton ratio to larger Q^2 relocates a zero in $G_E^n(Q^2)/G_M^n(Q^2)$ to smaller Q^2; there is likely a value of momentum transfer above which $G_E^n > G_E^p$; and the presence of strong diquark correlations within the nucleon is sufficient to understand empirical extractions of the flavour-separated form factors. Regarding the $\Delta(1232)$-baryon, we find that, *inter*

Reaching high Q^2 in Lattice QCD

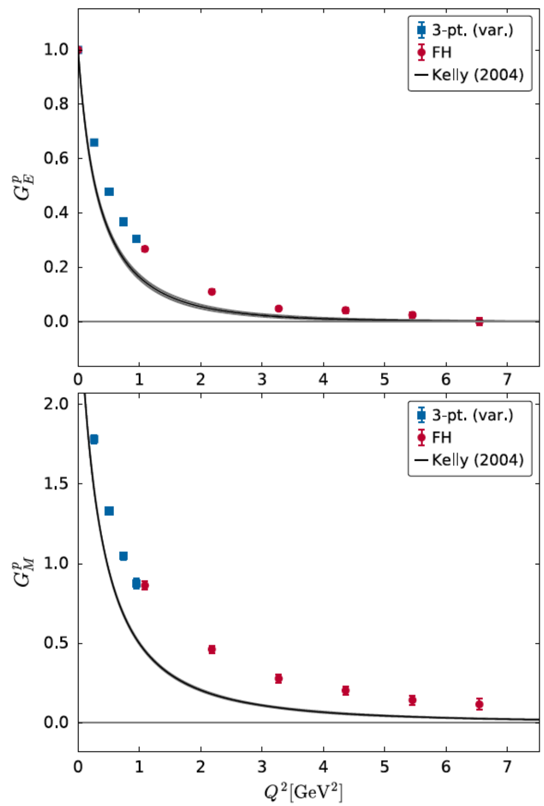

FIG. 3. G_E and G_M for the proton from the Feynman-Hellmann method and from a variational method described in Ref. [29] employed on the same ensemble. The experimental parametrization is from Ref. [49].

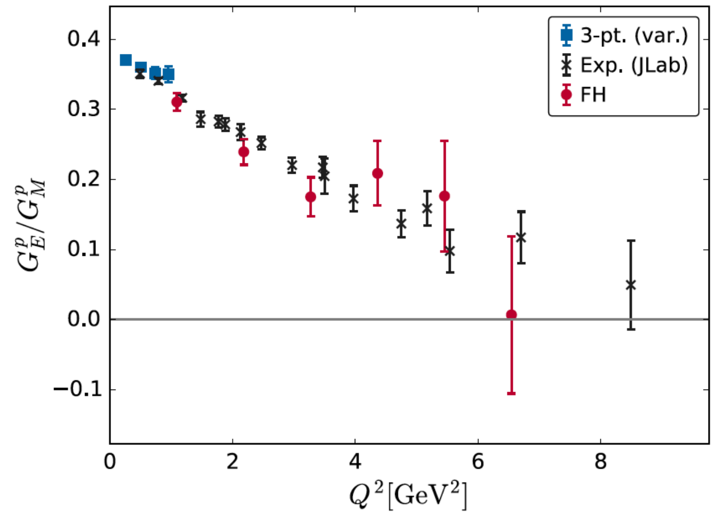

FIG. 4. Ratio G_E/G_M for the proton from the application of the Feynman-Hellmann method, from a variational analysis of three-point functions [29], and from experiment [5–7]. Note this is not scaled by the magnetic moment of the proton μ_p, as this would require phenomenological fits to the low-Q^2 data, which is not the focus of this work.

$$\frac{\partial E_\psi}{\partial \lambda} = \left\langle \psi \left| \frac{\partial H}{\partial \lambda} \right| \psi \right\rangle$$

A. J. Chambers *et al.*, (QCDSF/UKQCD/CSSM Collaborations) Phys. Rev. D 96, 114509 (2017)

- Novel application of the Feynman-Hellman method: relates hadronic matrix elements to energy shifts, allowing access to form factors via two-point correlators as opposed to more complicated three-point functions; improves signal-to-noise ratio for high-momentum states

Transition to pQCD–onset of dimensional scaling?

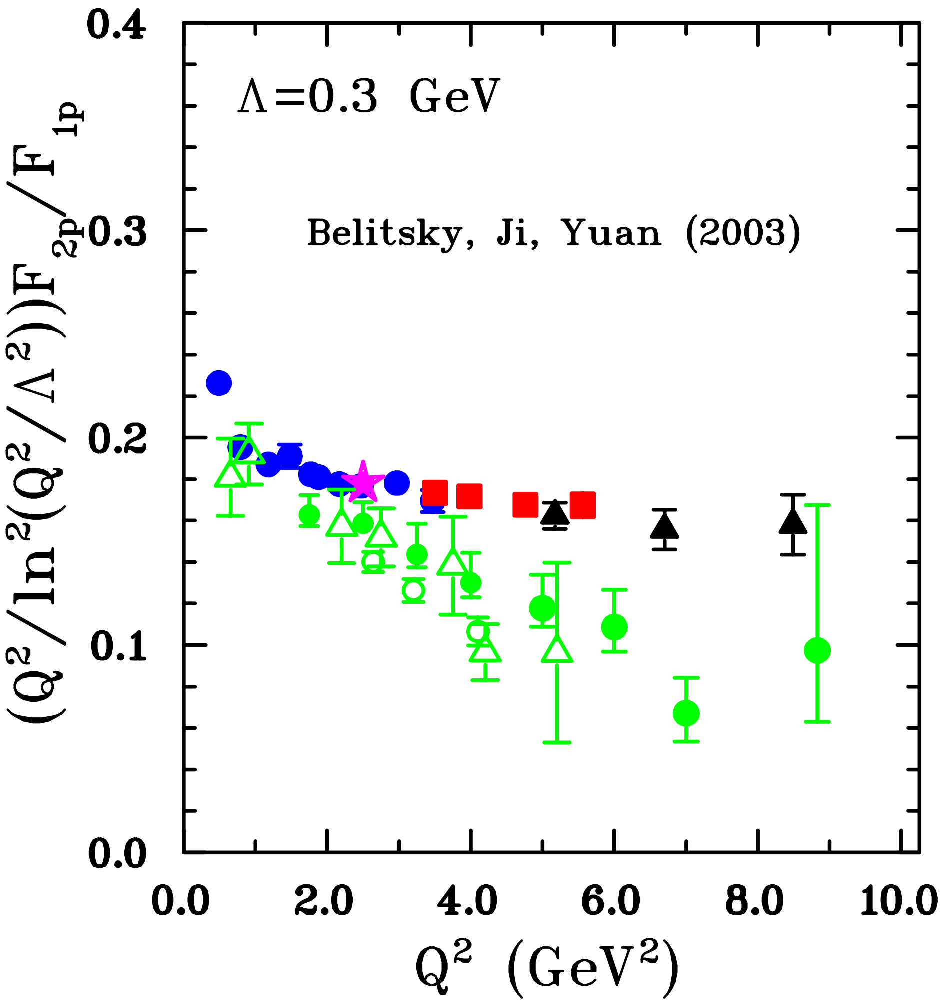

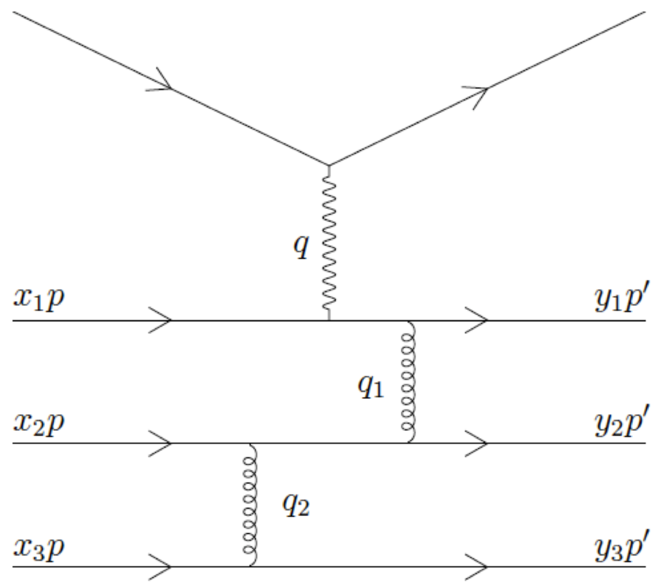

- Brodsky, Farrar, PRD 11, 1309 (1975) $\quad F_1 \propto \frac{\alpha_S^2}{Q^4}$
- Brodsky, Lepage PRL 43, 545 (1979) $\quad F_2 \propto \frac{F_1}{Q^2}$
- Belitsky, Ji, Yuan, PRL 91, 092003 (2003) $\quad \left(\frac{Q^2}{\ln^2\left(\frac{Q^2}{\Lambda^2}\right)}\right) F_2^p \propto F_1^p$

"Precocious" scaling observed in F_2^p/F_1^p not seen in F_2^n/F_1^n, for values of cutoff parameter Λ similar to that which describes proton data

Electron-nucleon scattering: Glossary

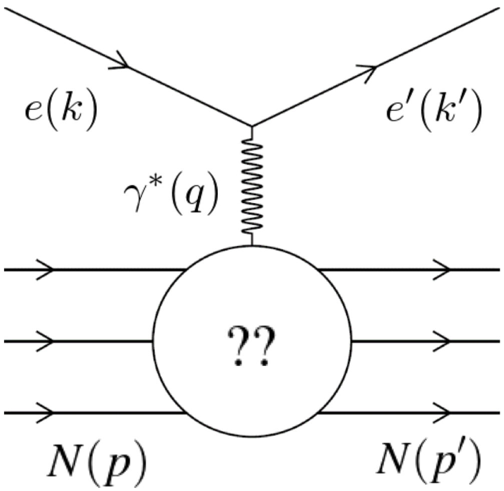

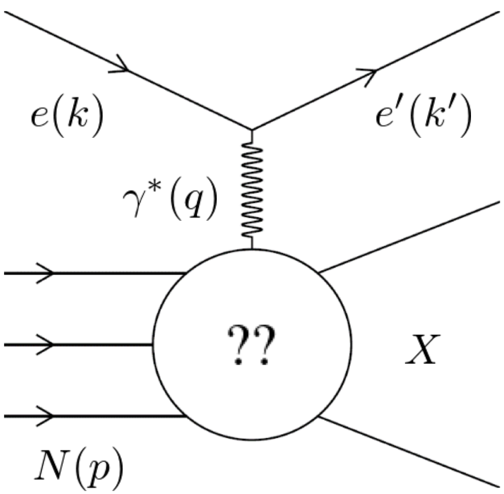

- ***Elastic scattering:***
  $e+N \rightarrow e+N$
- Nucleon stays intact and in its ground state
- ***Inelastic scattering:***
  $e+N \rightarrow e+X$
  - **X = anything** allowed by overall energy/momentum conservation and nucleon internal structure/reaction dynamics
- ***Inclusive reactions:***
  - *Only* the scattered electron is detected in the final state
  - All possible hadronic final states satisfying energy/momentum conservation are integrated over.
- ***Exclusive reactions:***
  - *All* final-state reaction products are detected either directly or via "missing mass"
  - Examples include elastic scattering (e+N→e+N), virtual Compton Scattering (e+N→e+N+γ), exclusive meson production (e+N→e+N+h, h = π, K, ...), etc.
- ***Semi-inclusive reactions:***
  - *Some (but not all)* final-state particles are detected
  - Example: semi-inclusive hadron production e+N→e+h+X, where e and h are detected in the final state, and "X" represents all unobserved particles.

Electron-Nucleon Scattering: Kinematics

$$k^\mu = (E_e, \mathbf{k}_e)$$ *Incident electron four-momentum*

$$k'^\mu = (E'_e, \mathbf{k}'_e)$$ *Scattered electron four-momentum*

$$p^\mu = (E_N, \mathbf{p}_N) \overset{N\ rest}{=} (M_N, \mathbf{0})$$ *Initial nucleon four-momentum*

$$Q^2 \equiv -q^2 = (k-k')^2 = 2E_eE'_e(1-\cos\theta_e) = 4E_eE'_e\sin^2\frac{\theta_e}{2}$$ *Squared Momentum Transfer*

$$\nu \equiv \frac{p\cdot q}{\sqrt{p^2}} \overset{N\ rest}{=} E_e - E'_e$$ *Energy Transfer (nucleon rest frame)*

$$x \equiv \frac{Q^2}{2p\cdot q} = \frac{Q^2}{2M_N\nu}$$ *Bjorken "x" variable*

$$y \equiv \frac{p\cdot q}{p\cdot k} \overset{N\ rest}{=} \frac{\nu}{E_e}$$ *Fractional electron energy loss (nucleon rest frame)*

$$W^2 \equiv (p+q)^2 = M_N^2 + 2M_N\nu - Q^2$$ *Invariant mass of virtual-photon + initial nucleon system*

$$= M_N^2 + Q^2\frac{1-x}{x}$$

The GEp-III and GEp-2γ experiments in Hall C

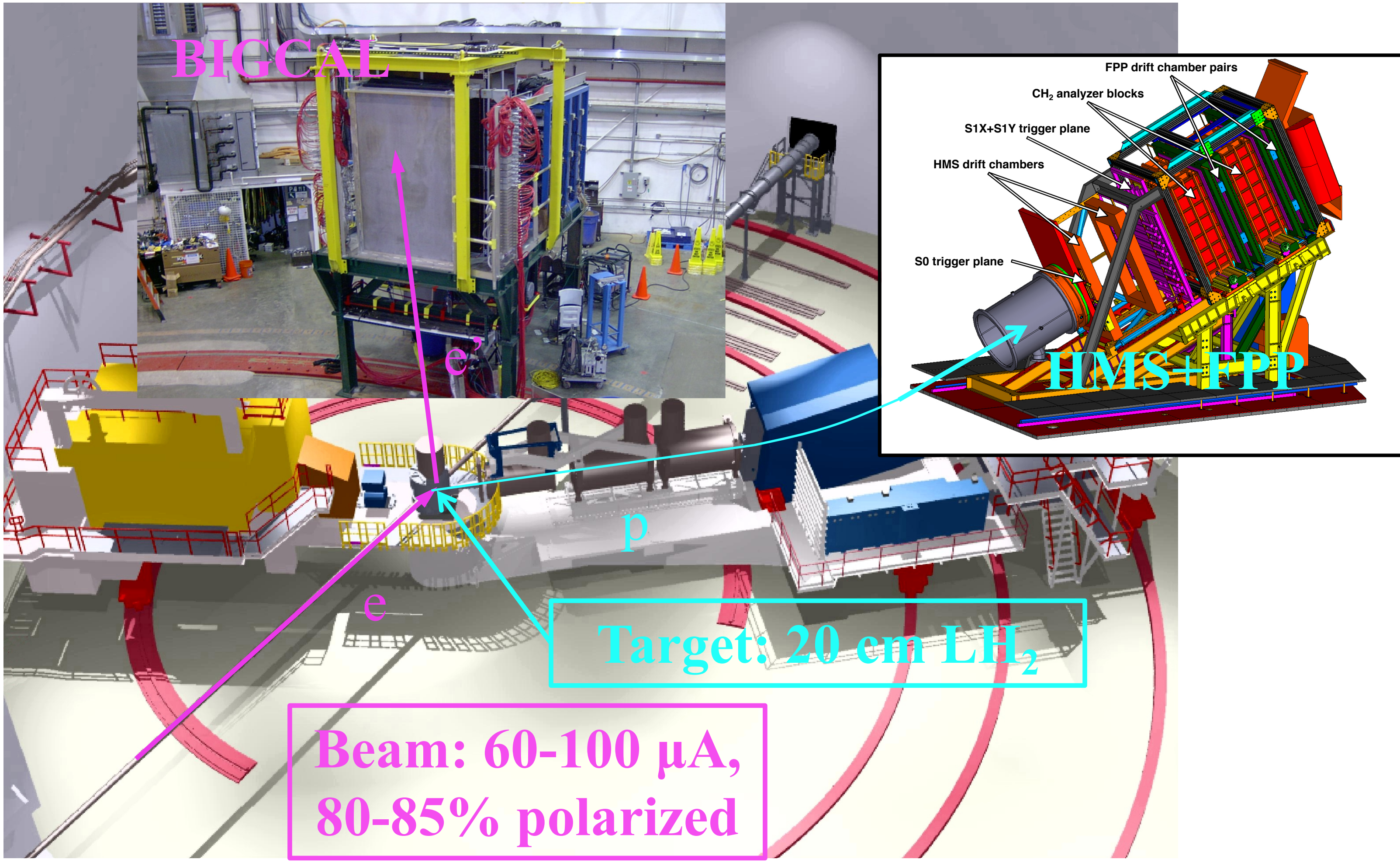

- Polarization transfer in ^{1}H(**e**,e'**p**). Nominal luminosity ~ 4×10^{38} Hz/cm^2
- "Fast" beam helicity reversal (30 Hz) cancels FPP instrumental asymmetry in polarization transfer observables

Neutron form factors—G_{Mn} existing data

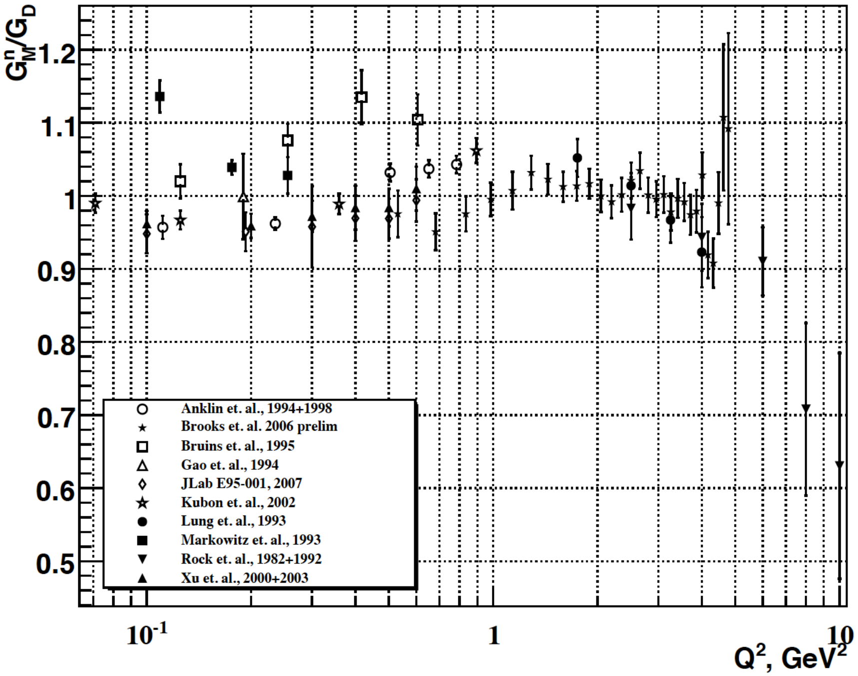

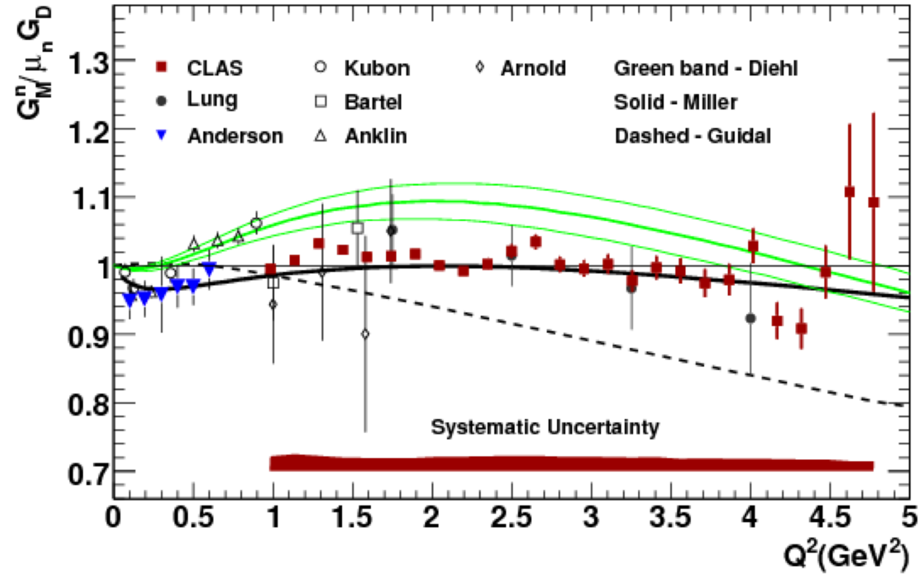

Lachniet *et al.*, CLAS Collaboration, Phys.Rev.Lett. 102 (2009) 192001

- Three main methods have been used to measure G_{Mn}:
  - "Ratio" method: measure cross section ratio of d(e,e'n)p/d(e,e'p)n in quasi-elastic kinematics
  - Absolute d(e,e'n)p quasi-elastic cross section measurement
  - Beam-target double-spin asymmetry* in inclusive quasi-elastic ^{3}He(e,e')

- **Note: double-spin asymmetry method for G_{Mn} would not work for a free neutron target, as the free nucleon asymmetry depends only on the ratio G_E/G_M, and not G_E or G_M independently.*
- Widest combined Q^2 coverage and precision from recent CLAS 6 GeV data from $1 < Q^2 < 5$ GeV^2—consistent with "standard" dipole
- Consistency issues in low-Q^2 data

The low-Q^2 regime and the proton radius puzzle

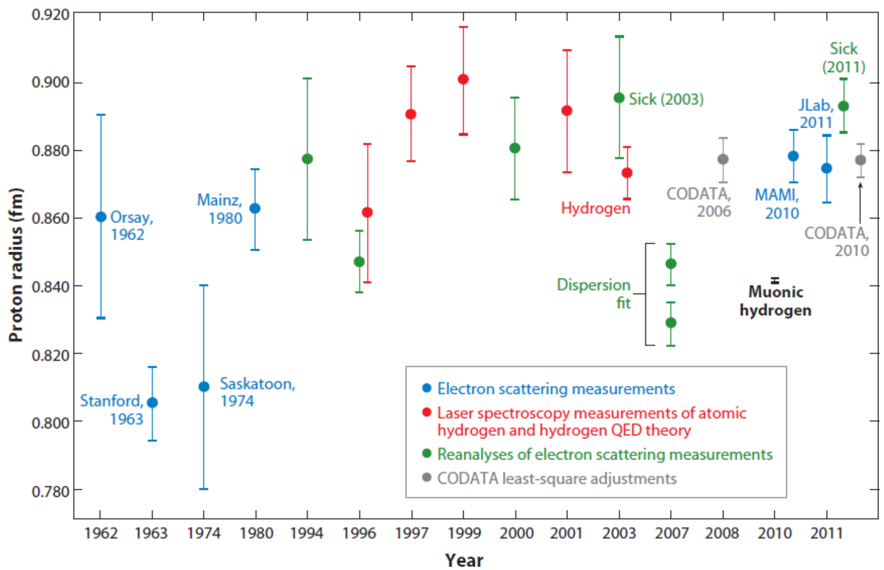

Pohl, Gilman, Miller, Pachucki: Ann. Rev. Nucl. Part. Sci. 63 (2013) 175-204

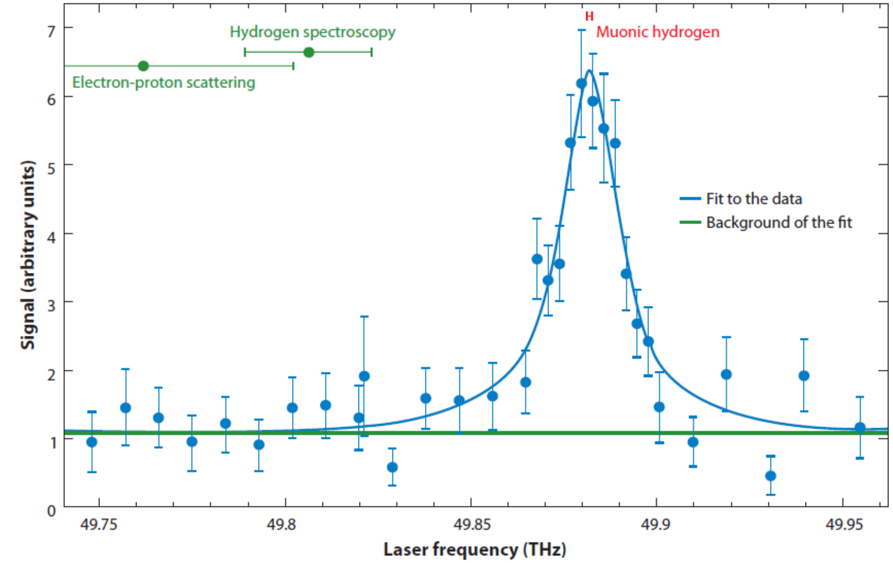

Pohl R, et al. (CREMA Collab.) *Nature* 466:213 (2010)

- Proton charge radius extractions from electronic hydrogen spectroscopy and elastic electron scattering agree on a value $r_p \sim 0.88$ fm
- Lamb shift in muonic hydrogen atom has much higher ($\sim 10^7$) sensitivity to proton radius because muon is much heavier than electron, spends more time "inside" the proton:

$$r_p^2 \equiv -6 \left.\frac{dG_E^p}{dQ^2}\right|_{Q^2=0}$$

$$a_{\mu H} = a_{eH}\left(\frac{m_e}{m_\mu}\right) \approx 256 \text{ fm}$$

- New experiments planned:
  - ep scattering at ultra-low Q^2
  - μp scattering
  - More precision spectroscopy

Is r_p from electron scattering consistent with muonic hydrogen results after all?

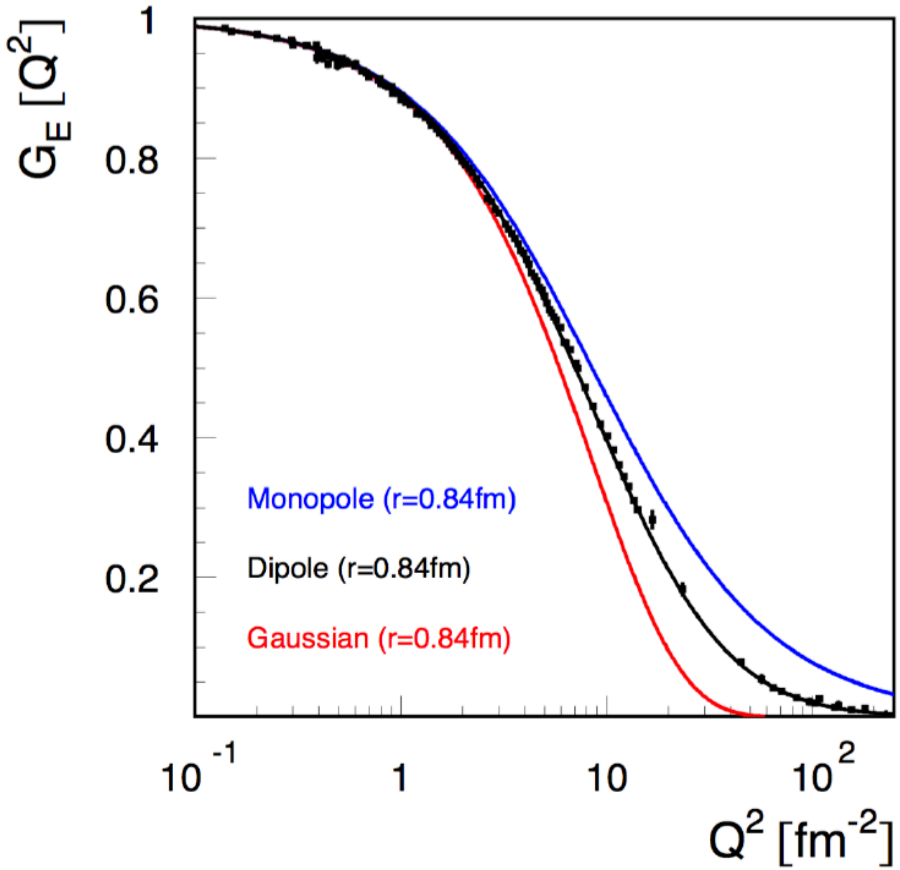

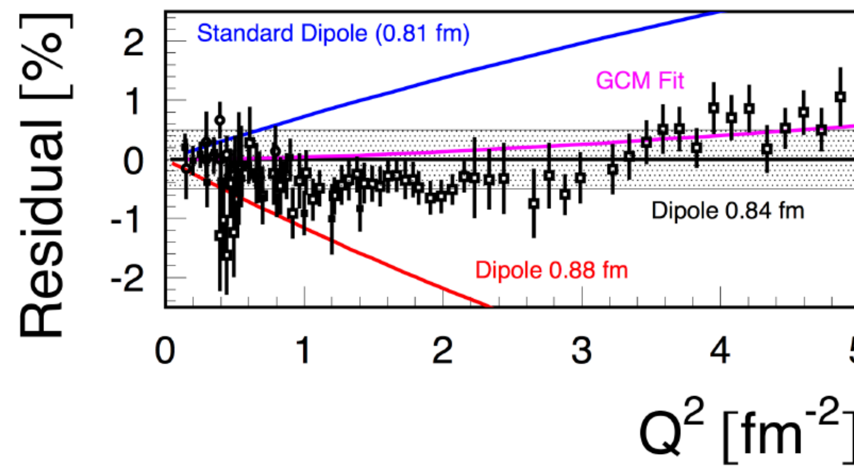

D. Higinbotham *et al.*, arXiv:1510.01293v2 [nucl-ex] 31 Mar 2016

- New statistical analysis of elastic *ep* scattering data suggests that electron scattering data are consistent with the muonic hydrogen determination of the proton charge radius, and that "the electronic hydrogen spectroscopy data are the outliers"
- Extension of modified dipole fit with r_p = 0.84 fm to large Q^2 describes cross section data rather well, but does not (and cannot) describe the observed falloff of the polarization data. The range of data described is notable nonetheless (and the conclusion of a smaller r_p compared to some other analyses does not depend on the dipole assumption).

The low-Q^2 region

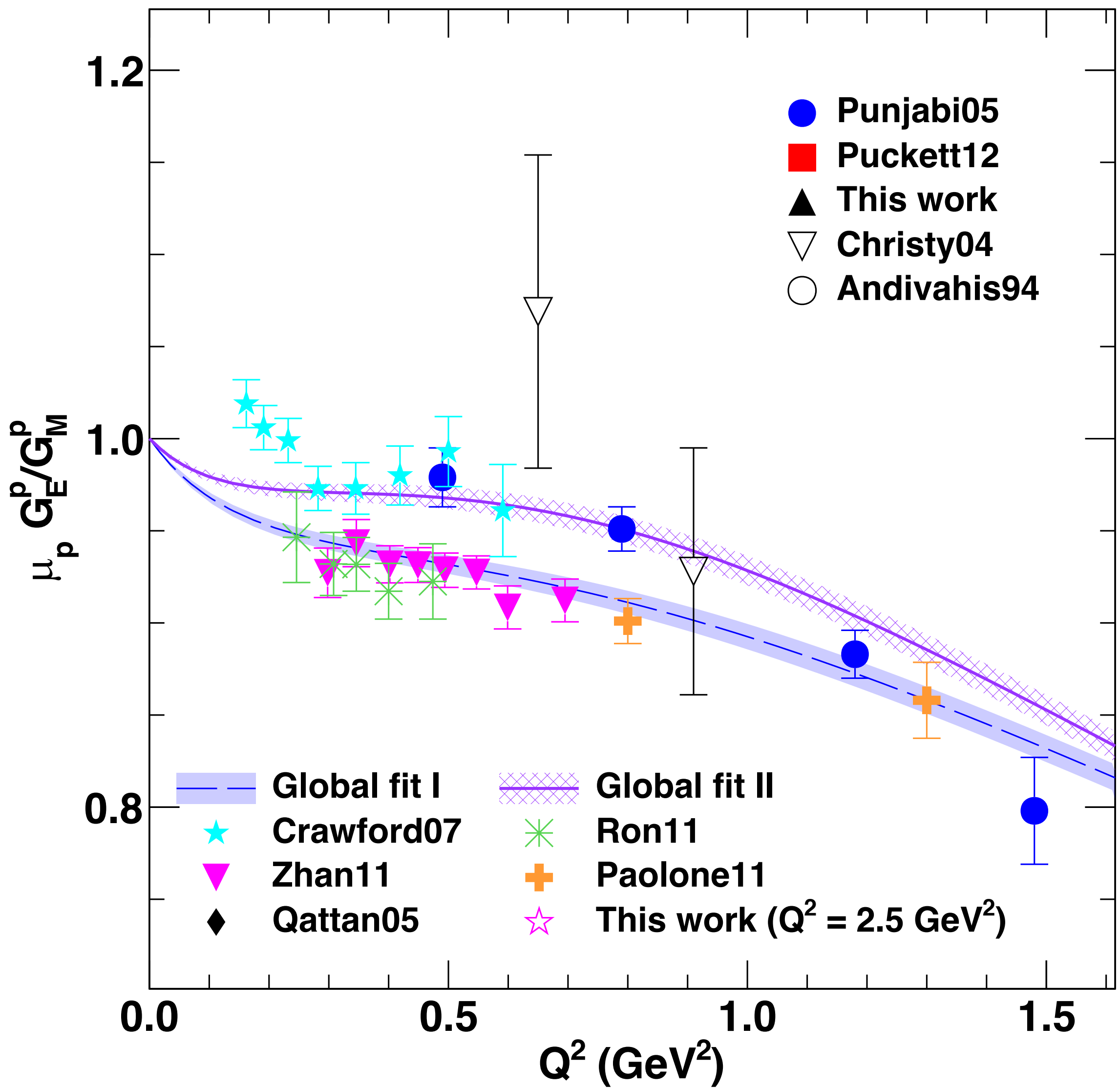

- Unresolved tension among polarization data in the low-Q^2 region.
- The two global proton FF fits differ only in the selection of low-Q^2 data
- Awaiting low-Q^2 polarized target results from Hall A

Analyzing Power Calibration

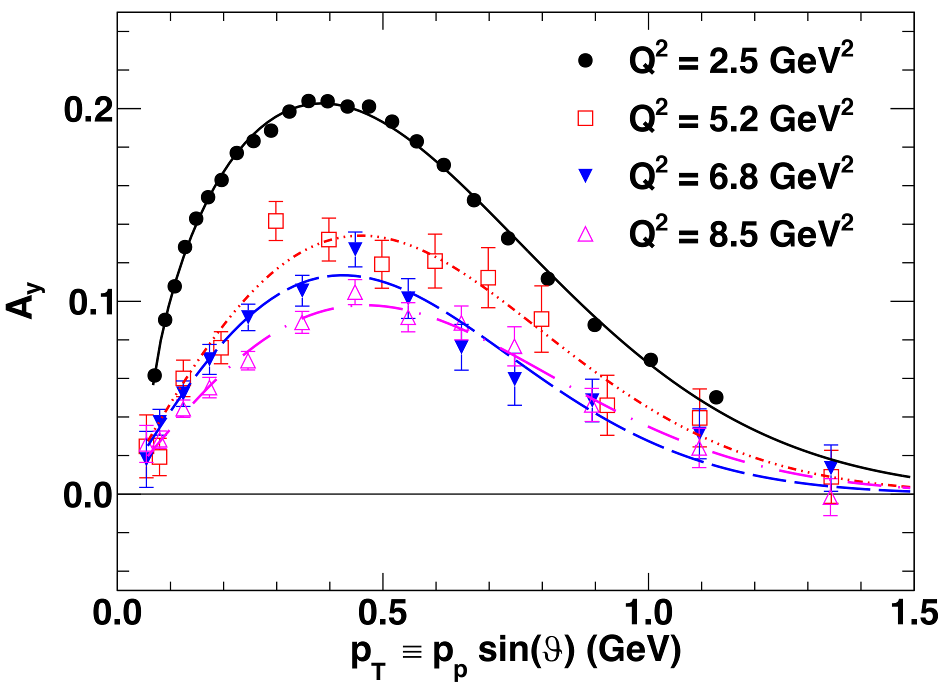

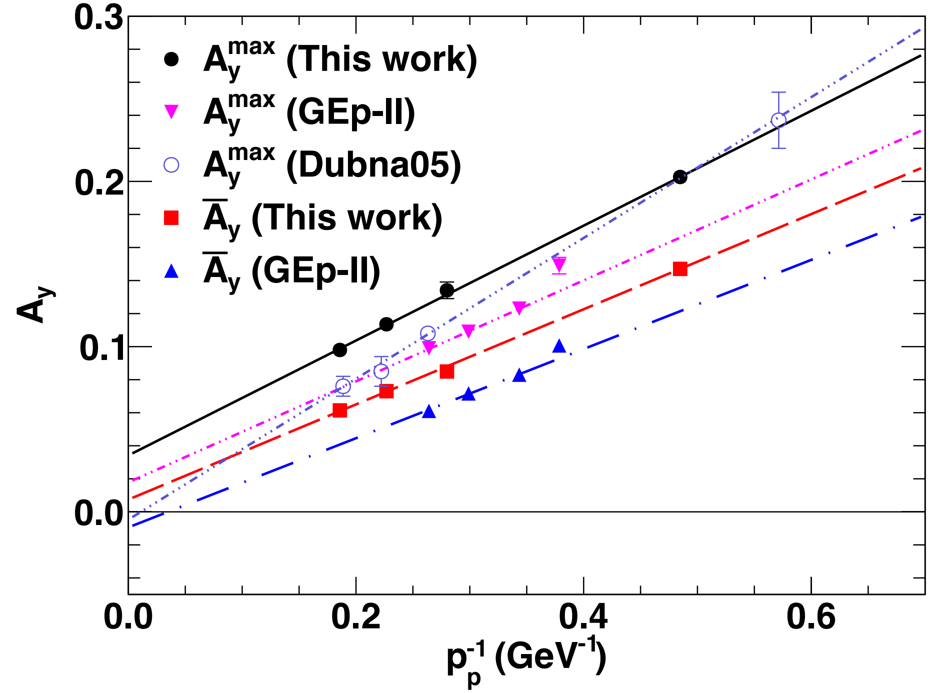

$$\hat{P}_t^{(A_y=1)} = \bar{A}_y P_t$$

$$\hat{P}_\ell^{(Ay=1)} = \bar{A}_y P_\ell$$

$$\bar{A}_y = \frac{\hat{P}_t^{(A_y=1)}}{P_t^{Born}} = \frac{\hat{P}_\ell^{(A_y=1)}}{P_\ell^{Born}}$$

$$A_y(p_p, p_T) = A_y^0(p_T)\frac{\bar{p_p}}{p_p},$$

- The analyzing power distribution in terms of $p_T = p_p \sin\vartheta$ is roughly Q^2-independent, up to an overall normalization constant, with a maximum at $p_T \approx 0.4$ GeV.
- Both the maximum and the average (for equivalent p_T ranges) analyzing power scale as p_p^{-1}.
- The analyzing power momentum dependence is corrected for event-by-event assuming an overall p_p^{-1} scaling, independent of ϑ.
- Hall C FPP effective A_y significantly exceeds that of other experiments using CH_2. This is attributable to the capability to isolate true single-track events, absent from Hall A and Dubna measurements

Doug Higinbotham's ranking of "Hall A" publications by citation count:

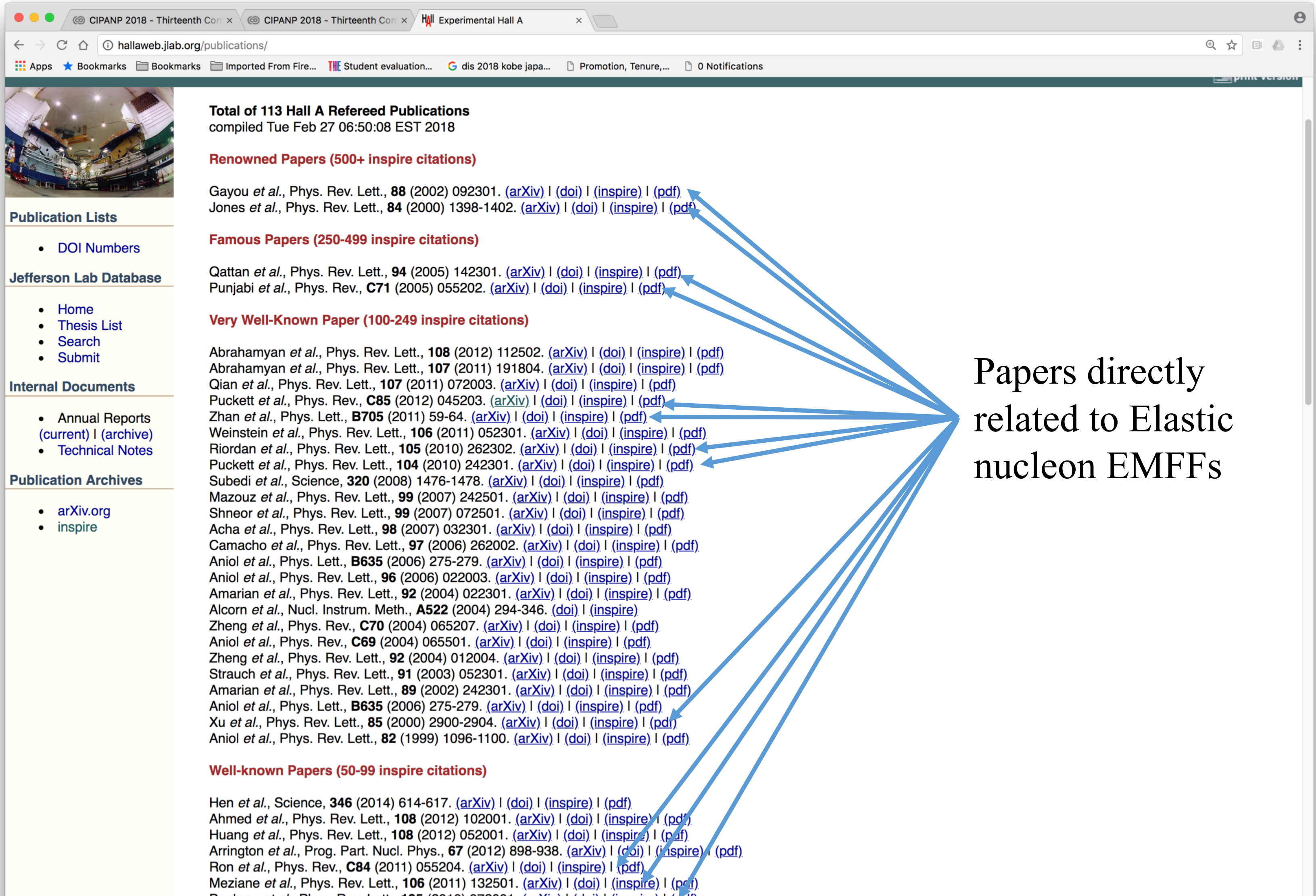

CIPANP 2018 - Thirteenth Con × | CIPANP 2018 - Thirteenth Con × | Experimental Hall A ×

hallaweb.jlab.org/publications/

Apps | Bookmarks | Bookmarks | Imported From Fire... | Student evaluation... | dis 2018 kobe japa... | Promotion, Tenure,... | 0 Notifications

Publication Lists

- DOI Numbers

Jefferson Lab Database

- Home
- Thesis List
- Search
- Submit

Internal Documents

- Annual Reports (current) | (archive)
- Technical Notes

Publication Archives

- arXiv.org
- inspire

Total of 113 Hall A Refereed Publications
compiled Tue Feb 27 06:50:08 EST 2018

Renowned Papers (500+ inspire citations)

Gayou *et al.*, Phys. Rev. Lett., **88** (2002) 092301. (arXiv) | (doi) | (inspire) | (pdf)
Jones *et al.*, Phys. Rev. Lett., **84** (2000) 1398-1402. (arXiv) | (doi) | (inspire) | (pdf)

Famous Papers (250-499 inspire citations)

Qattan *et al.*, Phys. Rev. Lett., **94** (2005) 142301. (arXiv) | (doi) | (inspire) | (pdf)
Punjabi *et al.*, Phys. Rev., **C71** (2005) 055202. (arXiv) | (doi) | (inspire) | (pdf)

Very Well-Known Paper (100-249 inspire citations)

Abrahamyan *et al.*, Phys. Rev. Lett., **108** (2012) 112502. (arXiv) | (doi) | (inspire) | (pdf)
Abrahamyan *et al.*, Phys. Rev. Lett., **107** (2011) 191804. (arXiv) | (doi) | (inspire) | (pdf)
Qian *et al.*, Phys. Rev. Lett., **107** (2011) 072003. (arXiv) | (doi) | (inspire) | (pdf)
Puckett *et al.*, Phys. Rev., **C85** (2012) 045203. (arXiv) | (doi) | (inspire) | (pdf)
Zhan *et al.*, Phys. Lett., **B705** (2011) 59-64. (arXiv) | (doi) | (inspire) | (pdf)
Weinstein *et al.*, Phys. Rev. Lett., **106** (2011) 052301. (arXiv) | (doi) | (inspire) | (pdf)
Riordan *et al.*, Phys. Rev. Lett., **105** (2010) 262302. (arXiv) | (doi) | (inspire) | (pdf)
Puckett *et al.*, Phys. Rev. Lett., **104** (2010) 242301. (arXiv) | (doi) | (inspire) | (pdf)
Subedi *et al.*, Science, **320** (2008) 1476-1478. (arXiv) | (doi) | (inspire) | (pdf)
Mazouz *et al.*, Phys. Rev. Lett., **99** (2007) 242501. (arXiv) | (doi) | (inspire) | (pdf)
Shneor *et al.*, Phys. Rev. Lett., **99** (2007) 072501. (arXiv) | (doi) | (inspire) | (pdf)
Acha *et al.*, Phys. Rev. Lett., **98** (2007) 032301. (arXiv) | (doi) | (inspire) | (pdf)
Camacho *et al.*, Phys. Rev. Lett., **97** (2006) 262002. (arXiv) | (doi) | (inspire) | (pdf)
Aniol *et al.*, Phys. Lett., **B635** (2006) 275-279. (arXiv) | (doi) | (inspire) | (pdf)
Aniol *et al.*, Phys. Rev. Lett., **96** (2006) 022003. (arXiv) | (doi) | (inspire) | (pdf)
Amarian *et al.*, Phys. Rev. Lett., **92** (2004) 022301. (arXiv) | (doi) | (inspire) | (pdf)
Alcorn *et al.*, Nucl. Instrum. Meth., **A522** (2004) 294-346. (doi) | (inspire)
Zheng *et al.*, Phys. Rev., **C70** (2004) 065207. (arXiv) | (doi) | (inspire) | (pdf)
Aniol *et al.*, Phys. Rev., **C69** (2004) 065501. (arXiv) | (doi) | (inspire) | (pdf)
Zheng *et al.*, Phys. Rev. Lett., **92** (2004) 012004. (arXiv) | (doi) | (inspire) | (pdf)
Strauch *et al.*, Phys. Rev. Lett., **91** (2003) 052301. (arXiv) | (doi) | (inspire) | (pdf)
Amarian *et al.*, Phys. Rev. Lett., **89** (2002) 242301. (arXiv) | (doi) | (inspire) | (pdf)
Aniol *et al.*, Phys. Lett., **B635** (2006) 275-279. (arXiv) | (doi) | (inspire) | (pdf)
Xu *et al.*, Phys. Rev. Lett., **85** (2000) 2900-2904. (arXiv) | (doi) | (inspire) | (pdf)
Aniol *et al.*, Phys. Rev. Lett., **82** (1999) 1096-1100. (arXiv) | (doi) | (inspire) | (pdf)

Well-known Papers (50-99 inspire citations)

Hen *et al.*, Science, **346** (2014) 614-617. (arXiv) | (doi) | (inspire) | (pdf)
Ahmed *et al.*, Phys. Rev. Lett., **108** (2012) 102001. (arXiv) | (doi) | (inspire) | (pdf)
Huang *et al.*, Phys. Rev. Lett., **108** (2012) 052001. (arXiv) | (doi) | (inspire) | (pdf)
Arrington *et al.*, Prog. Part. Nucl. Phys., **67** (2012) 898-938. (arXiv) | (doi) | (inspire) | (pdf)
Ron *et al.*, Phys. Rev., **C84** (2011) 055204. (arXiv) | (doi) | (inspire) | (pdf)
Meziane *et al.*, Phys. Rev. Lett., **106** (2011) 132501. (arXiv) | (doi) | (inspire) | (pdf)
Paolone *et al.*, Phys. Rev. Lett., **105** (2010) 072001. (arXiv) | (doi) | (inspire) | (pdf)

Papers directly related to Elastic nucleon EMFFs

JLab detector landscape

Figure credit: B. Wojtsekhowski (JLab)

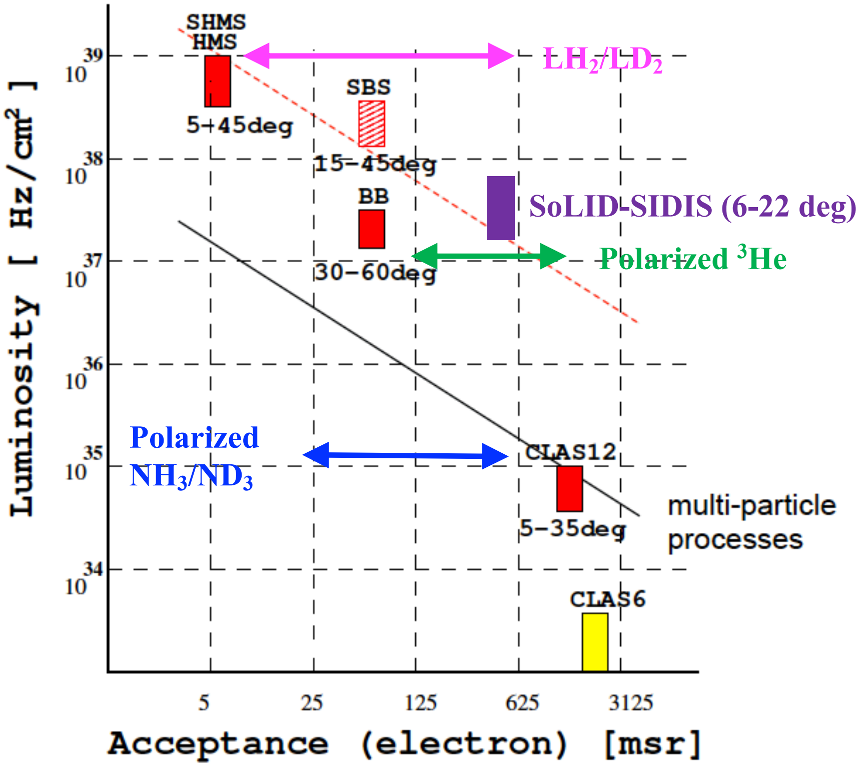

A range of 10^4 in luminosity.

A big range in solid angle:
from 5 msr (SHMS)
to about 1000 msr (CLAS12).

========================

The SBS is in the middle:
for solid angle (up to 70 msr)
and high luminosity capability.

In several A-rated experiments
SBS was found to be the best
match to the physics.

GEM allows a spectrometer
with open geometry (->large
acceptance) at high L.

11/16/15 Super Bigbite Spectrometer Review slide 9

- Complementary equipment/capabilities of Halls A, B, C allow optimal matching of (Luminosity x Acceptance) of the detectors to the luminosity capabilities of the targets, including state-of-the-art polarized target technology.

Proton FFs—Rosenbluth Separation Method

- The nucleon structure-dependent part of the cross section factorizes from the "point-like" part.
- The "reduced cross section" σ_R depends linearly on ϵ for a given Q^2, with slope G_E^2 and intercept τG_M^2.
- Experimentally, one measures $d\sigma/d\Omega$ while varying the beam energy and scattering angle to change ϵ while holding Q^2 constant

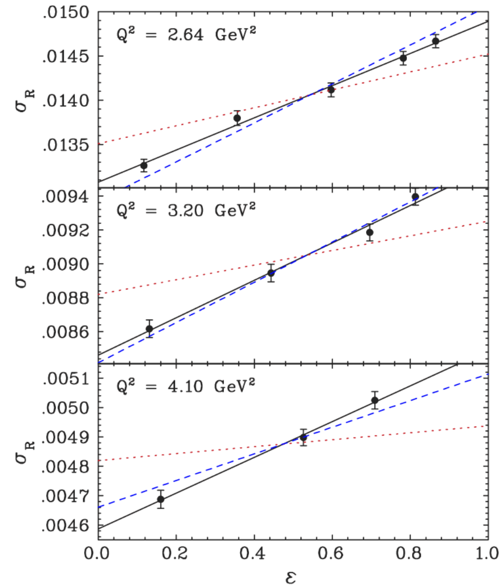

FIG. 2 (color online). Reduced cross sections as a function of ε. The solid line is a linear fit to the reduced cross sections, the dashed line shows the slope expected from scaling ($\mu_p G_E/G_M = 1$), and the dotted line shows the slope predicted by the polarization transfer experiments [6].

Qattan *et al.*, **Phys. Rev. Lett.** 94, 142301 (2005)

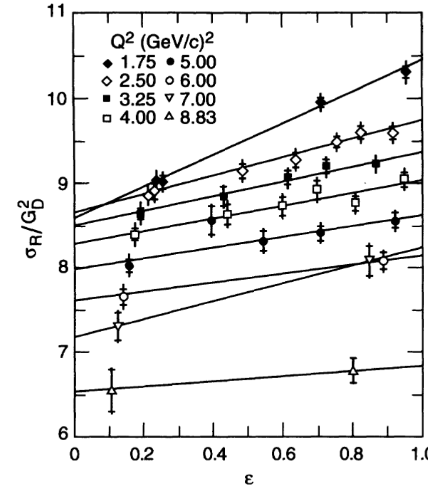

FIG. 22. Reduced cross sections divided by the square of the dipole fit plotted versus ϵ for each value of Q^2. The 1.6 GeV data points correspond to the leftmost point on each line, and the E136 data point is the rightmost point on the Q^2 = 8.83 (GeV/c)^2 line. The inner error bars show the statistical error, while the outer error bars show the total point-to-point uncertainty, given by the quadrature sum of the statistical and point-to-point systematic errors. An overall normalization uncertainty of ±1.77% has not been included.

Andivahis *et al.*, **Phys. Rev. D** 50, 5491 (1994)

$$\frac{d\sigma}{d\Omega_e} = \left(\frac{d\sigma}{d\Omega_e}\right)_{Mott} \frac{\epsilon G_E^2 + \tau G_M^2}{\epsilon(1+\tau)}$$

$$\left(\frac{d\sigma}{d\Omega_e}\right)_{Mott} = \frac{\alpha^2 \cos^2\left(\frac{\theta_e}{2}\right)}{4E_e^2 \sin^4\left(\frac{\theta_e}{2}\right)} \frac{E_e'}{E_e}$$

$$\sigma_R = \epsilon G_E^2 + \tau G_M^2$$

$$\tau \equiv \frac{Q^2}{4M_p^2}$$

$$\epsilon \equiv \left[1 + 2(1+\tau)\tan^2\left(\frac{\theta_e}{2}\right)\right]^{-1}$$